Fall 12-15-2017

Modeling of a Head - Neck Assembly Drop Tower Impact Test Using ABAQUS

Hussein Sharqi Owaid
Hussein.Owaid@maine.edu

MODELING OF A HEAD - NECK ASSEMBLY DROP TOWER IMPACT TEST USING ABAQUS

By

Hussein Sharqi Owaid
B.S. University of Thi Qar, 2009

A THESIS

Submitted in Partial Fulfillment of the

Requirements for the Degree of

Master of Science

(in Mechanical Engineering)

The Graduate School

The University of Maine

December 2017

Advisory Committee:

Vincent Caccese, Professor of Mechanical Engineering, Advisor

Senthil Vel, Arthur O. Willey Professor of Mechanical Engineering

Zhihe Jin, Professor of Mechanical Engineering

MODELING OF A HEAD - NECK ASSEMBLY DROP TOWER IMPACT TEST USING ABAQUS

By Hussein Sharqi Owaid

Thesis Advisor: Dr. Vincent Caccese

An Abstract of the Thesis Presented
in Partial Fulfillment of the Requirements for the
Degree of Master of Science
(in Mechanical Engineering)
December 2017

There are numerous potential causes of traumatic brain injury (TBI) and concussions, including traffic accidents, contact during sports and falls. Protection from these injuries is paramount because of the problems that result from TBI, such as loss of thinking and memory capability. Head impact from falls, especially in elderly, can also result in severe to fatal injury and some effects of brain injury are often not visible. For these reasons and more a need exists for protective head gear that can keep persons safe during at risk physical activity and that can protect fall prone persons from accidental injuries.

Part of the development of protective head gear includes standard methods to quantify the effectiveness of the protective device. Many studies have been conducted to design apparatus that can be used to quantify the response including

twin wire or monorail drop test apparatus and linear impactors. A combination of experimental and computational approaches can be used to develop new designs in an efficient manner. Experimental validation of head protection is typically done by using a standard apparatus. Accordingly, a validated Finite Element Analysis (FEA) model of the drop test system can be invaluable to new development efforts where FEA computer programs like ABAQUS can be used to save time and cost. The impact resisting material design can be evaluated by FEA prior to fabrication and experimental testing and adjustments made without the expense of a prototype.

The goal of this thesis work is to develop a validated FEA model of the head-neck assembly quantifying both the translational and angular accelerations based upon experimental testing of the apparatus under standard conditions. The translational and angular accelerations can be used to estimate and or mitigate the risk of the head injuries based on several head injury assessment criteria. Most apparatus calibration procedures use a rubber pad as an anvil during the testing. Accordingly, a rubber pad (MEP) was studied using experimental and FEA modeling approaches. The FEA model of a head-neck assembly test apparatus is intended to be used to study headgear response. It was developed to simulate a Hybrid III head/neck assembly drop test apparatus at the University of Maine that is currently being used to quantify the response of soft headgear. Soft headgear is the type that currently is used for soccer and in the design of headgear for elderly.

Through this thesis, a finite element model of the head-neck assembly was created and the geometric and material parameters were studied.

The first study presented was of the MEP rubber pad material response, and it material coefficients values were determined based on the experimental and the FEA results. An FEA model was created of the MEP rubber pad and impact testing apparatus including the projectile. The MEP rubber material is modeled as hyperelastic and its coefficients were estimated according to the Mooney- Rivlin theorem. The FEA model was run at different drop heights while incrementally changing the coefficients of the MEP rubber material. From this, a best fit curve was determined based upon experiment results to estimate the coefficients of the MEP rubber material.

A description of the finite element FEA model of a head-neck assembly test apparatus which is intended to be used to study headgear response is also presented. The FEA model was created using the computer program Abaqus. The material parameters of main parts of the model were studied. Some of them are assumed to be a hyperelastic material including the neck rubber, skin, rubber pads, etc. Others are liner isotropic elastic materials such as the beam and the drop arm component. The boundary conditions and the coefficient of friction COF between the head (front surface) and the impacted surface (MEP rubber pad) were studied. The peak

translational and angular accelerations versus the drop heights were determined for several sets of parameters and compared them to the experimental data.

A comparison between the FEA results and the experimental data for the head-neck assembly was performed. The study assessed the effect of a set of assumed parameters on the impact acceleration. The peak magnitudes of the translational and angular accelerations were compared at different drop height to the experimental response. The results of the experimental work were taken in the center of gravity CG of the head, particularly the CG accelerometer location which is in the head. Whereas, the FE model results were in an MPU location which was assumed the head center of gravity for the head-neck assembly. The comparison shows that the translational accelerations can be determined from the current FEA model with high confidence. A significant discrepancy exists with the current model in the assessment of peak angular acceleration.

DEDICATION

To my loving family.

ACKNOWLEDGEMENTS

I would like to thank Dr. Vincent Caccese for this opportunity and for advising me throughout the project and the two years study. I would like to thank The Higher Committee for Education Development in Iraq HCED for this opportunity to study and research and for their financial support. I am grateful to my advisory committee, Professor Zhihe Jin and Professor Senthil Vel, for their valuable input on my thesis. I would also like to thank all the students who worked in the Hybrid Structures Laboratory HSL and the group at the Advanced Manufacturing Center AMC for their support in all aspects of the project. I am grateful to the friends who provided support when needed. Last but not the least, I would like to thank my lovely wife for her support throughout my life.

TABLE OF CONTENTS

LIST OF TABLES

LIST OF FIGURES

CHAPTER 1

INTRODUCTION

Development of effective head protection can be enhanced by using a combination of experimental and computational approaches. Typical experimental validation of head protection devices usually is done using devices such as a drop testing apparatus or a linear impactor. These tests can be costly and need to be carried out subsequent to a prototype being fabricated. For that reason, development of validated finite element analysis (FEA) models can be invaluable to new development efforts. The impact resisting material design can be evaluated by FEA prior to fabrication and experimental testing and adjustments made without the expense of a prototype.

The focus of this thesis is to develop and validate the finite element model of a head-neck assembly test apparatus using the ABAQUS computer program. This model is intended to be used to study headgear response. It was developed to simulate a Hybrid III head/neck assembly drop test apparatus at the University of Maine that is currently being used to quantify the response of soft headgear. Soft headgear is the type that currently is used for soccer and in the design of headgear for elderly such as Alba Technic's SMARTY^{TM}. Through this thesis a finite element model of the head neck assembly was created and the geometric and

material parameters were studied and verified against the standard certification test specified in the ASTM F2439 standard test for soccer headgear.

According to the report of the Centers for Disease Control and Prevention (CDC), (Langlois JA, Rutland-Brown W, 2004) traumatic brain injury (TBI) is an important public health problem in the United States. Because of the problems that result from TBI, such as those of thinking and memory, effects are often not visible. Because awareness about TBI among the general public is limited, it is frequently referred to as the "silent epidemic.". Each year in the United States: At least 1.4 million people sustain a TBI. Of them, about 50,000 results in death, 235,000 are hospitalized, and 1.1 million are treated and released from an emergency department. Motor vehicle–traffic accidents result in the greatest number of TBI-related hospitalizations. Falls are also a significant cause of TBI; rates are highest for children ages 0 to 4 years and for adults age 75 years or older.

Another common cause of head injury is contact during sports. Concussion in sports is a continually occurring problem. Rowson and Duma (Rowson & Duma, 2013) reported as many as 3.8 million sports and recreation related concussion annually and an estimated 50% more incidents may go unreported.

Falls especially in elderly can result in severe to fatal head injury (U.S. Department of Health and Human Services, 2016). According to the CDC an older adult falls once every second making falls the leading cause of injury and death in

the older US population. A 2006 study published in the Journal of the American Geriatrics Society, more than one third of adults 65 and older fall each year in the United States, with falls being the most common cause of Traumatic Brain Injury (TBI) (Thompson, McCormick, & Kagan, 2006). In 2010, 2.3 million nonfatal fall injuries among older adults were treated in emergency departments and more than 662,000 of these patients were hospitalized (Faul M, Xu L, Wald MM, 2010).

Accidents injury can occur at significantly higher speed than in the case of falls and sports. As stated in (Marquis, Severson, & Tyrell, 1995) the occupant dynamics and predicted fatalities due to secondary impact for passengers involved in train collisions with impact speeds up to 140 mph is described where, the principal focus is on the effectiveness of alternative strategies for protecting occupants in train collisions, including friendly interior arrangements and occupant restraints. For example, the results indicate that compartmentalization can be as effective as a lap belt in minimizing the probability of fatality for the 50th percentile male. On the other hand, the car crash pulse varies with the impact speed, the position of the car within the trainset, and the structural design of the car.

1.1 Injury Predictor

Standard testing of headgear typically measures acceleration response during impact and the device is certified relative to a brain injury predictor. Many suggestions and studies have been performed over the years to develop and

determine accurately and systematically the predictors of a head injury in humans (Edgecomb, 2013). One injury predictor is the maximum translational acceleration magnitude, A_{max} that is used in numerous head gear testing certifications including the ASTM soccer headgear standard. The Gadd Severity Index GSI and Abbreviated Injury Scale (AIS) are one of the first head injury predictors where GSI was introduced in 1961 and AIS was created in 1969. The formula for the GSI is given below:

$$GSI = \int^{T} a(t)^{2.5} \quad dt \tag{1.1}$$

where: a(t) = resultant translational acceleration of the head in *g*'s

T = impact duration is seconds

The abbreviated injury scale AIS is an anatomic scale of the traumatic injuries. AIS includes a code from 0-6 that represents increasing injury severity from headache or dizziness to death. Table 1.1 shows details about AIS scale noting that AIS of zero means no injury.

The Head Injury Criterion HIC is currently the most widely accepted predictor, and it is used to measure the likelihood of the head injury due to translational impact (Edgecomb, 2013). It is thought to be a good predictor of the likelihood of skull fracture. Table 1.1 explains how the HIC is comparable with the AIS. The mathematical form of HIC is given in equation 1.2:

$$\mathrm{HIC} = \left\{\left[\frac{1}{(t_2 - t_1)}\int_{t_1}^{t_2} a(t)\,dt\right]^{2.5}(t_2 - t_1)\right\}_{\max} \quad (1.2)$$

where: t_1 and t_2 are any two times during the acceleration-time history

$a(t)$ = resultant translational acceleration of the head in *g*'s

t_1 and t_2 are selected to maximize HIC

The exponent 2.5 was taken from the Wayne State Tolerance Curve (WSTC), that is shown in Figure 1.1, which could be approximated by a straight line with a negative slope of 2.5 if it was plotted on a log-log scale (King, 2000). Typical HIC computations limit the analysis window (t_2 minus t_1) to 15 milliseconds. An analysis that invokes this limit is termed the HIC_{15}.

Table 1.1 Level of Head and Brain Injury According to GSI and HIC Predictors (Marquis et al., 1995)

Head Injury Criteria (HIC)	**AIS Code**	**Level of Brain Concussion and Head Injury**
135 – 519	1	Headache or dizziness
520 – 899	2	Unconscious less than 1 hour – linear fracture

Table 1.1 Continued

900 – 1254	3	Unconscious 1 – 6 hours – depressed fracture
1255 – 1574	4	Unconscious 6 – 24 hours – open fracture
1575 – 1859	5	Unconscious greater than 25 hours – large haematoma
> 1860	6	Non-survivable

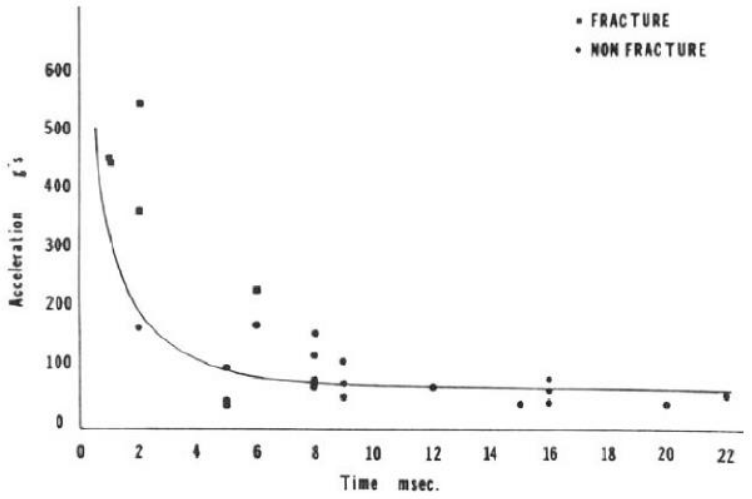

Figure 1.1 The Wayne State Tolerance Curve 15 (King, 2000)

The Generalized Acceleration Model for Brain Injury Threshold (GAMBIT) is a head injury predictor that was introduced in 1986 (Newman, 1986). In this prediction method, the resultants of both translational and angular

accelerations are been used to estimate the GAMBIT as explained in the original GAMBIT equation form:

$$G(t) = \left[\left(\frac{a(t)}{a_c}\right)^n + \left(\frac{\propto(t)}{\propto_c}\right)^m\right]^{1/s} \quad (1.3)$$

Where, a(t) in g's and α(t) in rad/s^2 are the instantaneous values of translational and rotational acceleration respectively.

a_c and $\propto_c$ are equal to 250 g's and 25000 rad/s^2 respectively.

n, m and s are empirical constants selected to fit the available data and they are equal to 2 in two kinds of motion (translational and rotational).

There are other head injury predictors such as peak translational acceleration of the center of gravity (COG) of the head, peak resultant rotational acceleration of the COG of the head, linear impact velocity, angular impact velocity, strain and strain rate, and Head Impact Power (HIP).

According to the "Final Report of Workshop on Criteria for Head Injury and Helmet Standards, 2005" Most mild traumatic brain injures MTBIs are caused by head motion (rotational and translational). The probability of a Mild Traumatic Brain Injury MTBI is correlated with a number of measures, according to Dr. Newman, including (Fenner et al., 2005):

• Maximum linear acceleration (50th percentile = 780 m/s^2)

• Maximum rotational acceleration (50th percentile = 6200 r/s^2)

• Severity Index (50th percentile SI = 300)

• Generalized Acceleration Model for Brain Injury and Tolerance (GAMBIT) (50th percentile GAMBIT = .4)

• HIC15 (50th percentile HIC15 = 230)

• Head Impact Power (HIP) (50th percentile HIP = 12.5kW)

Rowson and Duma stated that in the Head Impact Telemetry System HITS dataset, the combined probability of concussion and linear acceleration were significantly better predictors of concussion than rotational acceleration alone (Rowson & Duma, 2013). They presented a method to assess the combined use of the linear and angular accelerations, and they also used in their assessment the Head Impact Telemetry System (HITS) data and National Football League (NFL) data that collected from impact reconstructions using dummies (58 impacts including 25 concussions). The Combined Probability of Concussion Assessment formula (CP) that they used is shown below: Predictive Capability Assessment

$$\mathrm{CP} = \frac{1}{1+e^{-(\beta_0+\beta_1 a+\beta_2 \alpha+\beta_3 a\alpha)}} \tag{1.4}$$

Where: β_0, β_1, β_2 and β_3 are regression coefficients which are equal to -10.2, 0.0433, 0.000873, and -0.00000092 respectively

a is peak linear acceleration in g's

α is peak rotational acceleration in rad/s^2 and

CP is the combined probability of concussion

Equation (1.4) displays the risk function where it determines the likelihood of sustaining a concussion for a given impact, regardless of whether the injury would be reported or not. According to equation 1.4, risk contours relating peak linear and rotational head acceleration to concussion risk are shown in Figure 1.2.

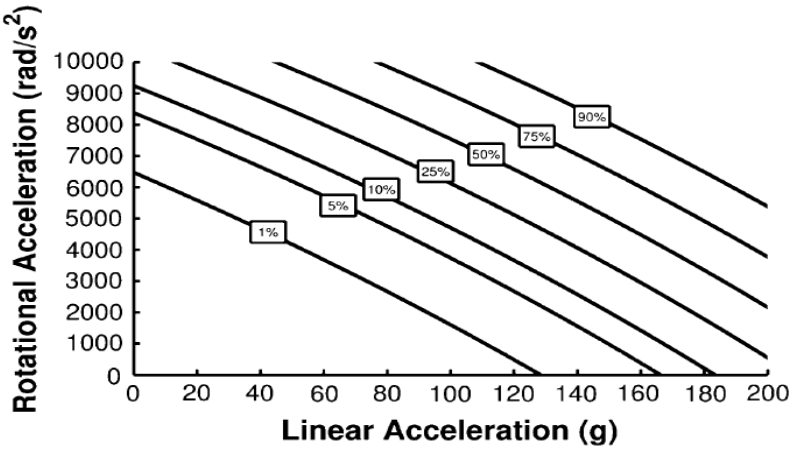

Figure 1.2 Combined Probability of Concussion Contours Relating overall Concussion Risk to Linear and Rotational Head Acceleration(Rowson & Duma, 2013)

Kimpara and Iwamoto presented predictors of a Mild Traumatic Brain Injury MTBI which are based on angular acceleration during impacts. They firstly substituted resultant angular acceleration of α(t) instead of resultant translational acceleration of a(t) in equation (1.2) that is the Head Injury Criterion HIC. This resulted in a new injury criterion called Rotational Injury Criterion RIC which is defined as follows, according to (Kimpara and Iwamoto 2012):

$$\mathrm{RIC} = \left\{(t_2 - t_1)\left[\frac{1}{(t_2 - t_1)}\int_{t_1}^{t_2} \alpha(t)\, dt\right]^{2.5}\right\}_{\max} \quad (1.5)$$

Where: t_1 and t_2 are any two times during the acceleration-time history

$\alpha(t)$ = resultant angular acceleration of the head in rad s^{-2}

Newman, Shewchenko, and Welbourne described the HIP (Head Injury Power) as a power expression of the human head injury when the kinematics of the head assumed as a rigid motion (Newman, Shewchenko, and Welbourne, 2000). According to that, Head Injury Power (HIP) as a power expression of the human head to predict head injuries due to both linear and angular accelerations was proposed as the following equation (Kimpara & Iwamoto, 2012):

$$\mathrm{HIP} = \sum m\, a_i \int a_i\, dt + \sum I_{ii}\, \alpha_i \int \alpha_i\, dt \quad (1.6)$$

Where m is a mass of the head (kg), a_i is linear acceleration (m s^{-2}), I_{ii} is a moment of inertia (MOI) (kg m^2), and α_i is angular acceleration (rad s^{-2}). Considering inertial properties of the mid-sized male of mass is 4.5 kg, and those of MOI for x, y, and

z directions are 0.016, 0.024, and 0.022 kg m^2, respectively (Kimpara et al. 2011). Fifty percent of the HIP for MTBI is determined as 12.8 kW (Newman et al., 2000).

In (Kimpara & Iwamoto, 2012; Kimpara, Nakahira, Iwamoto, Rowson, & Duma, 2011) studies the linear acceleration was omitted from the equation 1.6 then the HIP is become HIP_rot(t) which is shown in the equation 1.7:

$$HIP\_rot = \sum I_{ii}\, \alpha_i \int \alpha_i dt$$

$$= 0.016\, \alpha_x \int \alpha_x dt + 0.024\, \alpha_y \int \alpha_y dt + 0.022\, \alpha_z \int \alpha_z dt \qquad (1.7)$$

By substituting equation 1.7 as angular acceleration into equation 1.5, the final expression will be shown in equation 1.8, according to these studies. Power Rotational Head Injury Criterion (PRHIC) is:

$$\mathrm{PRHIC} = \left\{(t_2 - t_1)\left[\frac{1}{(t_2 - t_1)}\int_{t_1}^{t_2} HIP\_rot\, dt\right]^{2.5}\right\}_{\max} \qquad (1.8)$$

Time durations for angular acceleration obtained from football head impact data were greater than the 15 ms limit of the maximum time duration for HIC_{15}. Therefore, the maximum integral time duration for RIC and PRHIC was set to 36 ms, which was the time duration of HIC in some of the original studies. Therefore, this study proposed two new injury criteria of RIC_{36} and $PRHIC_{36}$ (Kimpara & Iwamoto, 2012; Kimpara et al., 2011). Table 1.2 shows the coefficients of correlation between head motion based brain injury criteria that include (RIC_{36} and

PRHIC$_{36}$) and head motions based on National Football League NFL(upper) and 6DOF device data (lower) (6DOF skull accelerations measured at CG of the head). Figure 1.3 shows the correlations of Cumulative Strain Damage Measure (CSDMs) against RIC$_{36}$ and PRHIC$_{36}$.

Table 1.2 Coefficients of Correlation Between Head Motion Based Brain Injury Criteria and Head Motions Based on NFL (upper) and 6DOF Device Data (lower) (Kimpara and Iwamoto, 2012).

Injury criteria	Max. linear acceleration	Max linear velocity	Max. angular acceleration	Max. angular velocity
HIC_{15}	**0.93****	0.889**	0.60**	0.38*
	0.93**	0.68**	−0.04	−0.27**
HIP	**0.89****	**0.93****	0.72**	0.58**
	0.92**	0.72**	0.08	−0.15*
KLC	0.70**	0.82**	0.78**	**0.91****
	−0.13	−0.11	0.61**	0.71**
RIC_{36}	0.50**	0.66**	0.81**	0.86**
	−0.03	−0.09	**0.90****	0.63**
$PRHIC_{36}$	0.08	0.31	0.49**	0.77**
	−0.04	−0.02	0.59**	0.56**

*$p < 0.01$, **$p < 0.001$.

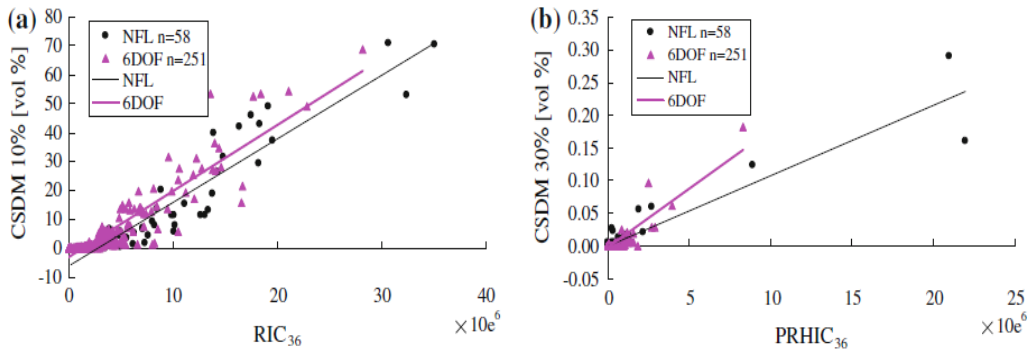

Figure 1.3 Correlations of CSDMs Against RIC_{36} and $PRHIC_{36}$. (a) RIC_{36} vs. CDSM 10%, (b) $PRHIC_{36}$ vs. CDSM 30% (Kimpara and Iwamoto, 2012)

In the past years, head rotation as a mechanism for brain injury was proposed so that a multitude of research studies by various institutions were conducted to confirm/reject this hypothesis. Kinematic rotational brain injury criterion – BRIC – which offers additional protection to an automotive occupant is one of the studies included the rotational head motion. Kinematic Brain Injury Criteria (BRIC) were developed for each tested dummy typically used in automotive studies (Hybrid III, ES2-re, and WorldSID) as well as human volunteers based on college football data (Takhounts, Ridella, Rowson, & Duma, 2011). The mathematical formula to estimate the BRIC is as follows:

$$\text{BRIC} = \frac{\omega_{max}}{\omega_{cr}} + \frac{\alpha_{max}}{\alpha_{cr}} \tag{1.9}$$

Where, ω_{max} and α_{max} are maximum angular velocities and accelerations for each test respectively, and The critical values of angular velocity and acceleration for:

the Hybrid III dummy, they were found to be ω_{cr} = 46.41 rad/s and α_{cr} = 39,774.87 rad/s^2, the WorldSID dummy, they were found to be ω_{cr} = 153.18 rad/s and α_{cr} = 11,527.92 rad/s^2, the critical values of angular velocity and acceleration for the college football players were found to be ω_{cr} = 42.05 rad/s and α_{cr} = 363,268.91 rad/s^2 and the critical values of angular velocity and acceleration for the ES-2re dummy were found to be ω_{cr} = 65.68 rad/s and α_{cr} = 23,063.90 rad/s^2.

According to the update of the BRIC expression in 2013 which after finding that angular velocity alone was sufficient to predict FE model strains in pendulum and occupant crash tests so that the updated criterion, BrIc, is formulated using the maximum magnitudes of the three orthogonal head angular velocity components as shown in Equation 1.10 (Takhounts, E. G., Craig, M. J., Moorhouse, K., McFadden, J., & Hasija, 2013):

$$\text{BrIc} = \sqrt{\left(\frac{\omega_x}{\omega_{xc}}\right)^2 + \left(\frac{\omega_y}{\omega_{yc}}\right)^2 + \left(\frac{\omega_z}{\omega_{zc}}\right)^2} \tag{1.10}$$

Where: ω_x, ω_y, and ω_z are maximum angular velocities about X-, Y-, and Z-axes respectively, and ω_{xc}, ω_{yc}, and ω_{zc} are the critical angular velocities in their respective directions, as shown in Table 1.3 all are in rad/s.

Table 1.3 Critical Max Angular Velocities in Each Direction Based on CSDM, MPS, and their Average. Note: the values are the same for all ATDs (and humans) (Takhounts, E. G., Craig, M. J., Moorhouse, K., McFadden, J., & Hasija, 2013)

Critical Max Angular Velocity	Rad/s (CSDM Based)	Rad/s (MPS Based)	Rad/s (Average of CSDM and MPS)
ω_x	66.20	66.30	66.25
ω_y	59.10	53.80	56.45
ω_z	44.25	41.50	42.87

In (Mueller, MacAlister, Nolan, & D. Zuby, 2015), the critical angular velocities ω_{xc}, ω_{yc}, and ω_{zc} are used where they performed these average values that are shown in the Table 1.3 which are 66.25, 56.45 and 42.87 rad/s respectively. They also estimate the risk of brain injury based on an AIS_{3+} and BrIc equation as follows:

$$PR_{AIS3+} = 1 - e^{-(\frac{BrIc}{0.987})^{0.294}} \quad (1.11)$$

$$PR_{AIS4+} = 1 - e^{-(\frac{BrIc}{1.204})^{0.294}} \quad (1.12)$$

Where, PR_{AIS3+} and PR_{AIS4+} are brain risk injury based on AIS_{3+} and AIS_{4+} with BrIc respectively.

1.2 Testing Methods

Most impact tests are designed to achieve a repeatable input condition and may not necessarily need to reproduce actual fall conditions. The Hybrid III 50th percentile male anthropomorphic test device (ATD) is the most widely used surrogate for human impact testing. The ATD has historically been used in automotive or military testing for applications evaluating athletic helmet protectively, quantifying head impact and estimating injury risk (Bartsch, Benzel, Miele, Morr, & Prakash, 2012).

The Hybrid III Head Neck assembly impact test at the University of Maine, as shown in Figure 1.4, has been used in this thesis. According to (Caccese et al., 2016), the University of Maine drop test apparatus was fabricated for assessing fall protective headgear with guidance from ASTM F2349 the standard for headgear used in soccer, and it was developed to impart and measure both linear and angular acceleration components of the headform simultaneously during impact. The Hybrid-III head was selected for the purpose that it is readily instrumented with a nine-accelerometer array and its response has been extensively quantified.

The drop mechanism consists of a twin wire fall system equipped with a drop arm that includes a 50th percentile male Hybrid- III head/neck assembly that is provided by Humanetics™, Plymouth, MI. The twin-wire drop tower, shown in

Figure 1.4, has a 5.5 m maximum drop height. It was originally built for an ASTM F1446 type test however, it has been retrofit with the head/neck apparatus.

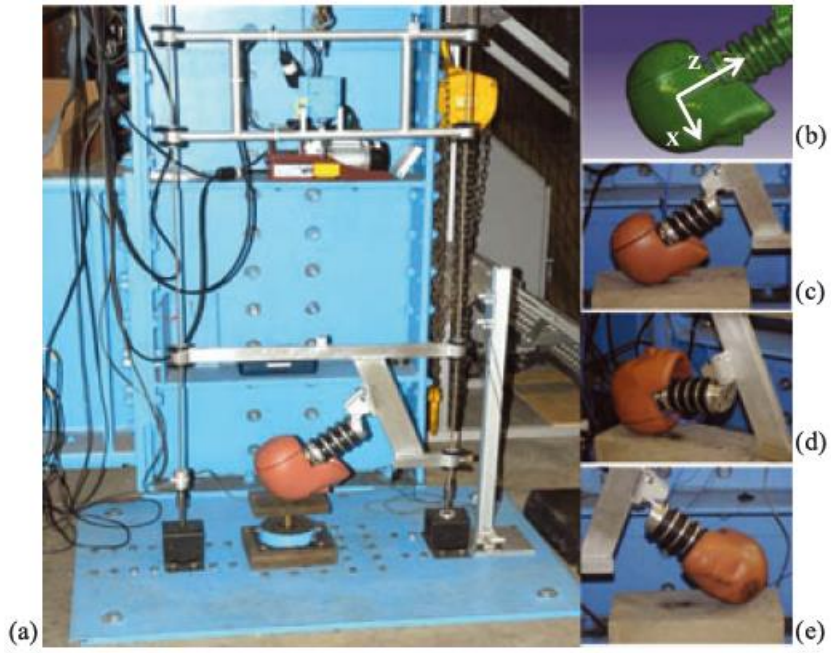

Figure 1.4 Photograph of the University of Maine drop test setup. (a) Drop tower with assembly; (b) coordinate system, (c) front drop; (d) rear drop; and (e) side drop. (Caccese et al., 2016)

The coordinate system used for the data acquisition is shown in Figure 1.4 (b). An aluminum tubing fly arm carries the head and neck, as shown in Figure 1.4, and its dimensions are shown in Figure 1.6. The head can be configured to strike in a frontal (Figure. 1.4(c)), rear (Figure. 1.4(d)), or side (Figure. 1.4(e)) impact orientations that are depended on the special adapters fabricated which can be placed between the neck and fly arm support as they are shown in Figure 1.7.

Impact locations as shown in Figure 1.5 include a $\pm 7^0$ rotation angle around an axis parallel to Y going through the neck mount, and these rotated positions were studied as they can be easily set up using the adjustment mechanism in the standard frontal mount of the ATD. The total mass of the arrangement outfitted with the head/neck assembly is 8.2 kg including the fly arm mass.

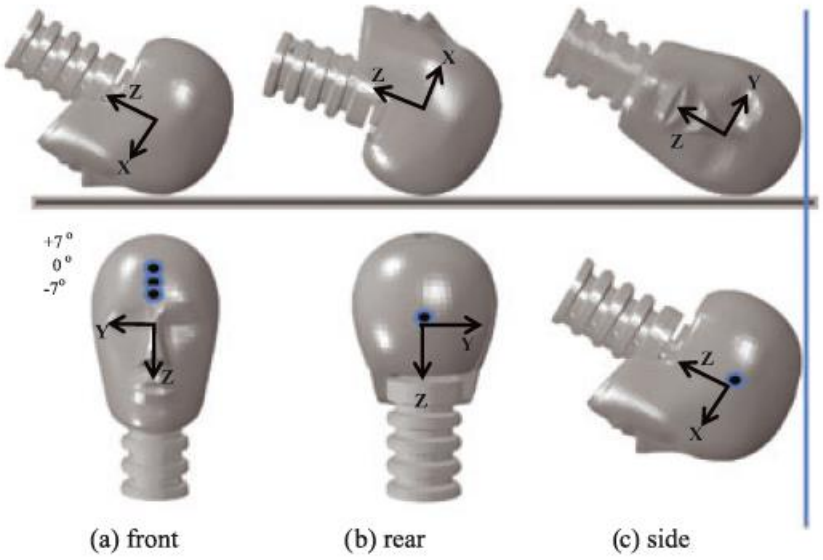

Figure 1.5 Impact Locations (Caccese et al., 2016)

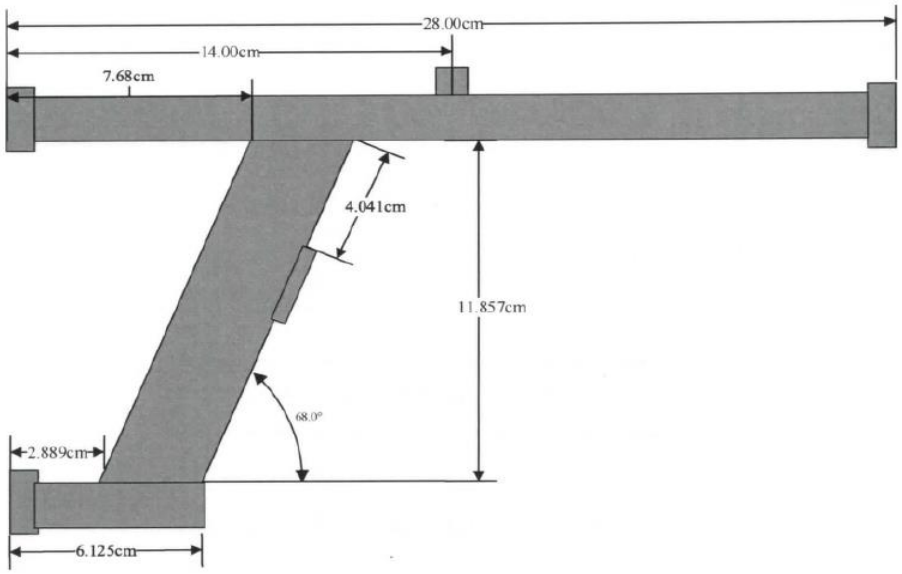

Figure 1.6 Fly Arm Dimensions (Seidi, 2015)

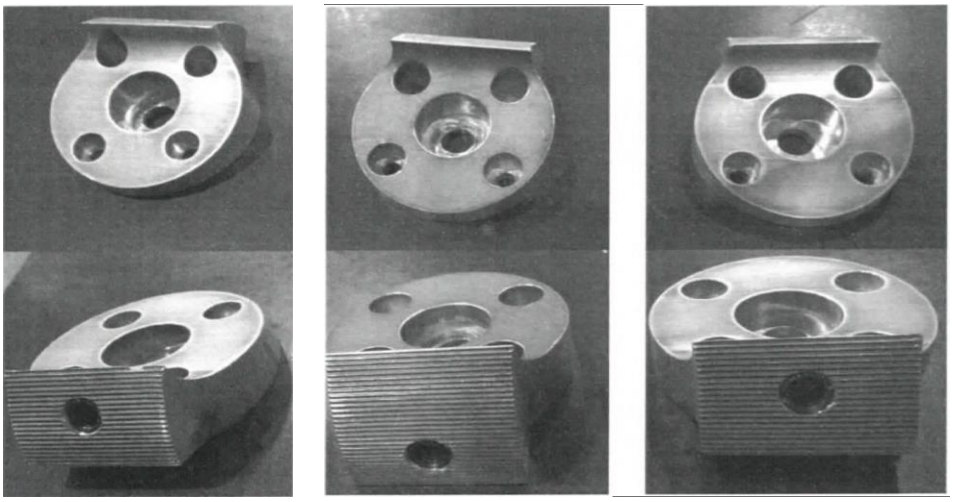

a) front b) rear c) side

Figure 1.7 Adaptors for Mounting Head and Neck Assembly to the Fly Arm

(Seidi, 2015)

The apparatus has three anvil types as shown in Figure 1.8 can be used depending on the study purpose, concrete, steel, and MEP. Concrete anvil is formed from a 102 mm × 204 mm × 406 mm long solid concrete masonry unit with a vinyl composition tile (VCT) bonded to the top using standard construction practices. Steel anvil is formed as flat 25mm thick steel. Modular Elastomeric Programmer (MEP) anvil consists of a 60 shore A durometer, 25-mm-thick neoprene rubber mounted over a 25-mm steel plate.

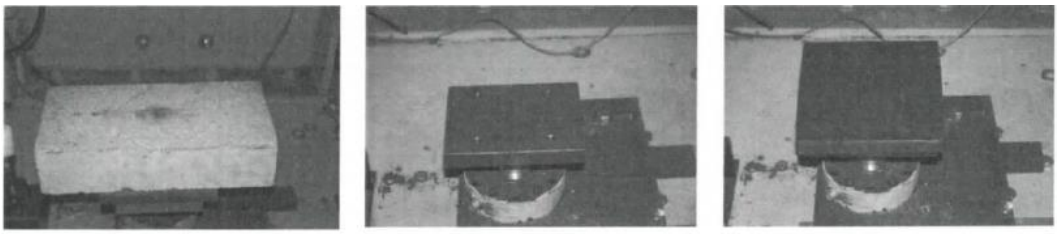

Figure 1.8 Anvils Used for Testing (Seidi, 2015)

The UMaine apparatus works with a specially written computer program which is used to control the drop test system. The experimental results data is recorded through a measurement computing simultaneous sampling 16-bit data acquisition system operating at 20 kHz. A velocity gate used to record impact velocity is comprised of a pair of photodiodes spaced at 38 mm aluminum apart. Impact signals from four triaxial accelerometers were arranged in an array so that angular acceleration is calculated directly from the filtered linear acceleration signals using a method as described by Padgaonkar in 1975 according to

(Padgaonkar, Krieger, & King, 1975). The accelerometers used were PCB model 356B21 triaxial accelerometer with a peak acceleration magnitude of 500 g. The HIC_{15}, RIC_{36}, and $PRHIC_{36}$ are computed within the data acquisition program using the magnitude of the center of gravity (CG) acceleration signal and angular acceleration-time histories, where appropriate. Impulse period of the primary impact is also estimated from the CG linear acceleration magnitude (Caccese et al., 2016).

A vertical drop on an anvil is one of the basic tests that are used by industry standards which are typically accomplished by using either a twin wire drop tower or monorail system as shown in Figure 1.9, according to the ASTM F1446 - 15b standard for protective headgear performance testing. By this method of tests, the produced motion is essentially linear and only the vertical linear acceleration component is typically measured during these tests so that the instrument specifications typically require translational acceleration to be recorded at the center of gravity CG without consideration of the angular acceleration. However, in (Caccese et al. 2016) they used a special procedure to estimate the angular acceleration. A velocity gate measures the impact velocity according to the required drop height.

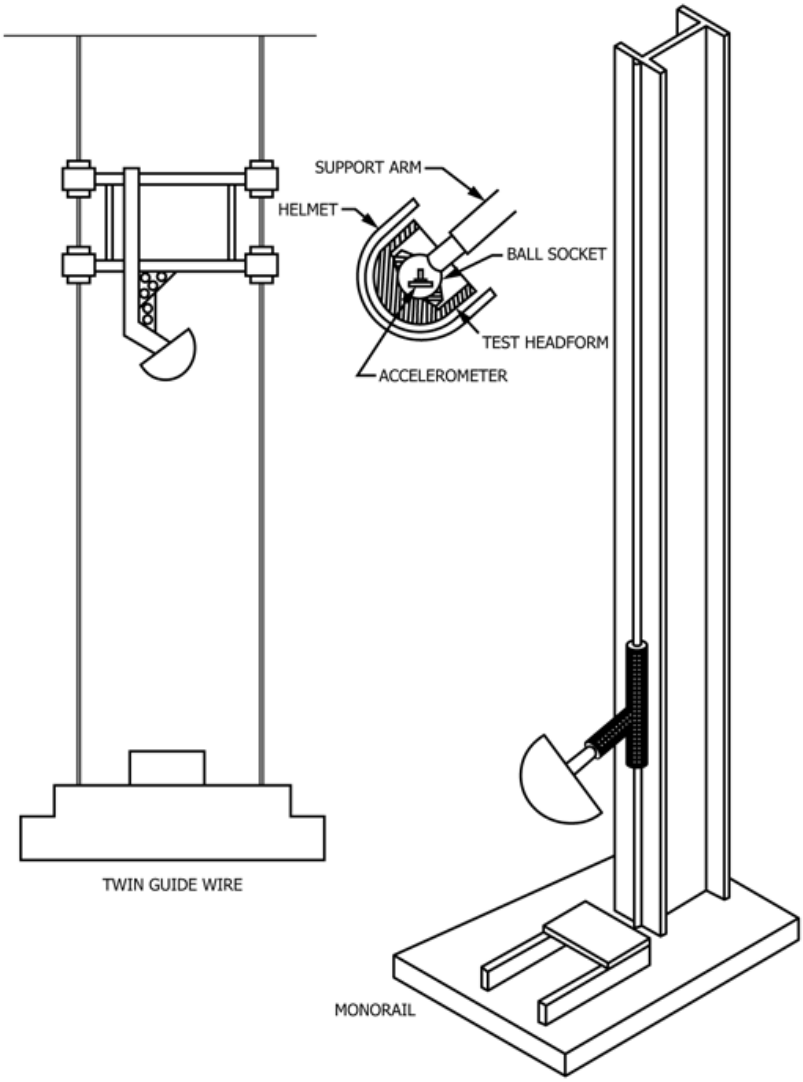

Figure 1.9 Typical Apparatus for Impact Test -Vertical Type - (ASTM, 2015b)

Headform size and the material that formed are basically being selected in the test depending on the headgear or a helmet that will be tested and the procedure of test. The headform is usually made of rigid materials such as magnesium, titanium, or in some cases; a relatively stiff urethane may be used. Numerous types

of the impact anvils that can be used in the tests depending on the type of tests where the selection of anvils to be used for testing any given kind of helmet is noted in the individual performance standards. ASTM F1446 standard described 6 anvil types which must be solid (that is, without internal cavities) and all are made from steel except the MEP anvil where these anvils are shown in the following Figures and shaped flat, hemispherical, cylindrical, Triangular Hazard, and curbstone. The ASTM F1446 standard also described the MEP anvil as 152 mm in diameter and 25 mm thick with a 60 ± 2 Shore A durometer hardness, and it is affixed to the top surface of a flat, 6.35-mm thick aluminum plate.

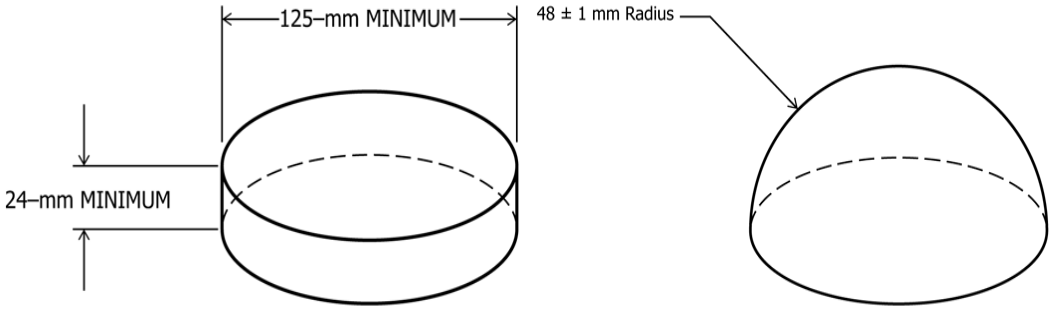

Figure 1.10 Flat Anvil(Left) and Hemispherical Anvil (Right) (ASTM, 2015b)

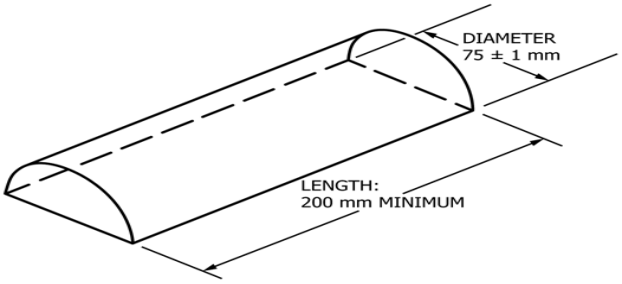

Figure 1.11 Cylindrical Anvil (ASTM, 2015b)

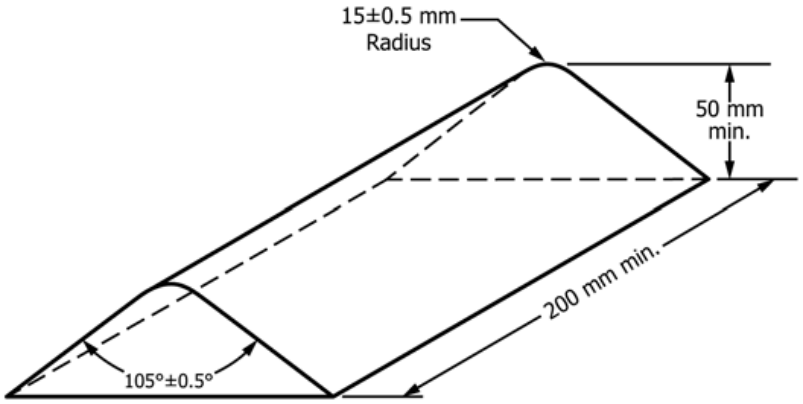

Figure 1.12 Curbstone Anvil (ASTM, 2015b)

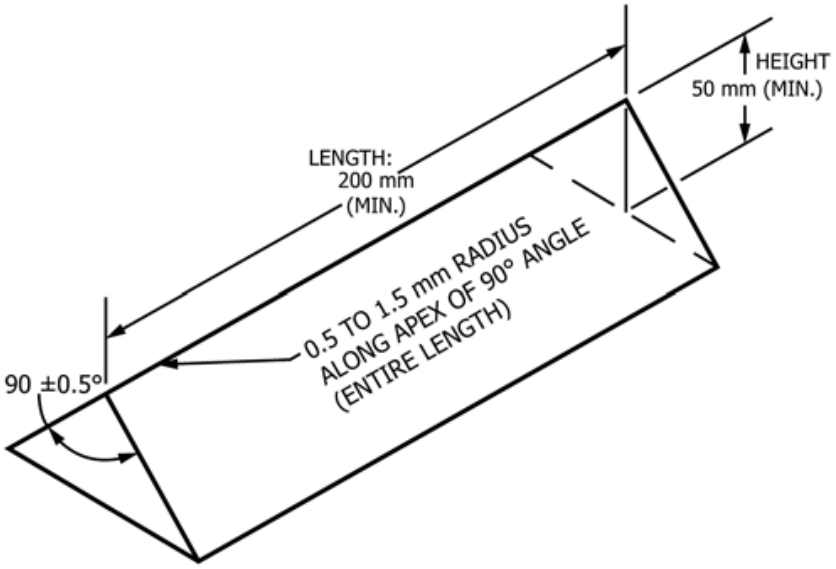

Figure 1.13 Triangular Hazard Anvil (ASTM, 2015b)

National Operating Committee on Standards for Athletic Equipment (NOCSAE) sets standards for a drop impact test method for several types of headgear tests, which is NOCSAE 001. Headform, as shown in Figure 1.14 used in

testing under this standard, is in three different sizes; namely $6\frac{5}{8}\,in$, $7\frac{1}{4}\,in$ and $7\frac{5}{8}\,in$ where each specific dimension is provided in the appropriate specification at this standard. Two type anvils can be used in the tests: ½ in Test MEP Pad with approximately dimensions ½ in (1.3 cm) thick by 6-inch (15.2 cm) and 1/ in Faceguard Test MEP Pad with approximately dimensions a 1/8 inch (3.2 mm) thick by 6-inch (15.2 cm) that must have a Shore "A" durometer >70.

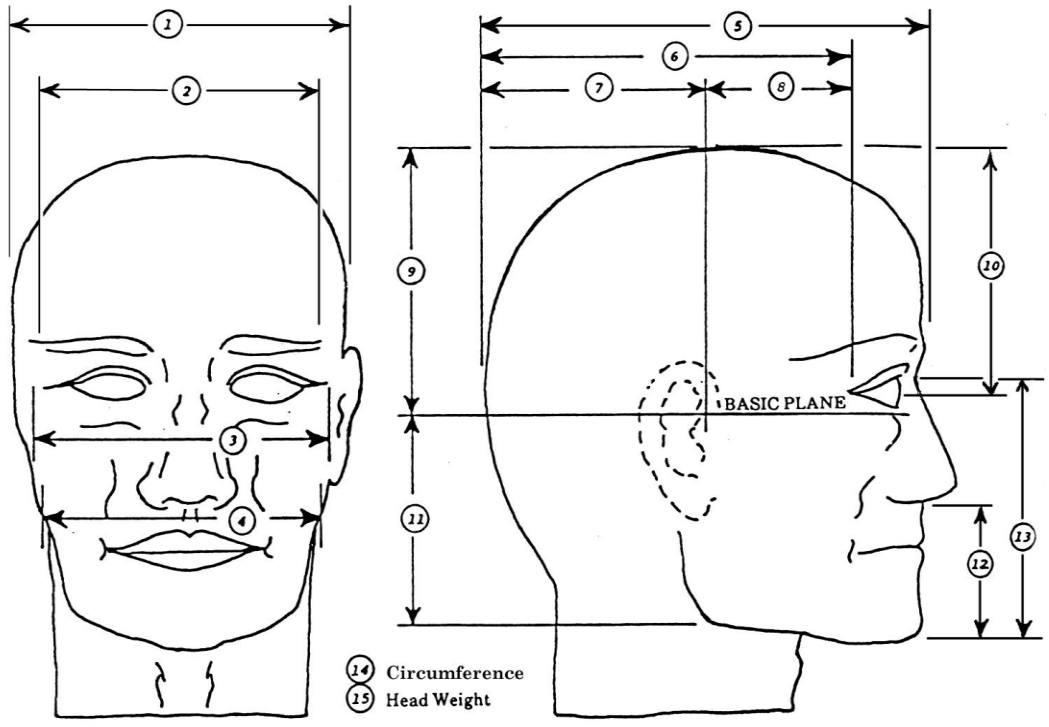

DIMENSIONING OF NOCSAE HEAD MODELS
(See Table 1)

Figure 1

Figure 1.14 Basic Headform (National Operating committee on Standards for Athletic Equipment, 2013)

According to the (Thom, D. R., Hurt Jr, H. H., Smith, T. A., & Ouellet, 1997), the Department of Transportation DOT, Federal Motor Vehicle Safety Standard 218 (FMVSS 218) sets standards for helmets tests that can be used by motorcycles drivers. in these standards, monorail test apparatus is used as shown in Figure 1.15 where the helmet is positioned on a test headform which is then dropped in a guided fall onto a fixed steel anvil whatever the anvil is flat or hemispherical. Headforms used to come in small, medium and large sizes where the specification for all three sizes can be found in DOT FMVSS 218. The comparison between the used headform DOT and the three sizes of ISO headforms is shown in Table 1.4. Figure 1.16 shows the medium size DOT headform compared to an ISO and ISO ECE head form.

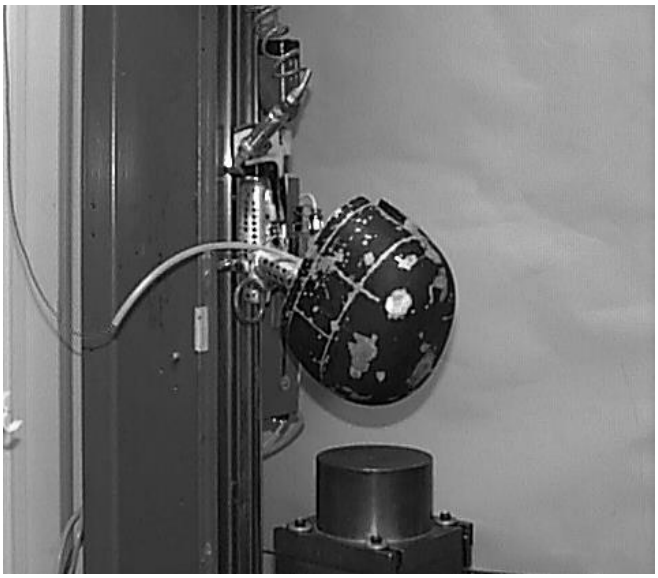

Figure 1.15 Monorail Test Apparatus with DOT Medium Headform and Flat Steel Anvil (Thom, D. R., Hurt Jr, H. H., Smith, T. A., & Ouellet, 1997)

Table 1.4 Test Headform Comparison (Thom, D. R., Hurt Jr, H. H., Smith, T. A., & Ouellet, 1997)

Headform	DOT Small	DOT Medium	DOT Large	ISO E	ISO J	ISO M
Circumference	49 cm	56 cm	60 cm	54 cm	57 cm	60 cm
Assembly Weight	3.5 kg	5.0 kg	6.1 kg	4.1 kg	4.7 kg	5.6 kg

Figure 1.16 Comparison of Headform Types (Thom, D. R., Hurt Jr, H. H., Smith, T. A., & Ouellet, 1997)

A linear impactor test method that shown in Figure 1.17 was developed to more closely emulate on-field impacts believed to be responsible for Mild Traumatic Brain Injury MTBI and it is believed that compliance with this test method will reduce the likelihood of MTBI (NOCSAE081, 2006). According to NOCSAE 081 standard, all testing and requirements of this standard specification must be in accordance with NOCSAE.001 where appropriate the method test must

be in accordance with NOCSAE 001. The test apparatus impactor should be with a mass of 13.3 kg ±3% and capable of delivering impacts at velocities from 6m/s to 12m/s. A headgear is positioned on a headform that is mounted onto a Hybrid or NOCSAE III head/neck assembly which is rigidly mounted to a linear bearing table to achieve a somewhat realistic position during the impact situation. The instantaneous resultant acceleration results are measured by a triaxial accelerometer or 9 accelerometer arrays where various injury indexes can be calculated.

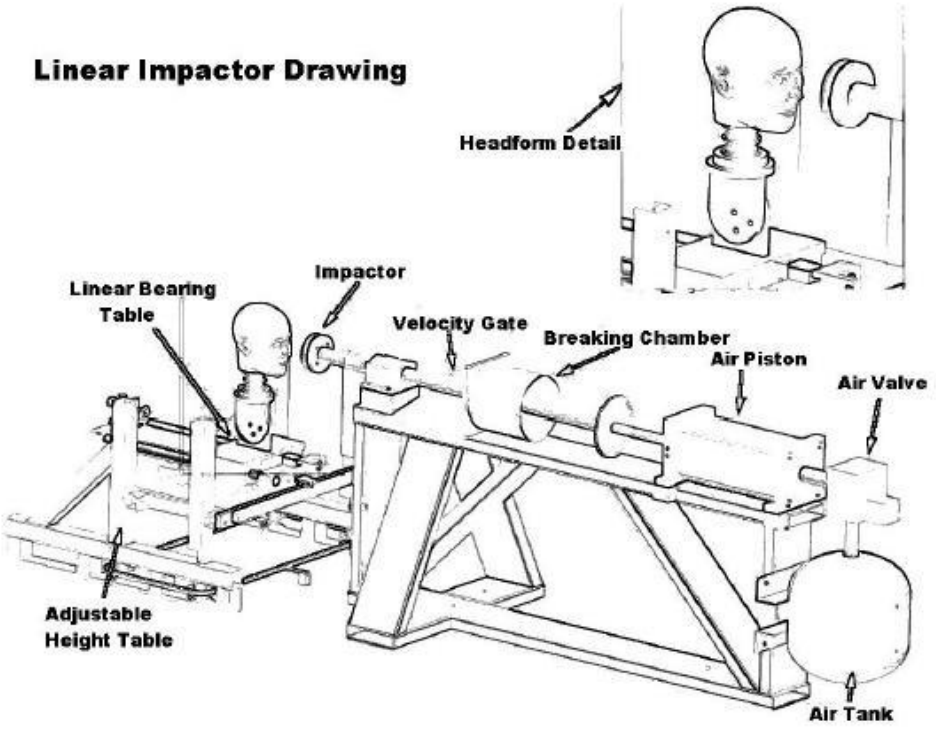

Figure 1.17 Linear Impactor (NOCSAE081, 2006)

The University of Maine linear impact test apparatus, as shown in Figure 1.18, was modeled after the NOCSAE version. The head/neck assembly model verified though this work is also applicable to the linear impactor setup and the Hybrid III head-neck assembly FEA model that we have quantified is applicable to both University of Maine test apparatus as shown in Figures 1.4 and 1.18.

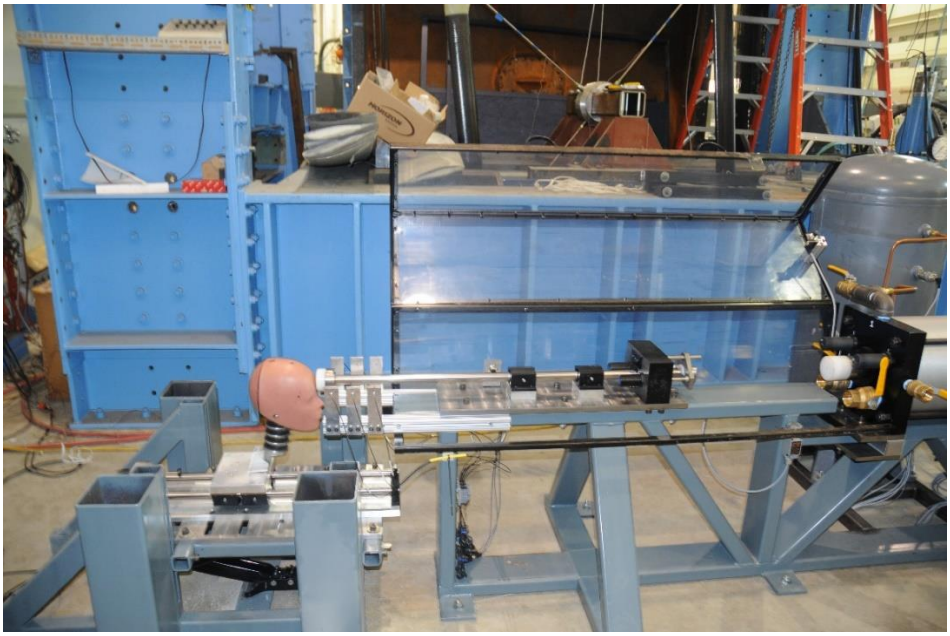

Figure 1.18 University of Mane Linear Impact Test Apparatus Photograph

Military helmet testing is described in (Brozoski et al., 2009), where they tested a critical component AH-64 Apache helicopter which is the Integrated Helmet and Display Sighting System (IHADSS) helmet. Blunt impact attenuation tests were performed on a guided, free fall drop tower as monorail drop tower as

shown in Figure 1.19 conforming to Federal Motor Vehicle Safety Standard number 218 (FMVSS 218) (Department of Transportation [DOT], 2006).

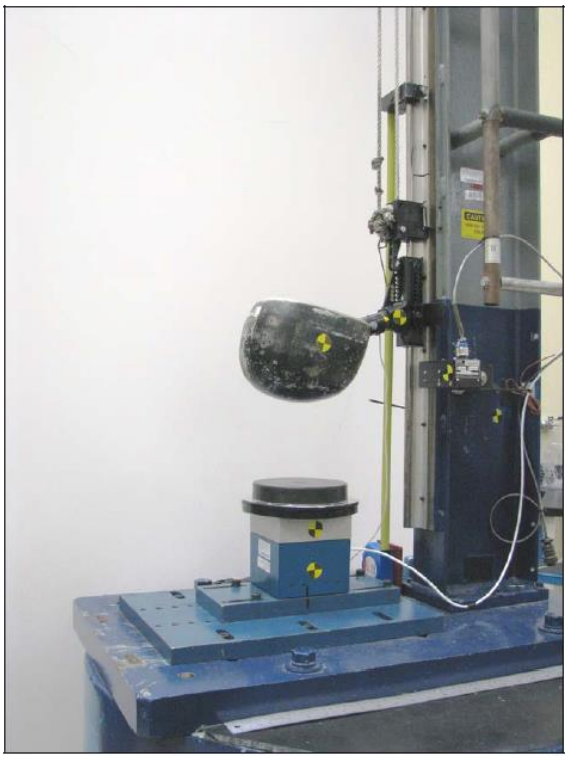

Figure 1.19 Guided, Free Fall Drop Tower (shown with the standard medium headform installed) (Brozoski et al., 2009)

Four magnesium headforms were available for use in these tests include the standard small (DOT size B), standard and modified medium (DOT size C), and modified large (DOT size D) headforms as shown in the Figure 1.20, and the test headform weights are provided in Table 1.5. The mass properties measurements, CM and mass moments of inertia (MOI), were made using a KSR330-60 mass

properties instrument (MPI) as shown in Figure 1.21 manufactured by Space Electronics, Inc. A flat steel anvil at the base of the drop tower is used in the test.

Table 1.5 Test Headform Drop Assembly Weight (Brozoski et al., 2009)

Headform size	Required weight (lbs)	Weight tolerance (lbs)***	Actual weight (lbs)
Small (size B)	10.1*	+0.2, -0.0	9.9
Medium (size C)	11.0**		11.2
Medium (size C) (modified)	11.0**		11.1
Large (size D) (modified)	13.4**		13.5

* Per FNS/PD 96-18 (DOD, 1996)
** FMVSS 218 (DOT, 2006)
*** Per ANSI Z90.1-1971 (American National Standards Institute [ANSI], 1971)

Figure 1.20 Drop Tower Headforms. Shown from left to right are the standard small (DOT size B), standard medium (DOT size C), modified large (DOT size D), and modified medium (DOT size C) headforms (Brozoski et al., 2009)

Figure 1.21 KSR330-60 Mass properties instrument (Brozoski et al., 2009)

1.3 Modeling of Hyperelastic Materials

The critical materials controlling the response of the drop testing apparatus are: the MEP anvil, head skin, neck rubber, rubber pad and the metal parts. In the finite element modeling the metal parts such as the fly arm, cablebeam, etc. were treated as an isotropic material with known modulus of elasticity and Passion's ratio, and they were modeled using a the common Hookean linear elastic material model. The rubberlike material was modeled using a hyperplastic modeling approach and significant studies were performed to assess how changing various properties influenced the model response.

Hyperelastic materials are the elastic materials that have high deformability, recoverability after deformation and nonlinearity in load-deformation behavior. For these materials, it is typical to use the strain energy density to describe the material response to load. Many attempts have been made to develop more general hyperelastic models which can include different aspects of materials behavior such as Saint Venant–Kirchhoff type, Neo-Hookean, and Mooney-Rivlin models which are the most widely used in commercial finite element packages (Darijani & Naghdabadi, 2010). Hyperelasticity also can be used to model or describe biological materials, like tissue (R. Jakel, 2010).

The strain energy density W of such a material can be expressed as the half value of the double dot product of stress tensor S and strain tensor E as shown in equation 1.13.

$$W = \frac{1}{2} S \cdot\cdot E \tag{1.13}$$

Where: W is the strain energy, S and E are stress and stain tensors respectively.

For a linear elastic material, the strain energy can be evaluated as the area under the stress-strain curve as shown in Figure 1.22a. Also, Figure 1.22b shows a typical stress strain curve for a hyperelastic material that is a nonlinear elastic response.

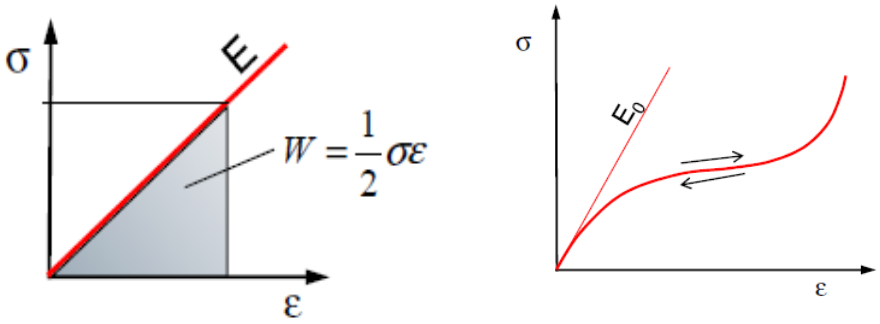

Figure 1.22 Linear Elastic Material Behavior in the Left and the Hyperelastic Material with the Elastic Linear Behaviors in the Right (R. Jakel, 2010)

As stated in (R. Jakel, 2010), usually the Elastomers (like rubber) are modeled as hyperelastic even if the elastomers typically have a viscous behavior. Elastomers basically have large strains (oftentimes > 100 %) at small loads with a low modulus of elasticity for example just 10 MPa. This means that the material is nearly incompressible, with the Poisson's ratio very close to 0.5. Also, their loading and unloading stress-strain curve is not the same as shown in Figure 1.23, depending on different influence factors (time, static or dynamic loading, frequency, etc.).

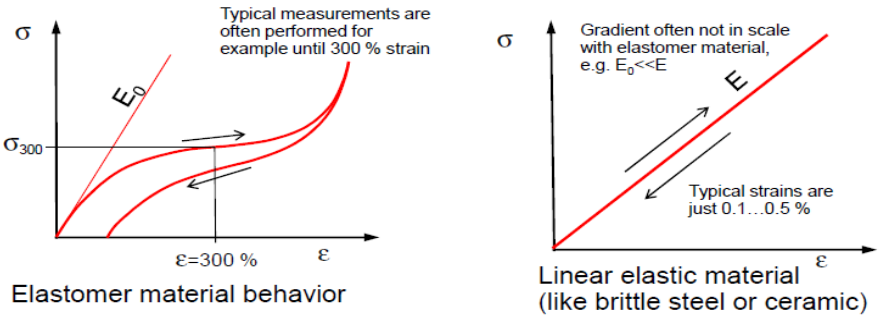

Figure 1.23 Elastomer (like rubber) and linear elastic materials behaviors (R. Jakel, 2010)

The description of the strain energy density W as shown in equation 1.14 is more complex compared to linear elastic material equation 1.13. In general, the strain energy density function in hyperelastic materials is a function of the stretch invariants $W = f(I_1, I_2, I_3)$ or principal stretch ratios $W = f(\lambda_1, \lambda_2, \lambda_3)$. For typical hyperelastic material models, often phenomenological models are used, where the strain energy function has the form: (R. Jakel, 2010).

$$W = \sum_{i+j=1}^{N} C_{ij}(I_1 - 3)^i (I_2 - 3)^j + \sum_{k=1}^{N} \frac{1}{D_k}(J-1)^{2k} \qquad (1.14)$$

Where C_{ij} and D_k are material constants which are determined by tests, I_1 and I_2 are the stretch invariants and J is total volumetric ratio; equally one if incompressible. Stretch invariants(I), the stretch ratio (λ) and J are related to each other as follows:

$$I_1 = \lambda_1^2 + \lambda_2^2 + \lambda_3^2 \tag{1.15}$$

$$I_2 = \lambda_1^2\lambda_2^2 + \lambda_2^2\lambda_3^2 + \lambda_1^2\lambda_3^2 \tag{1.16}$$

$$I_3 = \lambda_1^2\lambda_2^2\lambda_3^2 = 1 + \left(\frac{\Delta V}{V}\right)^2 = J^2 \tag{1.17}$$

Where the stretch ratio is another fundamental quantity to describe material deformation. It is defined as the current length divided by the original length as shown in the following equation:

$$\lambda = \frac{l_1}{l_0} = \frac{l_1 - l_0 + l_0}{l_0} = \varepsilon + 1 \tag{1.18}$$

where ε is the strain

ABAQUS supports modeling of hyperelastic materials based on various theorems. Options available in ABAQUS are shown in Figure 1.24. Mooney-Rivlin and Neo-Hookean are two of the commonly used approaches, which are described in equations 1.19 and 1.20 respectively.

$$W = C_{10}(I_1 - 3) + C_{01}(I_2 - 3) + \frac{1}{D_1}(\mathrm{J}_e - 1)^2 \tag{1.19}$$

$$W = C_{10}(I_1 - 3) + \frac{1}{D_1}(\mathrm{J}_e - 1)^2 \tag{1.20}$$

Where, J_e is the elastic volume ratio given by equation 1.21:

$$J_e = \frac{J}{J_{th}} = \frac{J}{(1+\varepsilon_{th})^3} \tag{1.21}$$

J = the total volumetric ratio, and J_{th} = thermal volume ratio

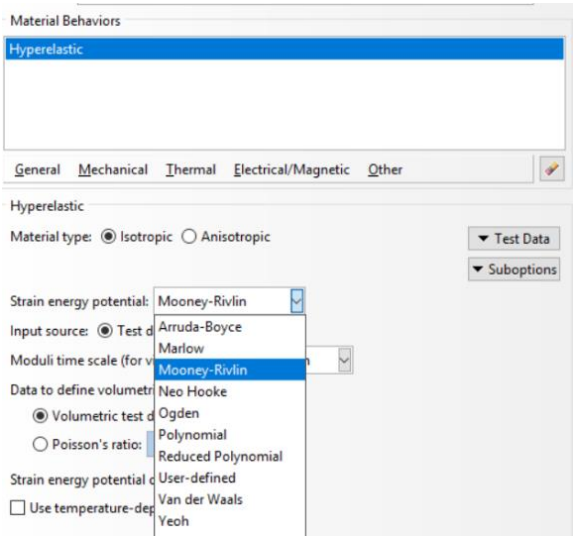

Figure 1.24 Hyperelastic Material Modeling Option at ABAQUS- Version 2017

Estimatation of the coefficients(C_{10}, C_{01} and D_1) of hyperelastic materials modeled according to Mooney-Rivlin theory these coefficients is typically done from from experiments. Estimation can also emply empirical formala, for example by prescribing the durometer of the rubberlike material (Shore A hardness), the initial modulus of elasticity of the material can be estimated from the following equation:

$$E_0 = e^{\frac{H-35.22735}{18.75847}} \tag{1.22}$$

Where equation 1.22 is expressed from the experiments according to (R. Jakel, 2010), E_0: Initial Modulus of elasticity in MPa and H: Shore A hardness in MPa

Then, the Mooney Rivlin constants (C_{10}, C_{01}, and D_1) can be evaluated by using the following equations: (R. Jakel, 2010).

$$G_0 = \frac{E_0}{2*(1+\nu)} \quad (1.23), \qquad K_0 = \frac{E_0}{3*(1-2\nu)} \quad (1.24)$$

$$\mu = G_0 \quad (1.25)$$

and $\mu = 2 * (C_{10} + C_{01})$ (1.26) (R. Jakel, 2010)

and $\alpha = \frac{C_{01}}{C_{10}}$ (1.27)

By plugging equation (1.26) into equation (1.25) and using equation (1.27), (1.23) and (1.24), we can find:

$$C_{10} = \frac{G_0}{2*(1+\alpha)} \quad (1.28)$$

$$C_{01} = \alpha * C_{10} \quad (1.29)$$

and from (R. Jakel, 2010) $D_1 = \frac{2}{K_0}$ (1.30)

Where, C_{10} and C_{01} are the material coefficients in MPa; D_1 is in Pa^{-1}; α is the relation between C_{10} and C_{01}; G_0 is the initial shear modulus in Pa; and Poisson's ratio ν equal to 0.4999 in this mode.

(Feng & Hallquist, 2017) stated two study cases for the rubber behaviors based on the loading type, uniaxial and biaxial, with set of various values of α as shown in Figures 1.25 and 1.26. They concluded that, the uniaxial tests cannot be used to determine α, while the biaxial tests have to be performed accordingly to the change in curve based on α change.

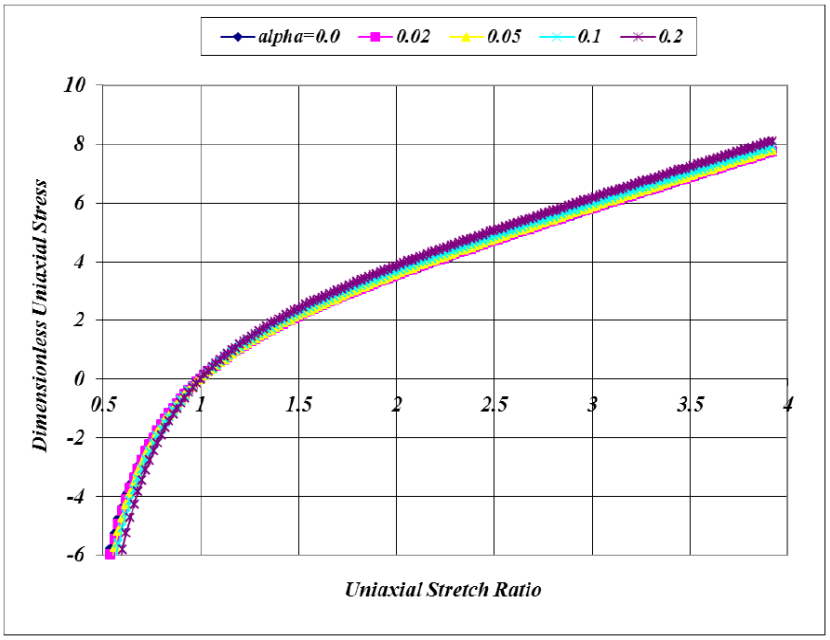

Figure 1.25 Uniaxial Stress- Strain Curves (Feng & Hallquist, 2017)

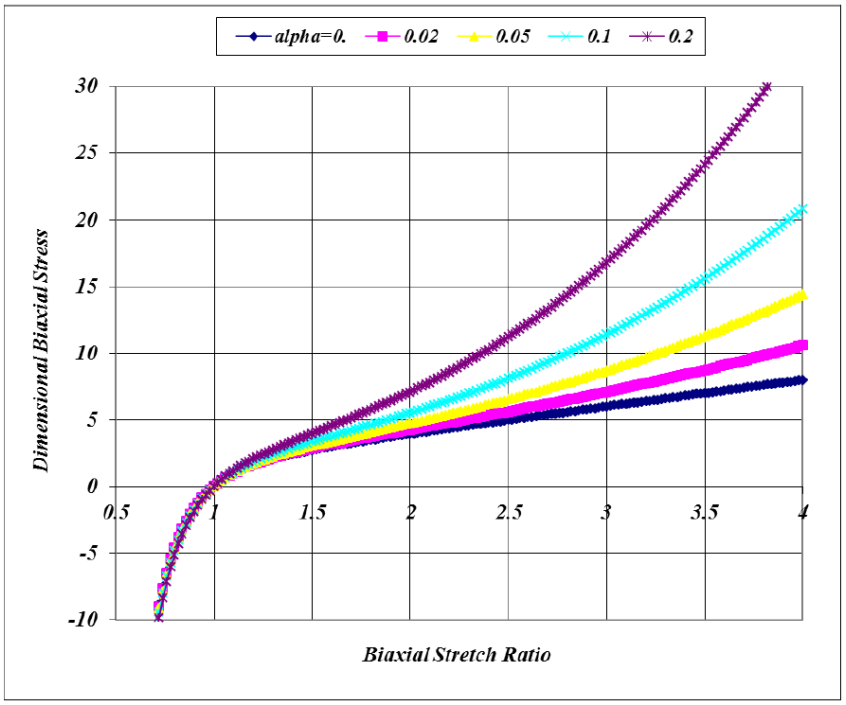

Figure 1.26 Homogenous Biaxial Stress-Strain Curves (Feng & Hallquist, 2017)

CHAPTER 2

MODULAR ELASTOMER PROGRAMMER MEP RUBBER PAD STUDY

The impact testing normally is used to study the response of materials for resisting impact forces. Typical measure is the acceleration of the impactor and the deformation during the impact event. In several cases, standard drop testing of helmets uses an anvil surface that is called a Modular Elastomer Programmer or MEP. The MEP is a critical part of the head/neck assembly drop testing apparatus. The MEP is a rubber pad of a specified durometer (60 Shore A typical) and thickness. In this chapter, the response of the MEP pad is isolated from the test apparatus and its dynamic response investigated to determine proper material properties for its modeling. Furthermore, the material coefficients (Invariants) of a Mooney-Rivlin model of the specific MEP rubber used in the soccer headgear testing was investigated theoretically and compared to experimental results.

2.1 Experimental Investigation

The experimental data of the MEP Rubber Pad impact test are used as results baseline to evaluate the coefficients of the MEP hyperelastic material. The experimental results shown in Section 2.1.3 are described by a curve of the peak translational acceleration in g versus dropped height in meters. The range of the drop height used is from 0.05m to 0.9m. In addition, the peak acceleration obtained in the testing should not exceed 300 g to avoid equipment failures.

2.1.1 Impact Testing Apparatus

The impact testing apparatus consists of four main parts: The tower, the impactor, sensors, and system data acquisition and control. All these parts are described with more details in Chapter 2 of AlQuaraishi (Alquraishi, 2017) . The essential differences between this description and the current test setup will be explained including the impactor type and the sensors used. Figure 2.1 shows a photograph of the University of Maine drop test tower. The impactor is made from aluminum with a modulus of elasticity 70 GPa, Poisson's ratio 0.33, and density 2700 kg/m^3. In the MEP rubber pad impact testing, the spherical tip shaped impactor with a 127 mm radius is used. Figure 2.2 shows the impactor that used in the impact testing in contact with the center of the MEP rubber pad sample.

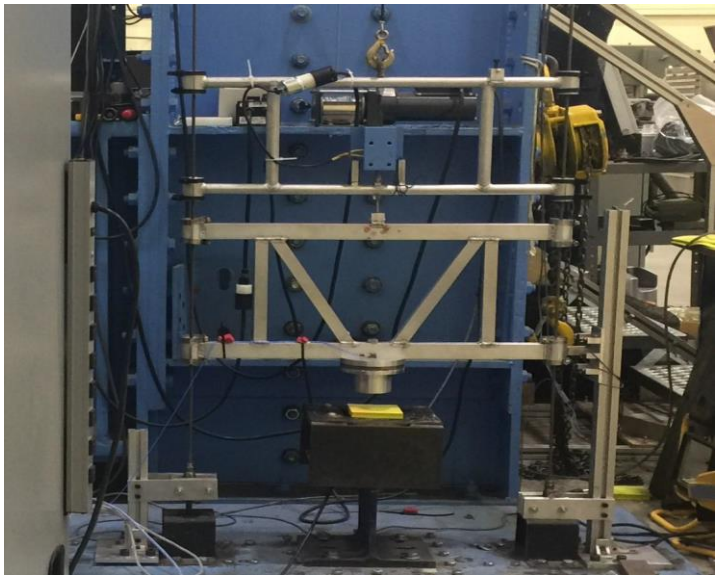

Figure 2.1 Photograph of the University of Maine Impact Testing Assembly(Alquraishi, 2017)

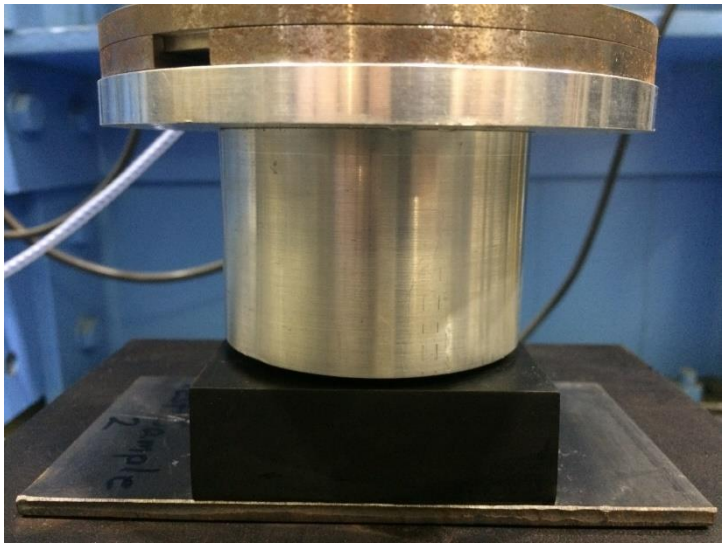

Figure 2.2 The Spherical Impactor Is Centered in the Center of the Sample

Four sensors are used in the apparatus for the linear impact testing:

A. The displacement laser that is located on the anvil. It measures the impact displacements by evaluating the reflected light that comes back from the fly arm surface. Figure 2.3 shows two views of the sensor location.

a) Top View b) Side View c) Zoomed the Side View

Figure 2.3 Two Views of the Displacement Sensors

B. The accelerometer that is located on the fly arm part as shown in Figure 2.4.a. It is used to measure the linear acceleration of the fly arm during the drop test.

C. The velocity gate photo sensor that consists of two photo diodes which are attached to the short column part with 39.37 mm space between them. These sensors read the time of the fly arm passing through the space. Eventually, the velocity gate photo sensor algorithm in the data acquisition/control program converts this time to the impact velocity. Figures 2.4.b and 2.4.c show two photographs of the sensors.

D. The fly arm position measuring string potentiometer that located in the top of the fly arm holder part as shown in Figure 2.5.

a) Accelerometer b) Velocity Sensors Gate c) Sensors Reading

Figure 2.4 The Accelerometer and the Velocity Sensors Photograph

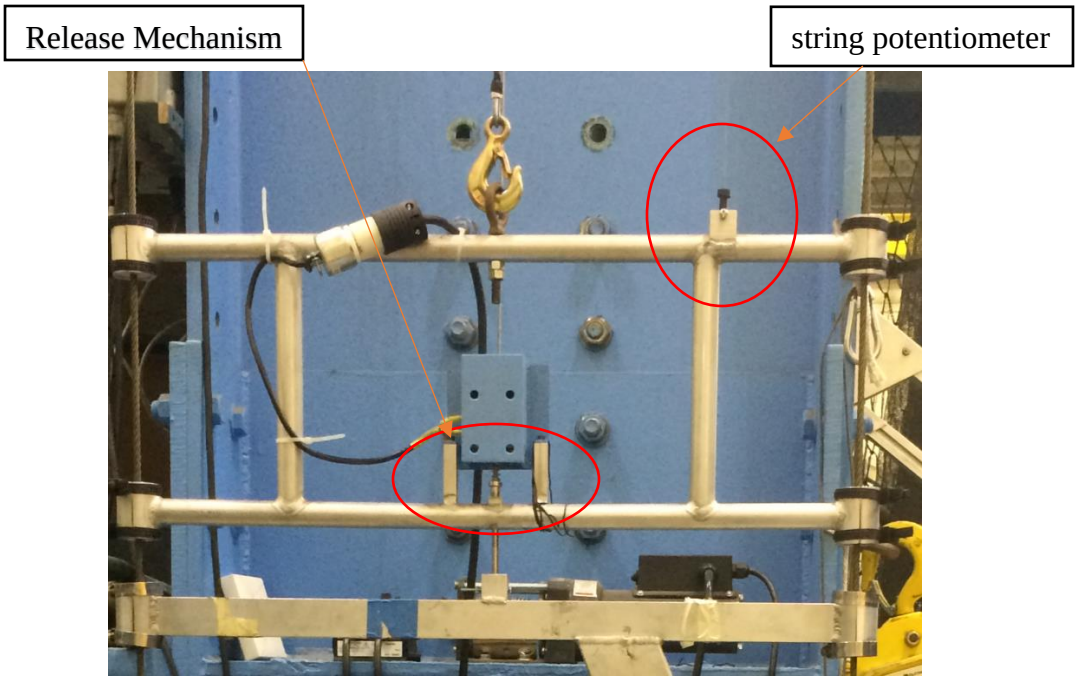

Figure 2.5 The Fly Arm Release Mechanism and the string potentiometer

2.1.2 Impact Testing Controls

The dimensions of the MEP rubber pad sample used for the impact test are: 7.62 cm (3 inches) width, 7.62 cm (3 inches) length, and 2.54 cm (1 inch) thickness. It has a 60 ± 5 Shore A durometer, 435psi (3 MPa) tensile strength(μ) and 300 % ultimate elongation in tension. The MEP rubber pad sample as seen in Figure 2.6 is bonded to a plate with dimensions of 15.24 cm (6 inches) length, 7.62 cm (3 inches) width and 7.4 mm thickness. The plate is made from steel material with a nominal modulus of elasticity 200 GPa, Poisson's ratio 0.3, and mass density 7850 kg/m^3. Locktite 409 was the adhesive used to adhere them together as shown in Figure 2.6.

The following procedure was performed to obtain the MEP impact test results:

1. Place the assembly of the MEP rubber pad sample and the steel plate which shown in Figure 2.6 on the anvil as close as to the laser light slot as shown in Figure 2.7. Additionally, insure that the top surface center of the MEP sample location is in the center of the spherical impactor surface as shown in Figure 2.2.

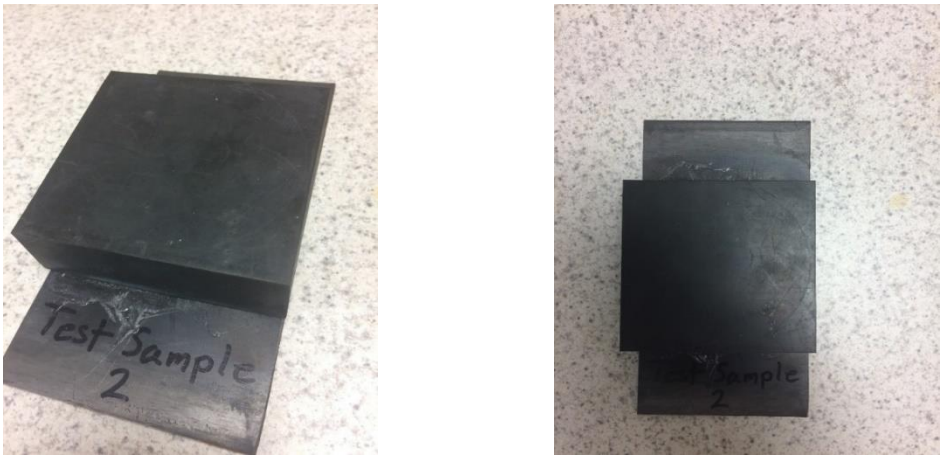

Figure 2.6 Two Views of the MEP Rubber Pad Sample Tied by an Adhesive with a Steel Plate

2. Move the fly arm toward the MEP Rubber Pad sample until the impactor touches the top surface of the sample. Insure visually that the impactor only touches the sample without displacing it as shown in Figure 2.8. The impactor position now is in the zero location for the apparatus.

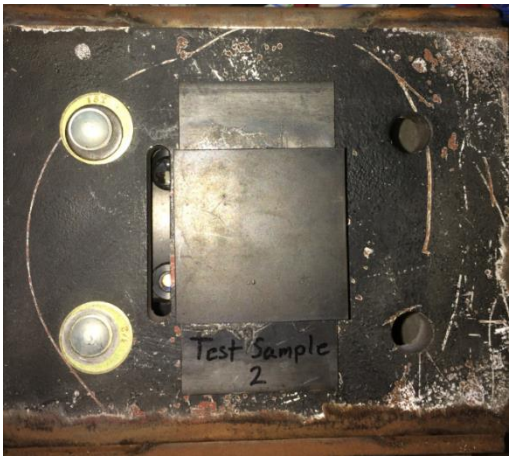

Figure 2.7 MEP Rubber Pad Sample Location at the Anvil

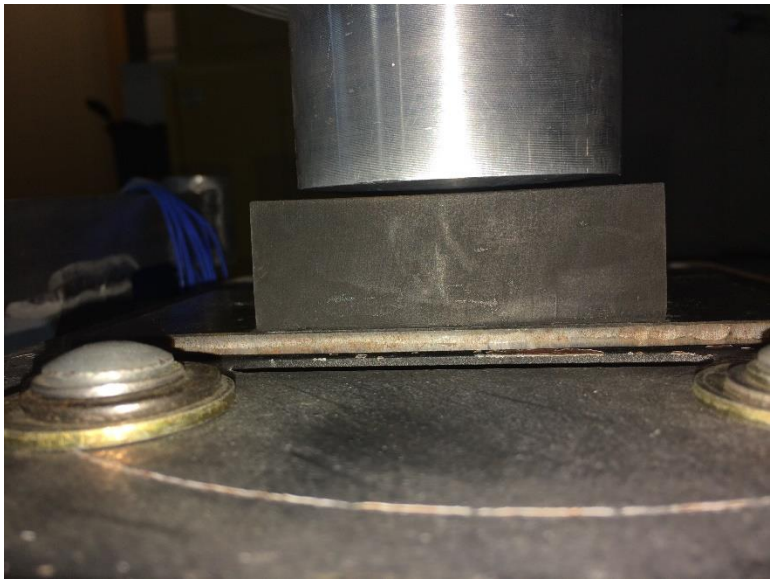

Figure 2.8 Impactor Touches the Sample

3. Move the velocity photo gate by sliding it down or up until the bottom red light turns off by the drop arm tab. Then, secure the gate to make sure it will not move during the impact. Figure 2.9 shows the velocity gate resetting.

4. In the controller part of the data acquisition program, reset the apparatus code by inserting and applying the suitable impact configuration file used for this type of impact testing. Check that the correct calibration factors are loaded. The file activation code should be reset before starting the next impact test step. The drop height should be reset to zero position to ensure that the test will start from zero drop height. Figure 2.10 shows the reset steps of the apparatus.

Figure 2.9 Resetting the Velocity Photo Gate

5. Insert the required drop height in to the edit box and move the fly arm accordingly to the desired height, and then release the fly arm by clicking on the drop button. Finally, use the write data button to obtain the test results.

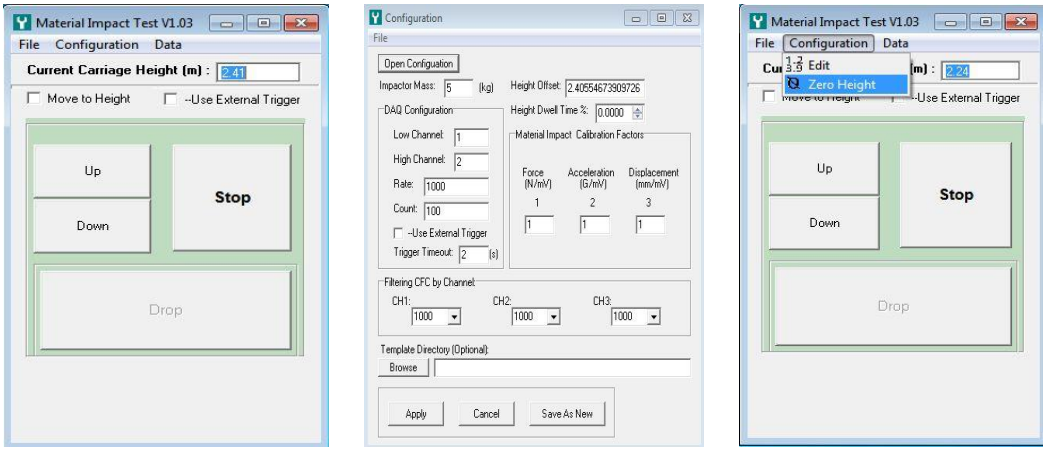

Figure 2.10 Three Steps to Reset the Apparatus Code and Zero the Fly Arm Position

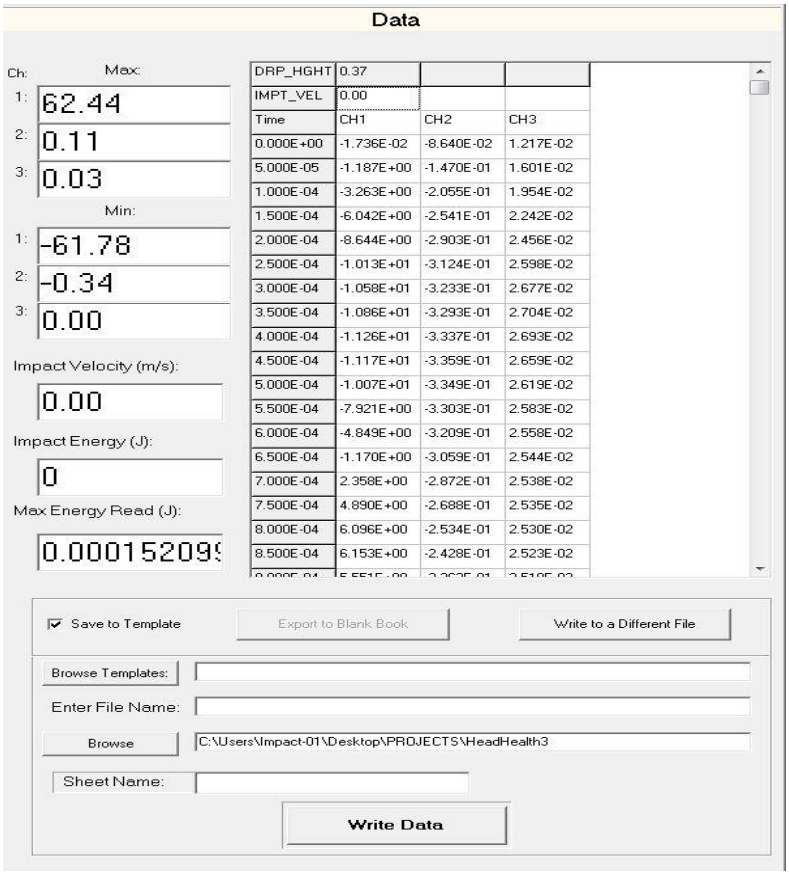

Figure 2.11 Last Step of Impact Testing Procedure

2.1.3 Impact Testing Results

The impact test results of MEP rubber pad sample are summarized in Table 2.1, where each test is repeated three times and the presented results are the average.

Table 2.1 Experimental Tests Results for MEP Rubber Pad

Test No	Drop Height, m	Impact Velocity, m/s	Peak Acceleration, g	Impact Energy, J	Peak Force, KN
1	0.05	0.9	42.33	2.01	2.08
2	0.1	1.29	64.69	4.19	3.17
3	0.15	1.58	83.78	6.28	4.11
4	0.2	1.83	99.95	8.39	4.9
5	0.25	2.04	114.4	10.45	5.61
6	0.3	2.24	126.87	12.51	6.22
7	0.35	2.44	138.13	14.9	6.78
8	0.4	2.59	148.2	16.77	7.27
9	0.45	2.74	158.63	18.71	7.78
10	0.5	2.9	168.63	21.07	8.27
11	0.55	3.03	177.73	23.01	8.72
12	0.6	3.16	185.97	24.98	9.12
13	0.65	3.29	194.57	27.1	9.54
14	0.7	3.41	200.87	29.02	9.61
15	0.75	3.54	209.77	31.25	9.9
16	0.8	3.64	215.53	33.07	10.07
17	0.85	3.73	224.07	34.76	10.33
18	0.9	3.87	232	37.47	10.6

Figure 2.12, Figure 2.13, Figure 2.14, Figure 2.15 and Figure 2.16 show the peak acceleration versus drop height, the drop height peak force curve, the impact energy versus drop height, acceleration versus time for various drop heights, force versus time for various drop heights respectively.

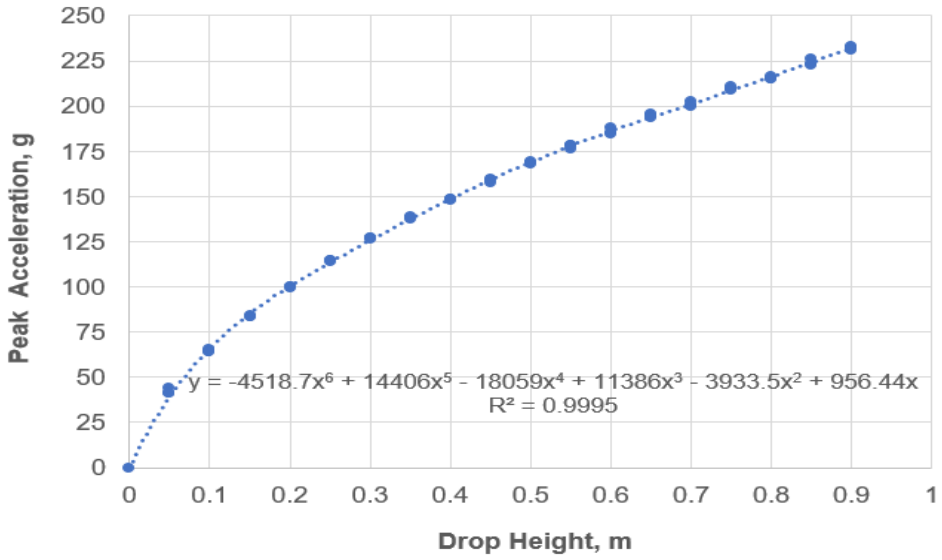

Figure 2.12 Peak Acceleration Versus Drop Height for the MEP Rubber Pad Tests

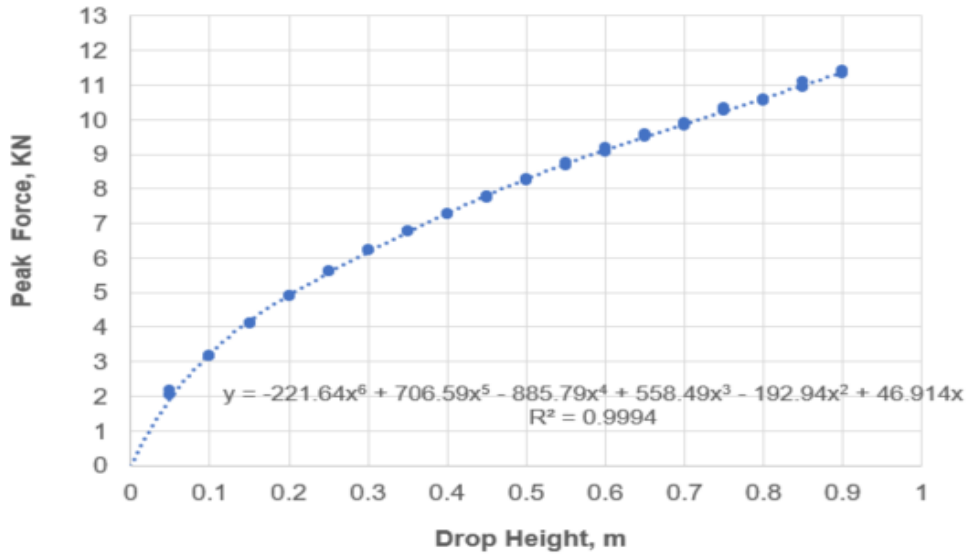

Figure 2.13 Peak Force Versus Drop height for MEP Rubber Pad Tests

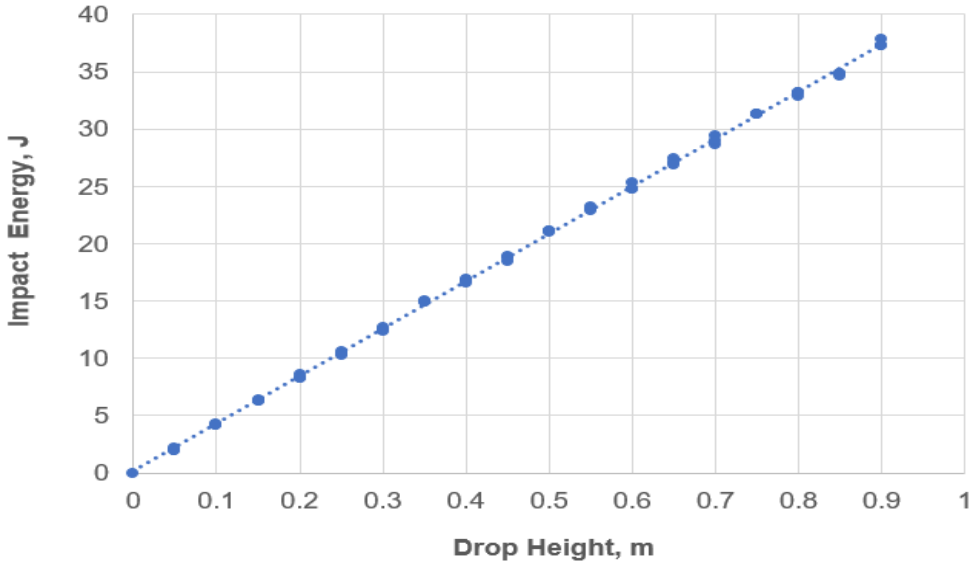

Figure 2.14 Impact Energy Versus Drop Height for MEP Rubber Pad Tests

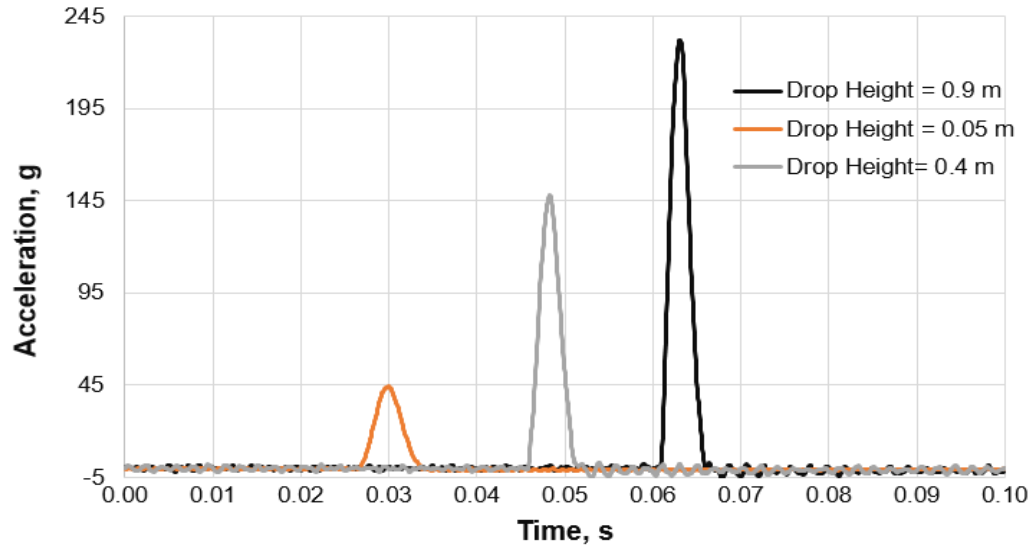

Figure 2.15 Acceleration Time Curve for MEP Rubber Pad Various Drop Heights Tests

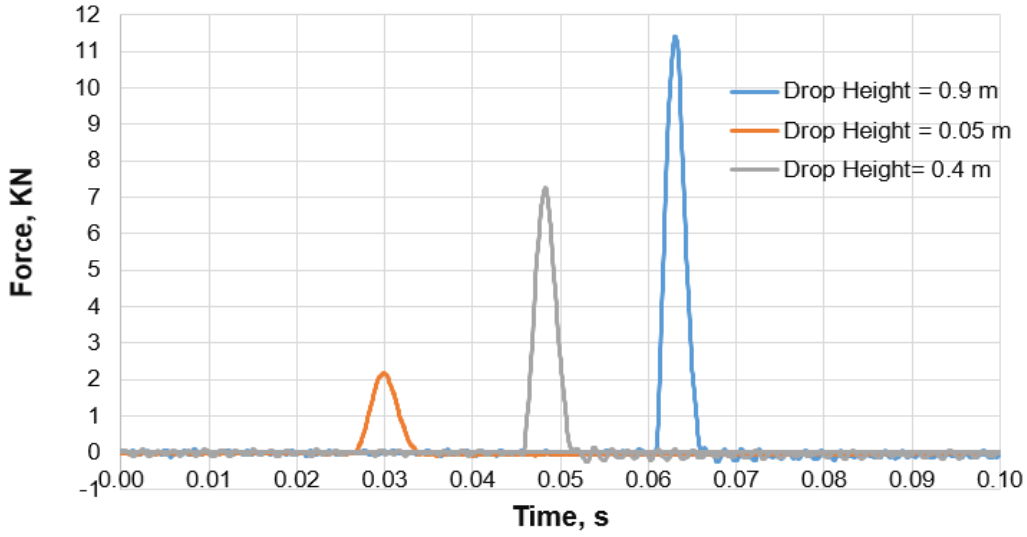

Figure 2.16 Force Time Curve for MEP Rubber Pad Various Drop Height Tests

2.2 Finite Element Analysis Impact Modeling

The finite element analysis (FEA) impact model is designed to evaluate the correct coefficients of the MEP Rubber pad material. The model results are compared to the experimental data that previously explained in Section 2.1.3. In addition, Section 2.4 shows additional details about the comparison between FEA model results and experimental data.

2.2.1 Description of FEA Impact Model

The FEA impact model consists of three parts: impactor, base, and MEP rubber pad sample. The FEA model is shown in Figure 2.17. The model is designed as a symmetric half of the experimental apparatus with ignoring some parts that do not highly affect the required results. The model design is used to reduce the analysis time.

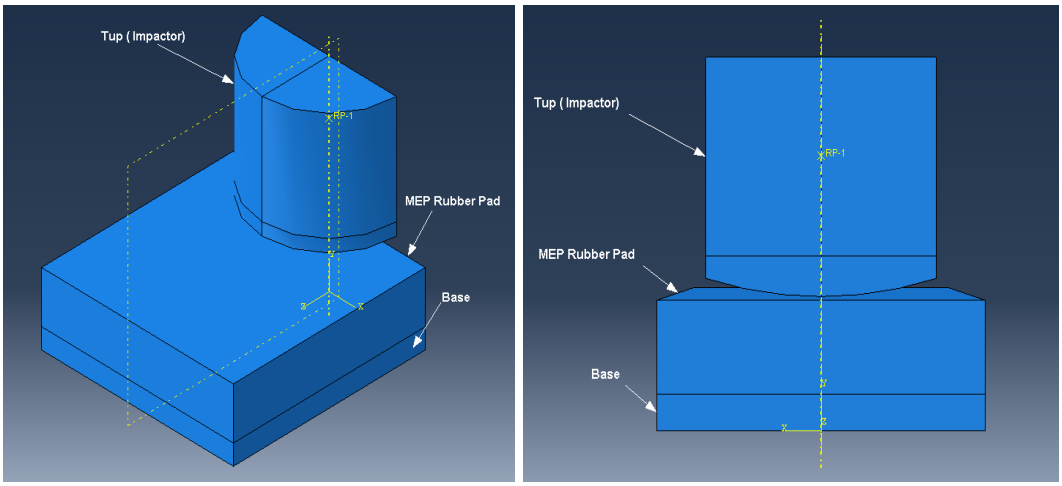

Figure 2.17 Two Views for the FEA Model of the MEP Rubber Pad Study

2.2.1.1 Impactor

There are three experimental impactors available for the impact testing study. In MEP rubber pad study model we have used an impactor that has spherical tip shape with a 127mm radius as explained in Figure 2.18. The total mass of the impactor should be equal to the experimental impactor mass as 5kg, and according to using a symmetric model, the total impactor mass shall be 2.5 kg. To set up that aspect in the model, we have computed the density of the impactor that satisfies the total mass of the impactor 2.5kg so that the density ρ= 40000 kg/m^3 is used in the model.

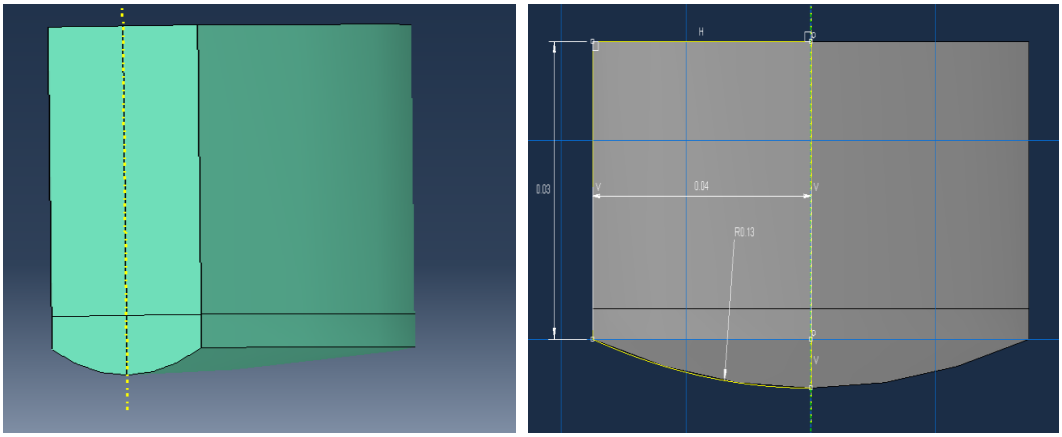

Figure 2.18 Radial Impactor Shape and its Dimensions

2.2.1.2 Base

The base part is made from structural steel that has a high modulus of elasticity as shown in Table 2.2. The base dimensions are 0.1 m, 0.1 m and 0.01 m

as the length, the width and the thickness respectively. Figure 2.19 shows more details.

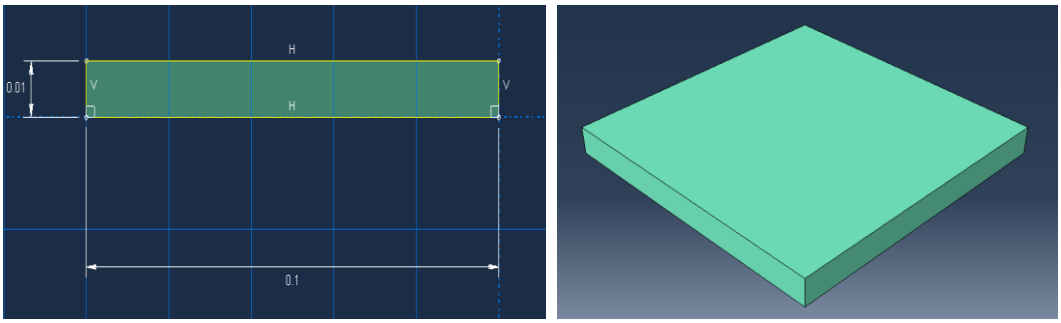

Figure 2.19 Base Part Details

2.2.1.3 MEP Rubber Pad

The MEP rubber pad sample is a hyperelastic material that has material properties based on the Mooney-Rivlin model. Figure 2.20 shows the MEP and more details are given on the material model in Section 2.2.3. The dimensions of the MEP Rubber Pad sample that used in the model are: 0.1 m length, 0.1 m width, and 0.0254 m (1 in) thick.

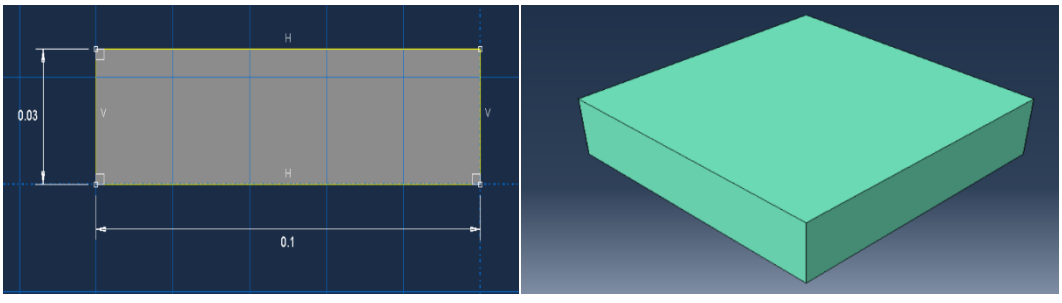

Figure 2.20 MEP Rubber Pad Details

2.2.2 Model Materials

The following Table shows the materials that are used in the model:

Table 2.2 Description of the Model Materials

Part Name	Material Name	Material Type	Details
Impactor	Aluminum	Isotropic Elastic	E = 70GPa, ν = 0.33, Beta damping is 1E-012
Base	Steel	Isotropic Elastic	E = 200GPa, ν = 0.3, Beta damping is 1E-012, ρ=7850kg/m^3
MEP Rubber Pad	MEP Rubber	Isotropic Hyperelastic	ρ = 1100 kg/m^3, with various invariants as studied in Section 2.2.3

2.2.3 Calculations of MEP Rubber Pad Material Invariants

The invariants of MEP Rubber material is evaluated accordingly to the Mooney Rivlin theory as shown in the following calculations: First, by using the durometer of the material (Shore A hardness, MPa), the modulus of elasticity of the MEP Rubber material can be estimated from the following equation:

$$E = e^{\frac{H-35.22735}{18.75847}} \quad \text{(R. Jakel, 2010)} \quad (2.1)$$

Where,

E: Modulus of elasticity, MPa

H: Shore A hardness, MPa

Then, the Mooney Rivlin constants (C_{10}, C_{01}, and D_1) can be evaluated by using the following equations:

$$G = \frac{E}{2*(1+\nu)} \quad (2.2), \qquad K = \frac{E}{3*(1-2\nu)} \quad (2.3)$$

$$\mu = G \quad (2.4)$$

and $$\mu = 2 * (C_{10} + C_{01}) \quad \text{(R. Jakel, 2010)} \quad (2.5)$$

and $$\alpha = \frac{C_{01}}{C_{10}} \quad (2.6)$$

By plugging equation (1.6) into equation (1.5) and using equation (1.4), we can find

$$C_{10} = \frac{G}{2*(1+\alpha)} \quad (2.7)$$

$$C_{01} = \alpha * C_{10} \quad (2.8)$$

and $$D_1 = \frac{2}{K} \quad \text{(R. Jakel, 2010)} \quad (2.9)$$

Where,

C_{10} and C_{01} are the material coefficients in MPa,

α is a relation between C_{10} and C_{01} as stated in Section 1.3 in Chapter1

D_1 is in Pa^{-1}

2.2.4 Model Mesh and Interaction Properties

Table 2.3 shows the mesh properties for each part in the model. The interaction properties that are used in the model are summarized here:

1. The contact properties are: Tangential Behavior by using the Coefficient of Friction COF as 0.3. and the Normal Behavior by using "Hard Contact".
2. General Contact (Explicit) for the whole model with contact property as shown above.
3. Surface-to-surface contact (Explicit) between the spherical surface of the impactor and the top surface of the MEP Rubber Pad with using the contact property as shown in 1.
4. The impactor is set up as a rigid body with a reference point, and the contact surfaces between the MEP Rubber Pad and the Base is a tie constraint.

Table 2.3 Mesh Properties of the Model Parts

Part Name	Element Controls		Element Type	
	Element Shape	Technique Type	Element Library	Geometric Order
Impactor (Tup)	Hex	Sweep	Standard	Linear, Reduced Integration
Base	Hex	Structured	Standard	Linear, Reduced Integration
MEP Rubber Pad	Hex	Structured	Standard	Linear, Reduced Integration

2.2.5 Model Applied Loads and Boundary Conditions

The impact velocity is used as an initial condition that causes the impact to occur. The caculations of the impact velocity is set up according to the equation 1.10 which is shown below. This is the theoretical velocity of a free-falling object similar principle to the theoretical head-neck drop tower assembly calculations which are shown with more detail in Section 3.2.6.

$$V_{impact} = \sqrt{2 * g * H} \tag{1.10}$$

Where,

g is gravity acceleration, equal to 9.81 m/s^2

H is desired drop height in m

V_{impact} is the impact velocity in m/s

Figure 2.21 shows the settings up of the applied load (Impact Velocity) in the model.

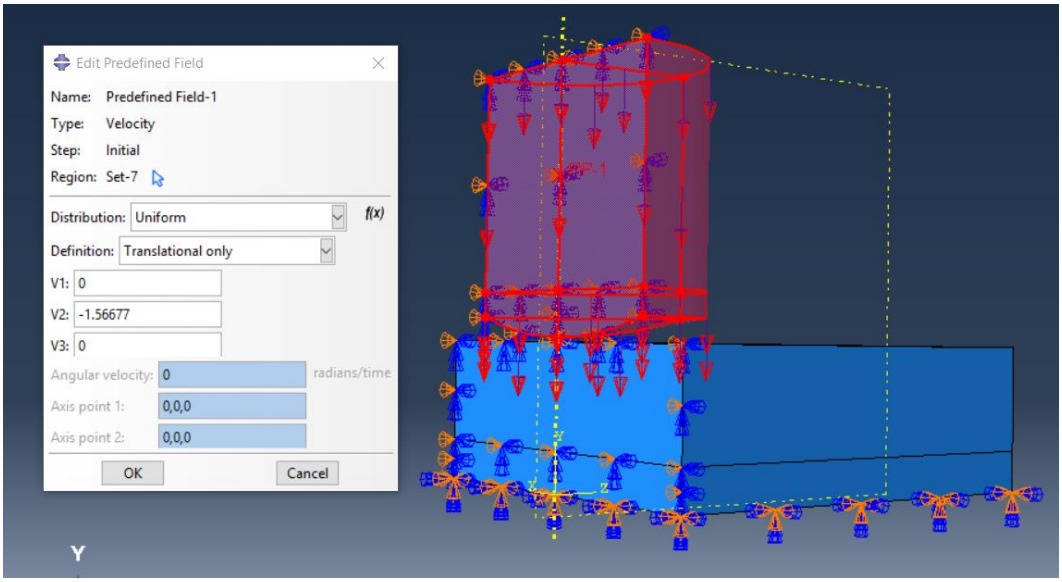

Figure 2.21 Impact Velocity Setting Up

For the model boundary conditions, we have set three conditions as shown in the following steps:

1. Make the symmetry plane to not displace in a direction transverse to the cut plane direction as shown in Figure 2.22.
2. Fix the bottom translation of the Base part in three directions as shown in Figure 2.23.

3. Fix two points on the impactor to guide it in the vertical direction, to insure the impact will occur in the center of the sample and to keep the impactor without rotation. Figure 2.24. Shows this step with more details.

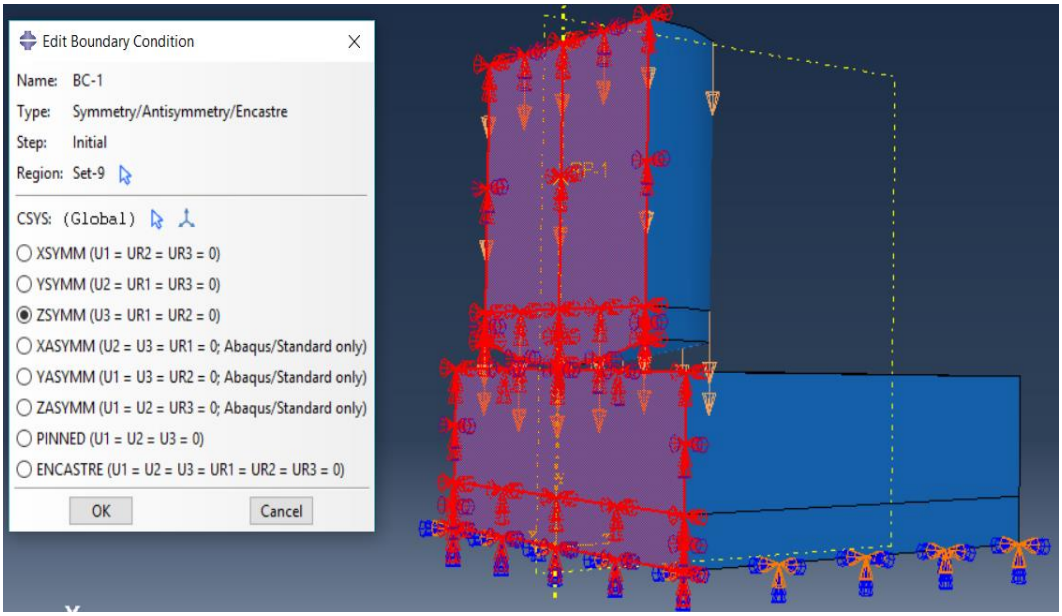

Figure 2.22 The First Step to Set Up the Boundary Conditions of the FEA Model

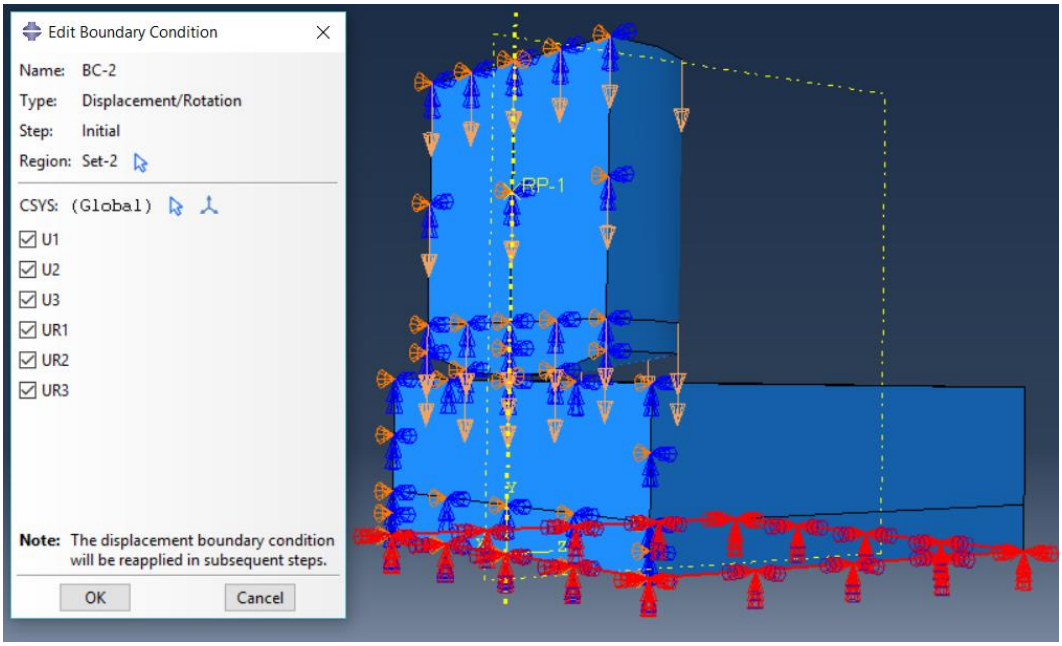

Figure 2.23 The Second Step to Set Up the Boundary Conditions of the FEA Model

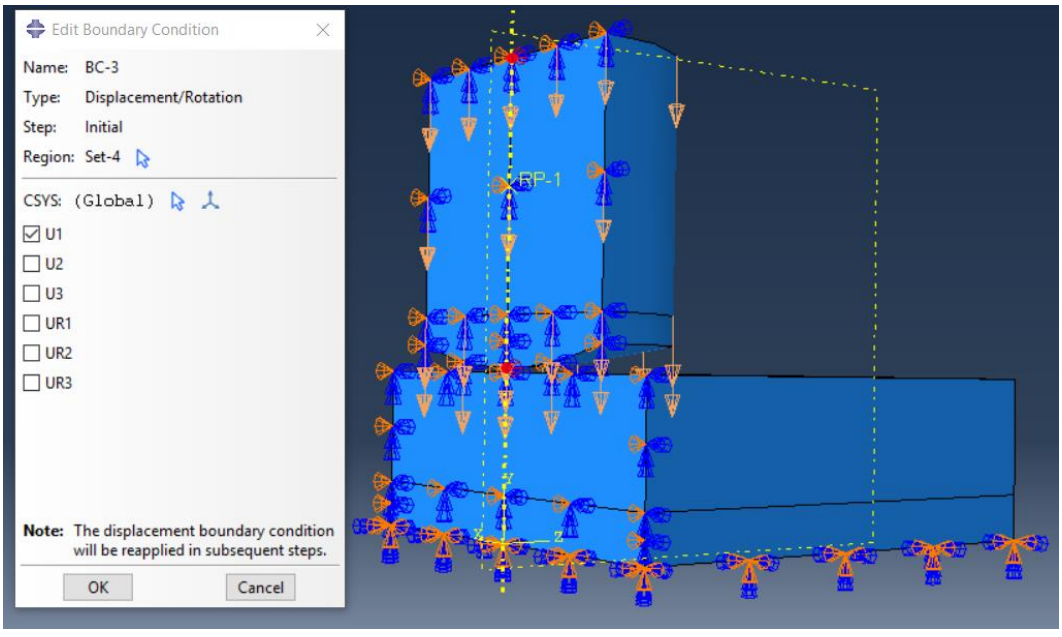

Figure 2.24 The Last Step to Set Up the Boundary Conditions of the FEA Model

2.2.6 Model Jobs and Results

2.2.6.1 Model Job Settings

In MEP study, the variants are the coefficients of the MEP rubber material that uses the Mooney-Rivlin hyperelastic material model. A parametric study of the influence of the coefficients was performed, which depended on the equations (2.7), (2.8) and (2.9). Figure 2.25 shows the process to set up the MEP rubber material properties in the FEA model.

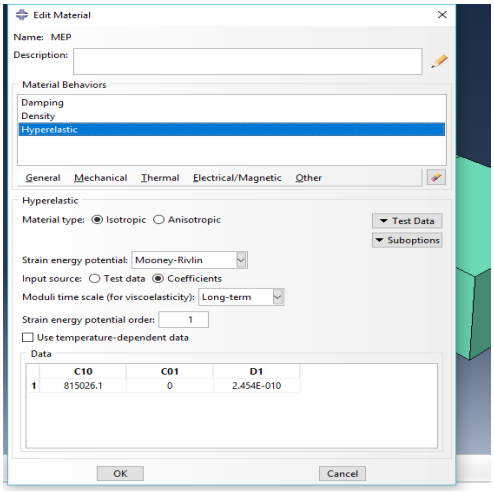

Figure 2.25 MEP Rubber Material Coefficients Settings

A total analysis time of 0.02 seconds was with the time step of 5E-5 seconds as shown in Figure 2.26.

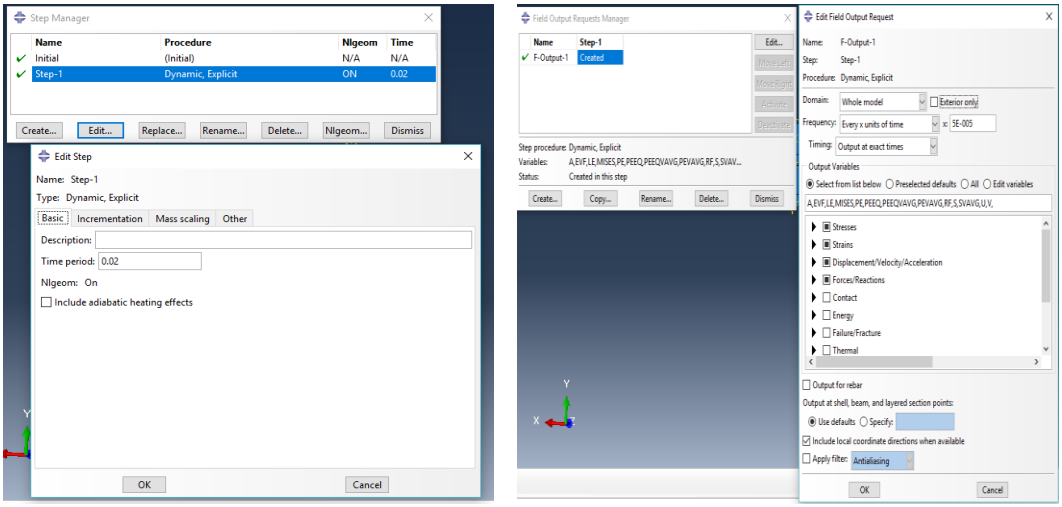

Figure 2.26 Total Time and Step Time Setting

2.2.6.2 Model Results Procedure

To obtain the required results after the job is completed, the following steps where used:

1. Go to the Job Manager and hit the Results button as shown in Figure 2.27.A.
2. Go to the Create XY Data, and point the OBD field output. Then, select the required results fields (Spatial Acceleration and Displacement) by choosing Unique Nodal. After that, choose the required node (Reference Point). Eventually, click on Save to save the data. Figures 2.27.B, C and D show more details.
3. A Butterworth filter was applied to the data set by the following process. After saving the required data as shown in Figure 2.28.a. Go to Create XY Data, and Operate on XY Data as shown in Figure 2.28.b. After that choose

"Butterworth Filter (X, F)" then click on the required data. The cutoff frequency was set at 1650Hz. This is the recommended value by the Society of Automotive Engineers (SAE) for similar experimental impact testing. Eventually the filtered data is saved as shown in Figure 2.28.c. Figure 2.29 that shows a sample of the differences between the filtered and non-filtered acceleration.

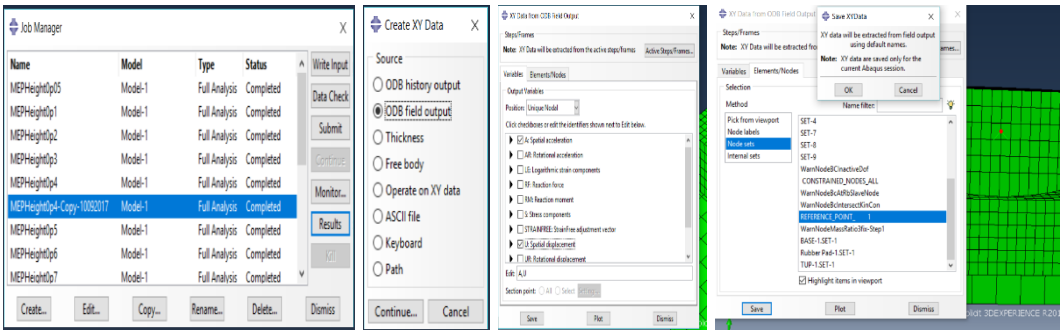

A) B) C) D)

Figure 2.27 Steps of Getting the Required Results

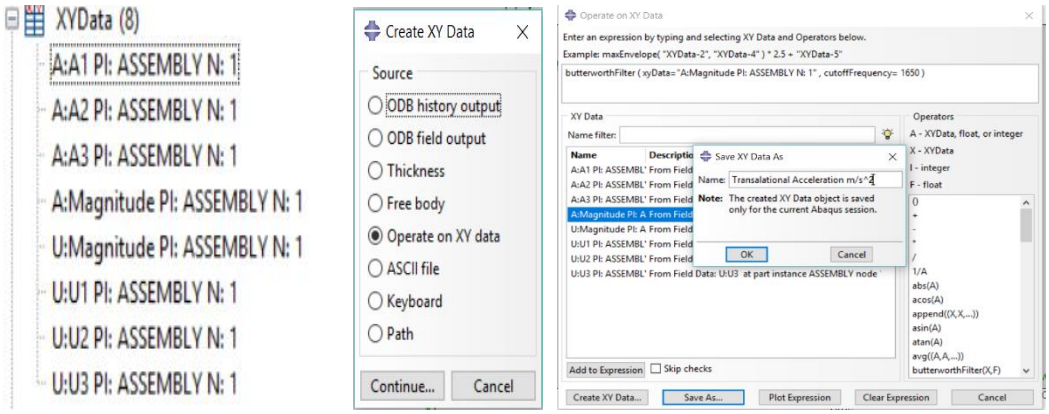

a) b) c)

Figure 2.28 Filter the Nosey Data Steps

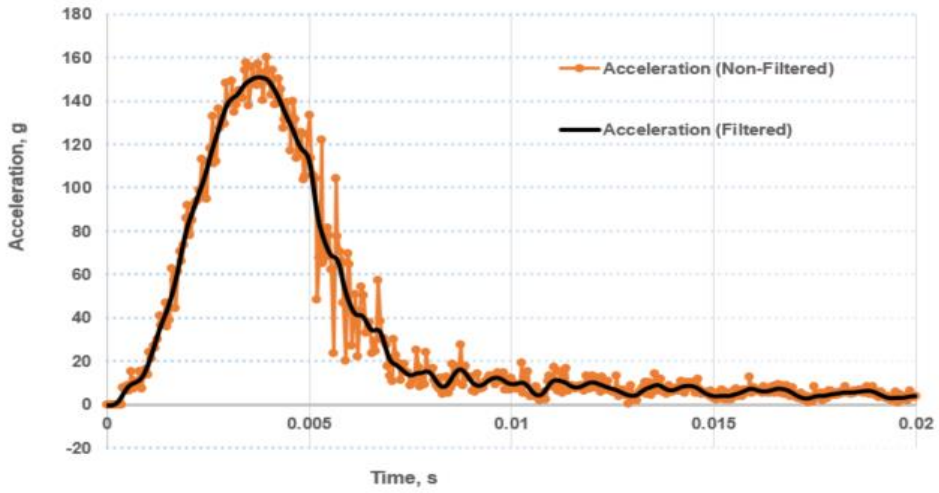

Figure 2.29 Sample of the Filtered and Non-Filtered Data

2.2.6.3 Model Results Data

The results of the FEA model analysis are summarized herein. Where, the constants of the MEP rubber material are evaluated accordingly to the equations (2.7), (2.8) and (2.9). The characters used in the tables and figures are designated as follows:

H: Drop Height, $V_{Imp.}$: theoretical impact velocity which is computed from equation 3.3 and used in the FEA model, A: Peak Acceleration, and D: Peak Displacement. In addition, durometer of material is the nominal Shore A hardness.

2.2.6.3.1 FEA Model Results of MEP Rubber Material with 60 Shore A Hardness

Peak acceleration in g's and displacement in mm for each impact FEA model test are shown in Tables 2.4, 2.5, 2.6 and 2.7. Where, in every theoretical impact test we have set the required impact velocity V_{Imp} which is evaluated according to the equation 3.3 and by using the required drop height H test range (0.05- 0.9) m. In addition to that, each FEA impact model test has to be set up with constants of the MEP Rubber material C_{10}, C_{01} and D_1 which are estimated according to the equations 2.7, 2.8 and 2.9 and by using various estimated α as shown in these Tables.

Table 2.4 Peak Accelerations Results for FEA Model Impact Test According to the Change of the MEP Material constants by using 60 Shore A Hardness Durometer, 1.25 MPa Tensile Strength(μ)

H (m)	$V_{Imp.}$ m/s	A, g α=0	A, g α=0.05	A, g α=0.1	A, g α=0.15	A, g α=0.2	A, g α=0.25	A, g α=-0.25
0.05	1	36.5	36.9	37.3	38.3	38.6	37.1	36
0.1	1.4	55.4	55.7	56.2	56.5	56.4	56.2	56
0.15	1.7	75	75.2	74.2	75	75.9	74.8	79.4
0.2	2	88.2	88.4	89.1	88.8	89.8	88.7	85.3
0.25	2.2	100.7	101.3	102	103.2	103.1	104	98
0.3	2.4	114.3	116.6	114.6	117.9	116.5	116.9	112.9
0.35	2.6	127.3	129.1	129.5	128.2	131.7	129.5	121.9
0.4	2.8	139.4	140.8	143.4	144.1	144.8	147.2	131.2
0.45	3.	150.5	152.7	152.9	156.2	151.4	154.8	142.8
0.5	3.1	160	163	162	163.4	163.1	163.5	151.6
0.55	3.3	171.5	175.8	174.8	177.2	178.8	175.6	163.6
0.6	3.4	181.9	184.7	185.8	187.1	188.8	188.7	173.7
0.65	3.6	192	194.6	198.6	197.2	195.7	199.5	180.8
0.7	3.7	203.1	206.7	208.8	209.4	208.7	210.9	189.9
0.75	3.8	216.7	215.2	221.6	219.2	221.6	224.5	198.4
0.8	4	224.1	230.1	232.4	227.9	231.1	235	207.5
0.85	4.1	233.3	237.5	239.5	250.5	243.1	247.4	221
0.9	4.2	245.9	246.4	252.4	252.1	253.4	256	226

Table 2.5 Peak Acceleration Results for FEA Model Impact Test According to the Change of the MEP Material constants by using 60 Shore A Hardness Durometer and 1.25 MPa Tensile Strength(μ)

H (m)	$V_{Imp.}$ m/s	A, g α=0.5	A, g α=-0.5	A, g α=1	A, g α=0.025	A, g α=10	A, g α=0.075	A, g α=100	A, g α=0.0001
0.05	1	37.8	37.8	40.3	37.3	39.3	39.2	37.3	37.1
0.1	1.4	57.2	57.2	57.3	55.4	58.4	56.2	58.1	56
0.15	1.7	74.6	74.6	76.6	74.3	78.5	75.2	76.8	74.6
0.2	2	91.5	91.5	92.9	87.9	95.3	89.8	94.6	87.7
0.25	2.2	103.9	103.9	106.3	102.2	109.1	101.9	111.1	100.8
0.3	2.4	117.5	117.5	120.7	116.6	124.8	118.9	125.4	115.1
0.35	2.6	132.1	132.1	133.3	126.9	140.1	129	141.4	127.9
0.4	2.8	147	147	144	138.5	151.7	141.3	153.3	139.1
0.45	3	156.7	156.7	159.1	152.1	167.4	152.7	167.8	150.8
0.5	3.1	168.1	168.1	174.6	160.2	179.2	162	183.1	160.6
0.55	3.3	181	181	182.6	173.5	191.4	175	193.3	171.7
0.6	3.4	190.8	190.8	195.5	182	205.6	186.8	206.8	182.1
0.65	3.6	206.3	206.3	205.4	195	220.5	195	224.9	194.4
0.7	3.7	211.5	211.5	221.9	211.9	235.2	207.4	232.2	203.2
0.75	3.8	226.2	226.2	233.4	213.6	242.6	216.8	246.6	216.2
0.8	4	236.2	236.2	241.8	225.3	257.5	225.3	266.7	225.7
0.85	4.1	263.6	263.6	267.2	239.2	270.9	238.5	270.5	236.6
0.9	4.2	261.6	261.6	267.1	250.3	286.4	249.5	290.8	245.8

Table 2.6 FEA Model Displacement Results According to the Change of the MEP Material constants by using 60 Shore A Hardness Durometer and 1.25 MPa Tensile Strength(μ)

No #	H (m)	$V_{Imp.}$ m/s	D, mm α=0	D, mm α=0.05	D, mm α=0.1	D, mm α=0.15	D, mm α=0.2	D, mm α=0.25	D, mm α=-0.25
1	0.05	1	3.7	3.7	3.7	3.7	3.7	3.7	3.7
2	0.1	1.4	4.7	4.7	4.6	4.6	4.6	4.6	4.7
3	0.15	1.7	5.3	5.3	5.3	5.3	5.3	5.3	5.4
4	0.2	2	5.8	5.8	5.8	5.8	5.8	5.8	5.9
5	0.25	2.2	6.3	6.3	6.3	6.2	6.2	6.2	6.4
6	0.3	2.4	6.6	6.7	6.6	6.6	6.6	6.6	6.8
7	0.35	2.6	7	7	7	7	7	6.9	7.2
8	0.4	2.8	7.3	7.3	7.3	7.3	7.3	7.3	7.5
9	0.45	3	7.6	7.6	7.6	7.5	7.5	7.5	7.8
10	0.5	3.1	7.9	7.8	7.8	7.8	7.8	7.8	8.1
11	0.55	3.3	8.1	8.1	8.1	8	8	8	8.3
12	0.6	3.4	8.4	8.3	8.3	8.3	8.2	8.2	8.6
13	0.65	3.6	8.6	8.5	8.5	8.5	8.5	8.4	8.8
14	0.7	3.7	8.8	8.7	8.7	8.7	8.7	8.6	9
15	0.75	3.8	9	8.9	8.9	8.9	8.9	8.8	9.2
16	0.8	4	9.2	9.1	9.1	9.1	9	9	9.4
17	0.85	4.1	9.3	9.3	9.3	9.2	9.2	9.2	9.6
18	0.9	4.2	9.5	9.5	9.4	9.4	9.4	9.3	9.8

Table 2.7 FEA Model Displacement Results According to the Change of the MEP Material constants by using 60 Shore A Hardness Durometer

No#	H (m)	$V_{Imp.}$ m/s	D, mm α=0.5	D, mm α=-0.5	D, mm α=1	D, mm α=0.025	D, mm α=10	D, mm α=0.075	D, mm α=100	D, mm α=0.0001
1	0.05	1	3.7	3.7	3.7	3.7	3.6	3.7	3.6	1
2	0.1	1.4	4.6	4.6	4.6	4.7	4.5	4.7	4.5	1.4
3	0.15	1.7	5.3	5.3	5.2	5.3	5.2	5.3	5.1	1.7
4	0.2	2	5.8	5.8	5.7	5.8	5.6	5.8	5.6	2
5	0.25	2.2	6.2	6.2	6.1	6.3	6	6.3	6	2.2
6	0.3	2.4	6.6	6.6	6.5	6.7	6.4	6.7	6.4	2.4
7	0.35	2.6	6.9	6.9	6.8	7	6.7	7	6.7	2.6
8	0.4	2.8	7.2	7.2	7.1	7.3	7	7.3	7	2.8
9	0.45	3	7.5	7.5	7.4	7.6	7.2	7.6	7.2	3
10	0.5	3.1	7.7	7.7	7.6	7.9	7.5	7.8	7.4	3.1
11	0.55	3.3	7.9	7.9	7.9	8.1	7.7	8.1	7.7	3.3
12	0.6	3.4	8.2	8.2	8.1	8.3	7.9	8.3	7.9	3.4
13	0.65	3.6	8.4	8.4	8.3	8.6	8.1	8.5	8	3.6
14	0.7	3.7	8.6	8.6	8.5	8.8	8.3	8.7	8.2	3.7
15	0.75	3.8	8.8	8.8	8.7	8.9	8.4	8.9	8.4	3.8
16	0.8	4	8.9	8.9	8.8	9.1	8.6	9.1	8.6	4
17	0.85	4.1	9.1	9.1	9.0	9.3	8.8	9.3	8.7	4.1
18	0.9	4.2	9.3	9.2	9.1	9.5	8.9	9.4	8.9	4.2

Additionally, the curves of accelerations in g's and displacements in mm versus the impact time (0.2 seconds) are shown herein for some of the FEA impact

model results in the following Figures 2.30, 2.31, 2.32 and 2.33. Where, Figures 2.30 and 2.31 include the results of 0.05 m drop height test with C_{10}= 0.6243268 MPa, C_{01}=0 and D_1=0.3204 GPa^{-1} (where, α=0, Neo-Hookean) and C_{10}= 0.3121634 MPa, C_{01}= 0.3121634 MPa and D_1=0.3204 GPa^{-1} (where, α=1) MEP Rubber material constants respectively that estimated according to equations 2.7, 2.8 and 2.9. In the other hand, Figures 2.32 and 2.33 include the results of 0.9 m drop height tests with the same MEP Rubber constants at α=0, (Neo-Hookean Theory) and α=1 respectively as shown above.

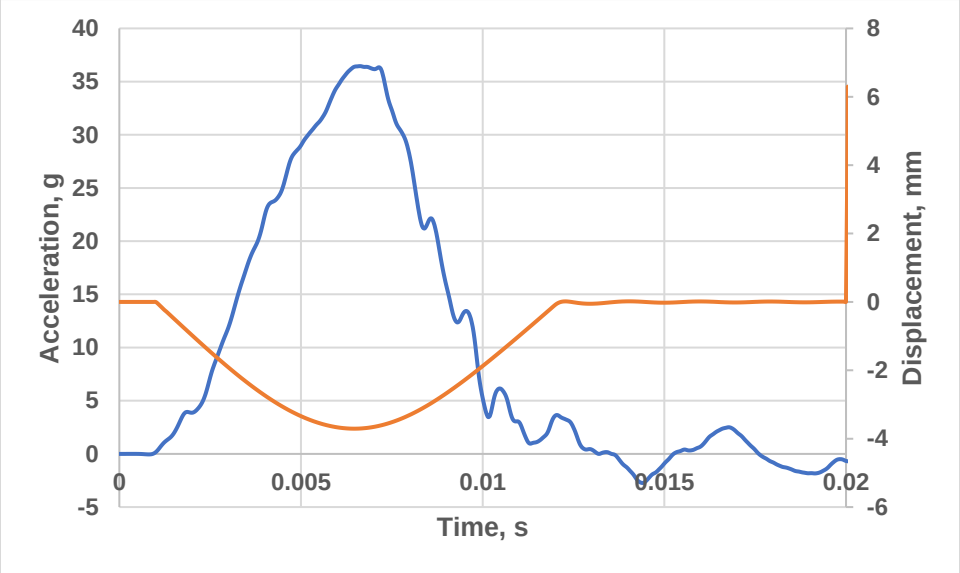

Figure 2.30 Acceleration and Displacement Versus Time for α=0 and Drop 0.05m

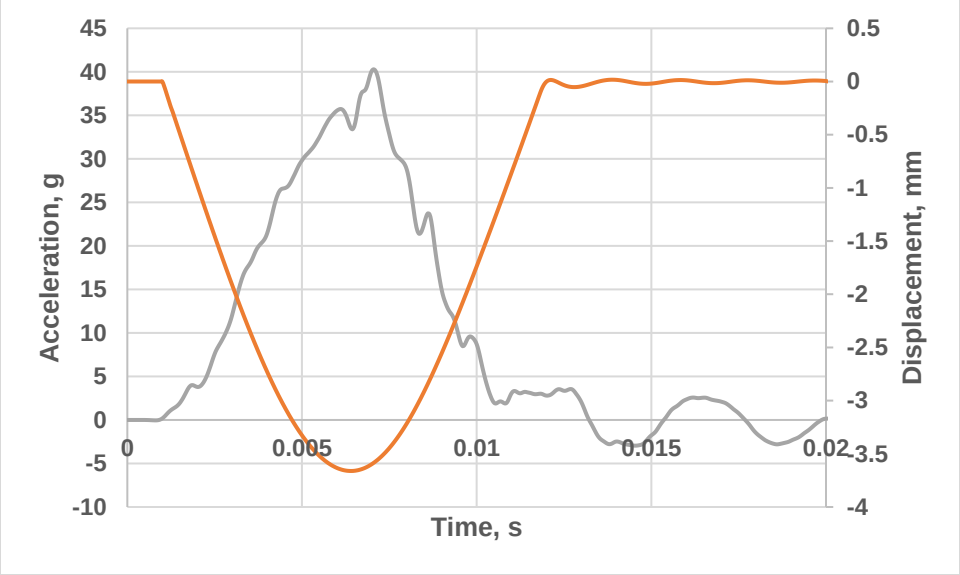

Figure 2.31 Acceleration and Displacement Versus Time for α=1 and Drop 0.05m

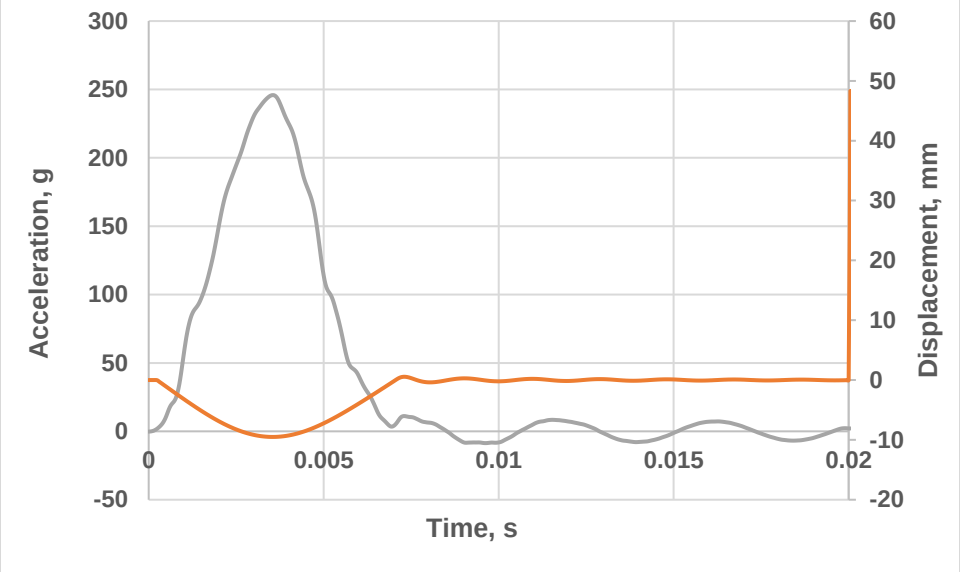

Figure 2.32 Acceleration and Displacement Versus Time for α=0 and Drop 0.9 m

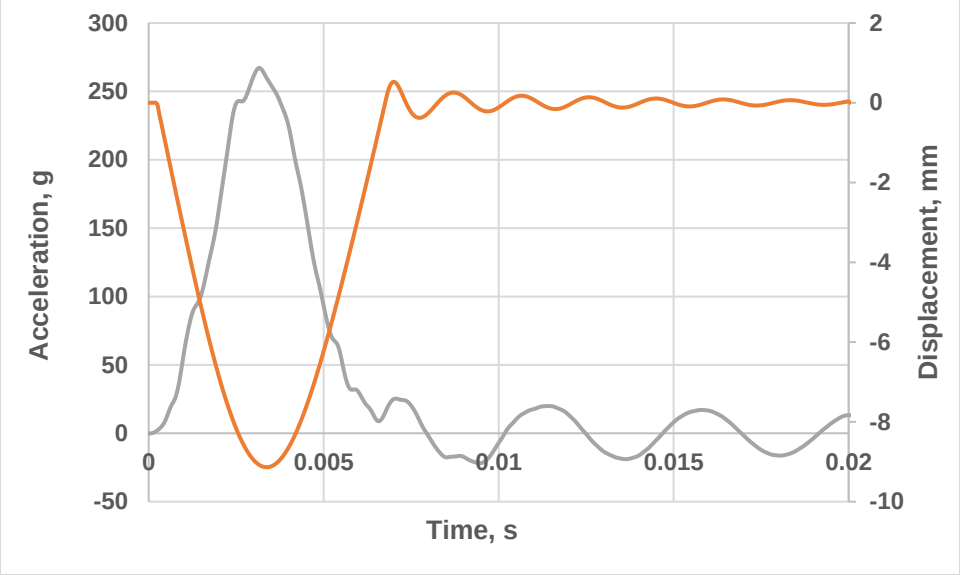

Figure 2.33 Acceleration and Displacement Versus Time for α=1 and Drop 0.9 m

2.2.6.3.2 FEA Model Results of MEP Rubber Material with a Various Shore A Hardness Durometer

Peak acceleration in g's and displacement in mm for each impact FEA model test are shown in Tables 2.8 and 2.9. Where, in every theoretical impact test we have set the required impact velocity V_{Imp} which is evaluated according to the Equation 3.3 and by using the required drop height H test range (0.05- 0.9) m. In addition to that, the FEA impact model test has to be set up with constants of the MEP Rubber material C_{10}, C_{01} and D_1 which are estimated according to the equations 2.7, 2.8 and 2.9 and by using α=1 and α=0 (Neo-Hookean Theory). These constants are estimated with depending on the following Shore A Hardness durometer: 55, 56, 57, 58, 60, 62.5 and 65.

Table 2.8 FEA Model Results of MEP Material with Various Durometer (Shore A)

H (m)	$V_{Imp.}$ m/s	Durometer =55		Durometer =56		Durometer =57	
		A, g α=0	A, g α=1	A, g α=0	A, g α=1	A, g α=0	A, g α=1
0.05	1	33.8	34.9	34.3	35.4	34.8	40.5
0.1	1.4	54.2	54.8	53.9	55.3	54.8	55.6
0.15	1.7	69.4	71.8	70.2	71.7	72	75
0.2	2	82.7	85.7	83.5	87.4	85.5	88.6
0.25	2.2	96.8	100.6	96.9	101	97.9	102
0.3	2.4	107.1	113.8	108	113.9	110.5	117
0.35	2.6	119.5	123.9	122	126.5	122.1	130.1
0.4	2.8	129.1	137.2	131.6	138.5	134.3	140.9
0.45	3	141.4	148.5	142.3	151.9	141.3	151.5
0.5	3.1	149.8	163.1	151.8	160.9	152.7	164.5
0.55	3.3	160.6	174.5	163	176.9	165.4	175.8
0.6	3.4	171.8	182.2	171.2	188	176.3	187.3
0.65	3.6	179.1	196.1	191	196.4	193.5	197.7
0.7	3.7	191.7	207.4	190	210.3	196.8	211.6
0.75	3.8	200.5	228	201.9	222.2	201.6	227.2
0.8	4	208.2	231.3	211.9	231.2	217.1	239.5
0.85	4.1	218.9	241.6	225.7	244.1	223.2	246.1
0.9	4.2	232.8	250.3	227.8	254.5	234.9	259.1

Table 2.9 FEA Model Results of MEP Material with Changing the Durometer (Shore A)

H (m)	$V_{Imp.}$ m/s	Durometer =58		Durometer =62.5		Durometer =65	
		A, g α=0	A, g α=1	A, g α=0	A, g α=1	A, g α=0	A, g α=1
0.05	1	38.8	38.9	36.9	36.9	37.4	38
0.1	1.4	55.1	57.4	58.2	58.6	58.5	60.4
0.15	1.7	74.2	79.9	80.1	77.6	76.3	79.1
0.2	2	85.4	89.5	93.4	95.9	94.5	96.8
0.25	2.2	98.6	104.8	104.3	110.8	110.9	114.3
0.3	2.4	113.6	117.7	119	125.2	125.1	130.6
0.35	2.6	125	131.5	132.7	139.3	137.8	143.8
0.4	2.8	136.4	142.6	145.7	153.2	148.7	158.3
0.45	3	145.1	155.2	157	165.8	163.3	171.3
0.5	3.1	157.1	168.8	165	178.7	176.1	191.1
0.55	3.3	166.1	176.9	179.5	194.5	184.6	201.2
0.6	3.4	179.1	197.5	189.2	208.5	197.5	204.1
0.65	3.6	185.7	208.7	199.6	219.3	206.5	227.5
0.7	3.7	207	213.7	214.7	227.7	220.5	238.9
0.75	3.8	233.2	224	225.3	245.9	233.3	251.3
0.8	4	217.9	234.6	236.7	257.9	244.1	259.1
0.85	4.1	230.2	247.3	244	265.4	254	273.5
0.9	4.2	236.6	263.1	254	273.8	262.9	292.4

The curves of accelerations in g's and displacements in mm versus the impact time (0.2 seconds) are shown herein for some cases of the FEA impact model results in the following Figures 2.34, 2.35, 3.36 and 2.37. Where, Figures 2.34 and 2.36 include the results of 0.05 and 0.9 m drop height test with C_{10}= 0.478 MPa, C_{01}=0 and D_1= 0.418 GPa^{-1} (where, α=0) and C_{10}= 0.239 MPa, C_{01}= 0.239 MPa and D_1= 0.418 GPa^{-1}(where, α=1) MEP Rubber material constants respectively that estimated according to equations 2.7, 2.8 and 2.9. In the other hand, Figures 2.35 and 2.37 include the results of 0.05 and 0.9 m drop height tests with C_{10}= 0.815 MPa, C_{01}=0 and D_1= 0.245 GPa^{-1} (where, α=0) and C_{10}= 0.408 MPa, C_{01}= 0.408 MPa and D_1= 0.245GPa^{-1}(where, α=1) MEP Rubber material constants respectively that estimated according to Equations 2.7, 2.8 and 2.9.

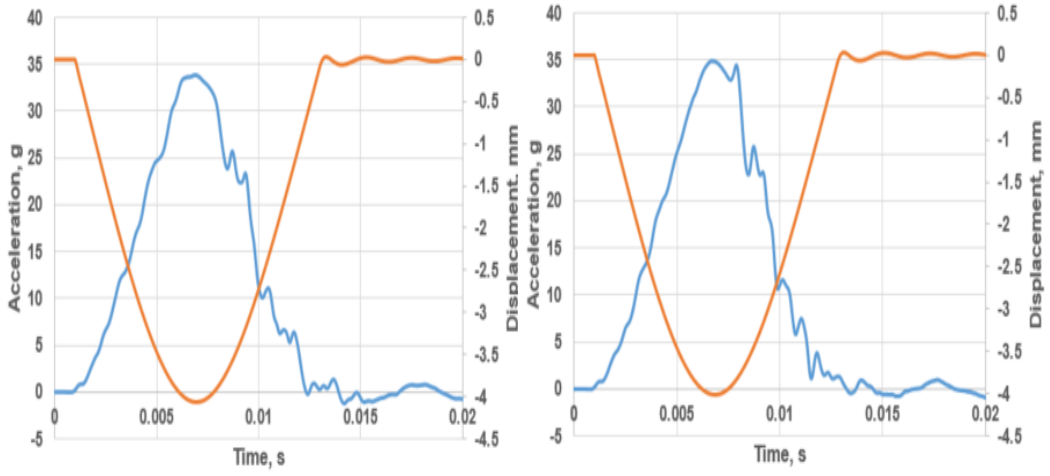

Figure 2.34 Acceleration and Displacement Versus Time for MEP Durometer Equal to 55 Shore A Drop 0.05 m at: Left Figure α=0 and Right Figure α=1

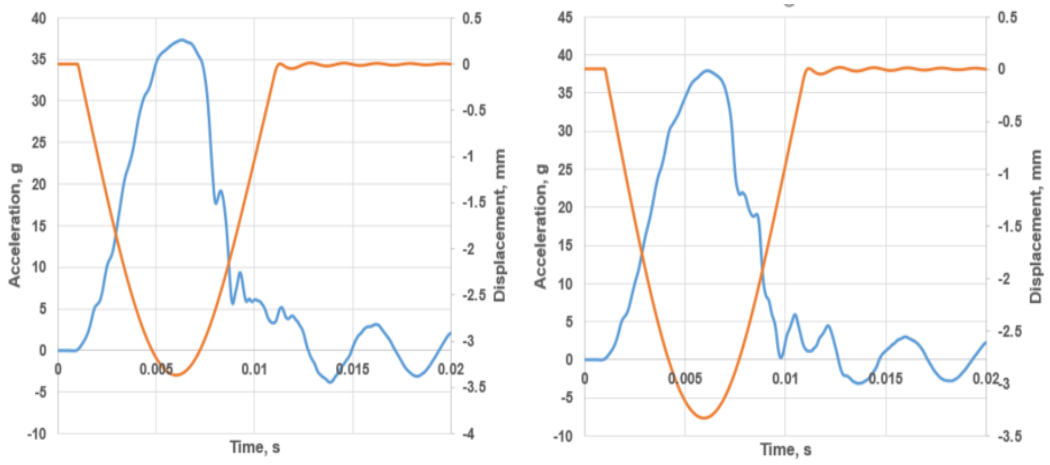

Figure 2.35 Acceleration and Displacement Versus Time for MEP Durometer Equal to 65 Shore A, Drop 0.05 m at: Left Figure α=0 and Right Figure α=1

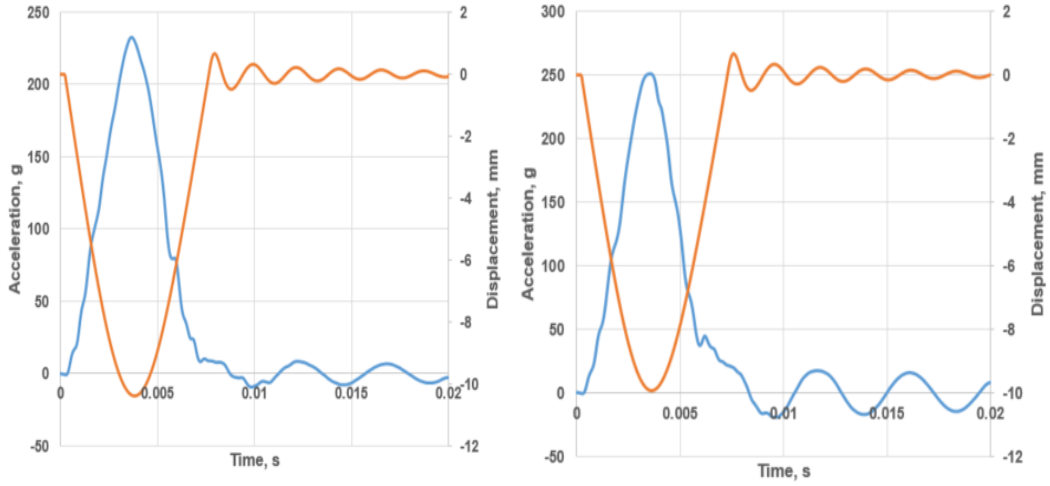

Figure 2.36 Acceleration and Displacement Versus Time for MEP Durometer Equal to 55 Shore A, Drop 0.9 m at: Left Figure at α=0 and Right Figure at α=1

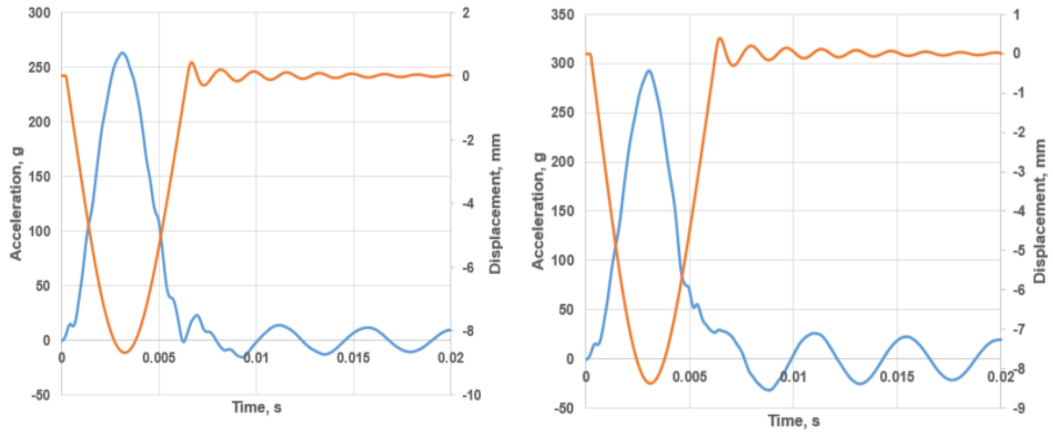

Figure 2.37 Acceleration and Displacement Versus Time for MEP Durometer 65 Shore A, Drop 0.9 m at: Left Figure α=0 and Right Figure α=1

2.3 Comparison Between the Experimental and Model Results

As mentioned in Section 2.1, the experimental data will be used as a baseline for MEP constants determination and the FEA model results will be compared with experimental performance. The peak acceleration versus drop height curve is used for the comparison between the results. To obtain which curve is more close to the experimental curve, we have used the following method: First, estimate the area under the experimental curve $A_{Experimental}$ by using Equation 2.11 and make its value (75.29 m*g) as a baseline number. Second, bring each curve (Peak acceleration versus drop height curve) for the FEA model results that studied in this chapter and estimate the area under this curve by using Equation 2.11 as shown in Table 2.10. Then, compare these computed areas values of the FEA model with the baseline number (75.29 m*g) by evaluating the error that shows which

curve might be closed to the experimental curve. Equation 2.12 uses to estimate the error between the required curve and the baseline number (experimental data). Eventually, it is observed that a few curves for FEA model results are similar to the baseline curve (Experimental data) as shown in Table 2.10. In addition, we can also perform a visually check regarding the quality of fit to the experimental data.

The equation used to estimate the area under the curve is:

$$A_{approximate} = \sum_{i=0}^{n} \big(f(x_{i+1}) - f(x_i)\big) * \left(\frac{x_{i+1} + x_i}{2}\right) \quad (2.11)$$

According to this equation, the area under the experimental results curve that shown in Figure 2.12 is 75.29 m*g. The computed error equation is:

$$\text{Error} = \frac{A_{\text{Required}} - A_{\text{Experimental}}}{A_{\text{Experimental}}} * 100\% \quad (2.12)$$

Where,

$A_{Required}$ is the computed area under the required curve, m*g

$A_{Experimental}$ is the computed area of the experimental results, m*g

Table 2.10 shows the computed area under the peak acceleration versus drop height curves that shown in Figure 2.38 by using equation 2.11, and it also shows the percentage of the error between the experimental data and the FEA model results.

Table 2.10 Computed Area under the Peak Acceleration Drop Height Curves for FEA Model Results in Figure 2.38

Durometer, Shore A	α	Area under the curve, m*g	Error, %
55	0	87.97	16.84
55	1	94.26	25.19
56	0	81.91	8.79
56	1	97.1	28.96
57	0	86.53	14.92
57	1	99.21	31.76
58	0	84.59	12.35
58	1	100.77	33.84
60	0	91.62	21.68
60	1	101.05	34.21
62.5	0	93.2	23.78
62.5	1	101.48	34.77
65	0	96.6	28.3
65	1	113.91	51.29

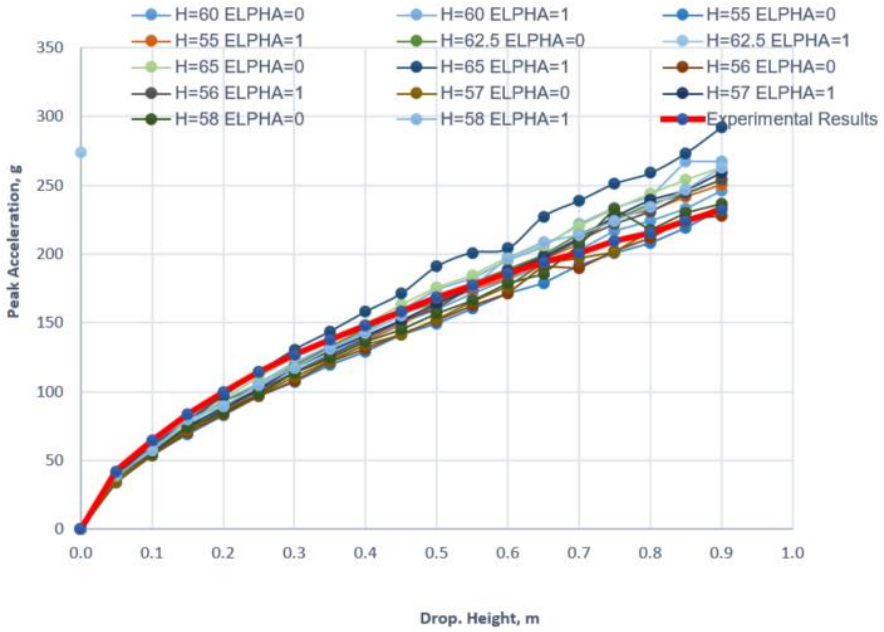

Figure 2.38 FEA Model Results According to change the MEP Rubber Pad Shore A Durometer(H) That Are Summarized in Tables 2.8 and 2.9

In conclusion, there are four MEP Rubber pad Shore A durometer material constant sets that can be reliably used to model the material according to the Table 2.10: Shore A 55, 56, 57 and 58. All these results were with Neo- Hookean Theory (α=0). However, the best curve that can be more converged to the experimental data is with Shore A (H=57) as shown in Figure 2.39. Where, the MEP Rubber Pad material constants are:

$$C_{10} = 0.532 \quad \text{MPa}, \quad C_{01} = 0 , \quad \text{and} \quad D_1 = 0.376 \ \text{GPa}^{-1} \tag{2.13}$$

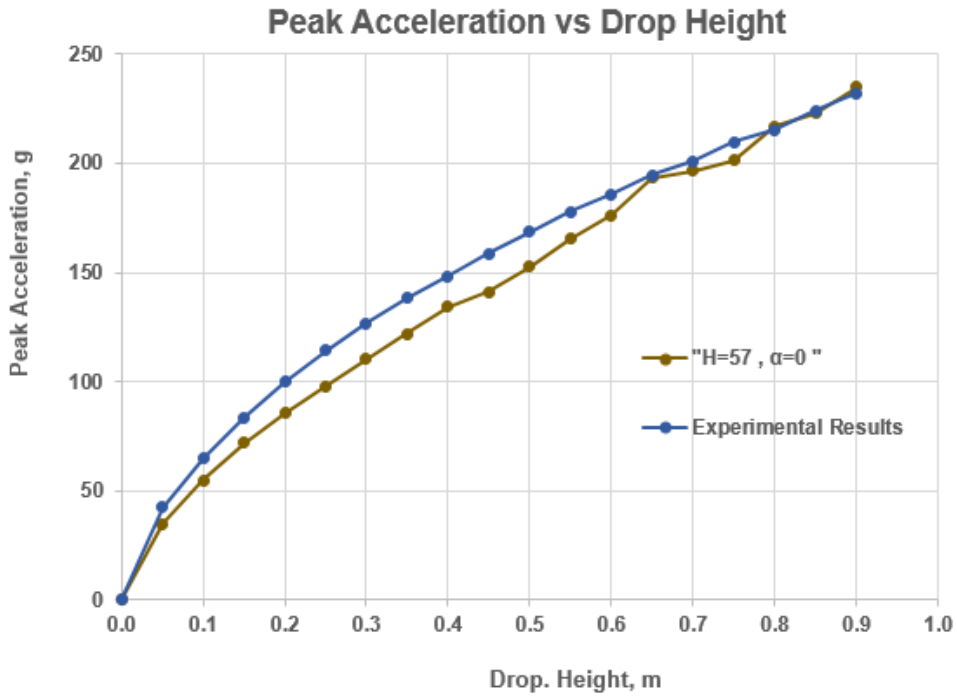

Figure 2.39 Best Converge Between the Experimental Results and the FEA Model

CHAPTER 3

MODEL VERIFICATION

This chapter includes a summary of the finite element model verification for the computer model of the head neck assembly used in the University of Maine drop tower. The immediate goal is to compare the response to designated standards and to experimental testing. The ASTM soccer headgear specification is one of the few standards that govern the response of soft type head protection. Its calibration procedure will be used to guide the verification process. These criteria give a standard calibration process for the translational acceleration but not the angular acceleration. Therefore, our experimental tests results will be used for the angular acceleration. The remainder of this chapter describes the target values and the calibration process.

3.1 Summary of Standard ASTM Specification

The calibration procedure stated in the ASTM F2439 standard for testing soccer headgear will be uses as a basis for the verification process. The standard specification of the American Society for Testing and Materials ASTM (F2439 / F1446) clearly state how to set up the test apparatus of impact tests and what the expected results are for these tests. The calibration tests are described by dropping the Hybrid III head and neck assembly onto the MEP (Modular Elastomer Programmer) rubber pad. The impact velocity for this test should be 2.8 m/s ± 2 %.

That means the height of the dropped Hybrid III head and neck assembly should be around 40 mm. The total mass of the entire drop system should be 8.8 kg ± 5 % (19.4 lb ± 5 %) including the flyarm and all attached parts. The peak acceleration during the impact test is also obtained as 112 ± 8 g. This acceleration was measured from the translational motion of the Hybrid III head and neck assembly at the head center of gravity. The ASTM (F2439 / F1446) standards do not state how to set up the apparatus for post-impact angular acceleration testing. In addition to that, the durometer hardness of Modular Elastomer Programmer (MEP) rubber pad is Shore A 60 ± 2 GPa. (ASTM, 2015a, 2015b).

3.1.1 Summary of Standard Values Used for Model Verification

One of the lab studies verifies the experimental response of the Head- Neck assembly drop tower at University of Maine. As part of that study translational and angular acceleration were recorded for several test conditions, including the MEP anvil among others. During this testing with the MEP anvil, a sample of 12 drops resulted in a peak translational acceleration of 110.28 g and angular acceleration of 4722.42 rad/sec^2. Accordingly, the target values for the calibration study are as follows:

MEP anvil: Shore A 60 ±5 MPa, 25.4 mm thick.

Impact velocity: 2.8 ± 3% m/s

Drop Height: 0.4 ± 1% m

Peak translational acceleration: 110.28 ± 3 g

Peak angular acceleration: 4722.52 ± 445 rad/s^2

3.2 Description of FEA Hybrid III Head-Neck Assembly Model

The Hybrid III Head-Neck Assembly model as shown in Figure 3.1 has a total mass of 8.27 kg with its FlyArm and all attachments. The mass was designated to match the mass of the University of Maine drop arm. Our focus is on the parts worked on to satisfy model verification standards and to compare the response to obtain experimental results.

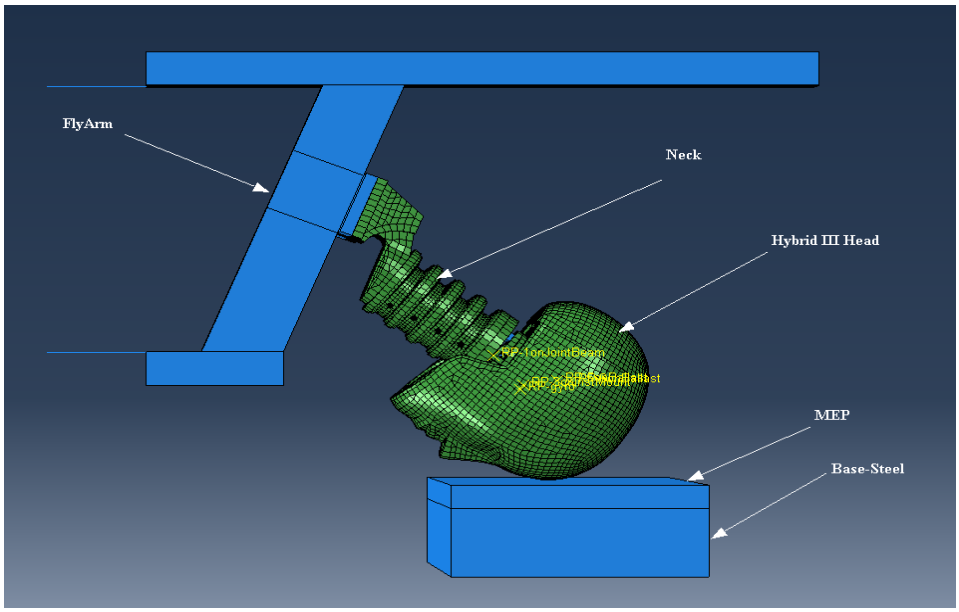

Figure 3.1 Hybrid III Head-Neck Assembly Model

These primary parts comprising the model are shown in Figures 3.2 and 3.3. The properties of the important elements to make the Hybrid III Head-Neck

Assembly model more acceptable and useful are shown. Generally, the properties of the main parts that have some control over the translation and angular acceleration response were varied parametrically so oberve the sensitivity of the analysis to their selection and to develop a set of parameters that precisely fit with the experimental results and the standards. Some of the major elements that will be discussed include the following:

1. MEP Mooney Material
2. NeckRubber Material
3. RubberPad Parts
4. Skin-Rubber-Mooney Material
5. CableBeam and MPU Parts

In addition, there were more than ten other minor parts contained in the model.

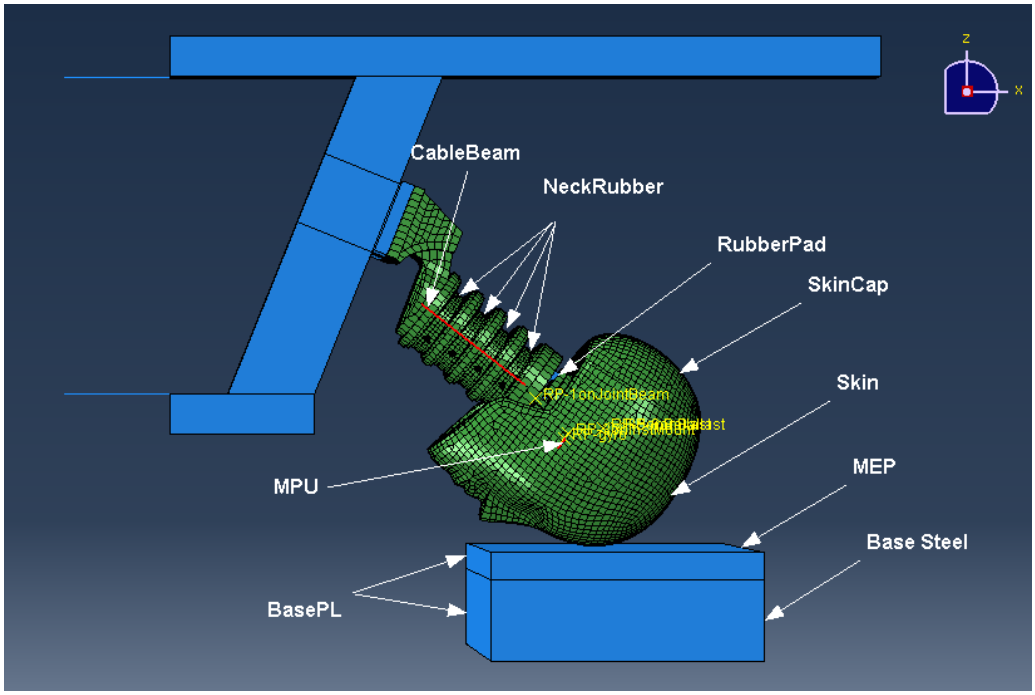

Figure 3.2 The Parts of the Study Model

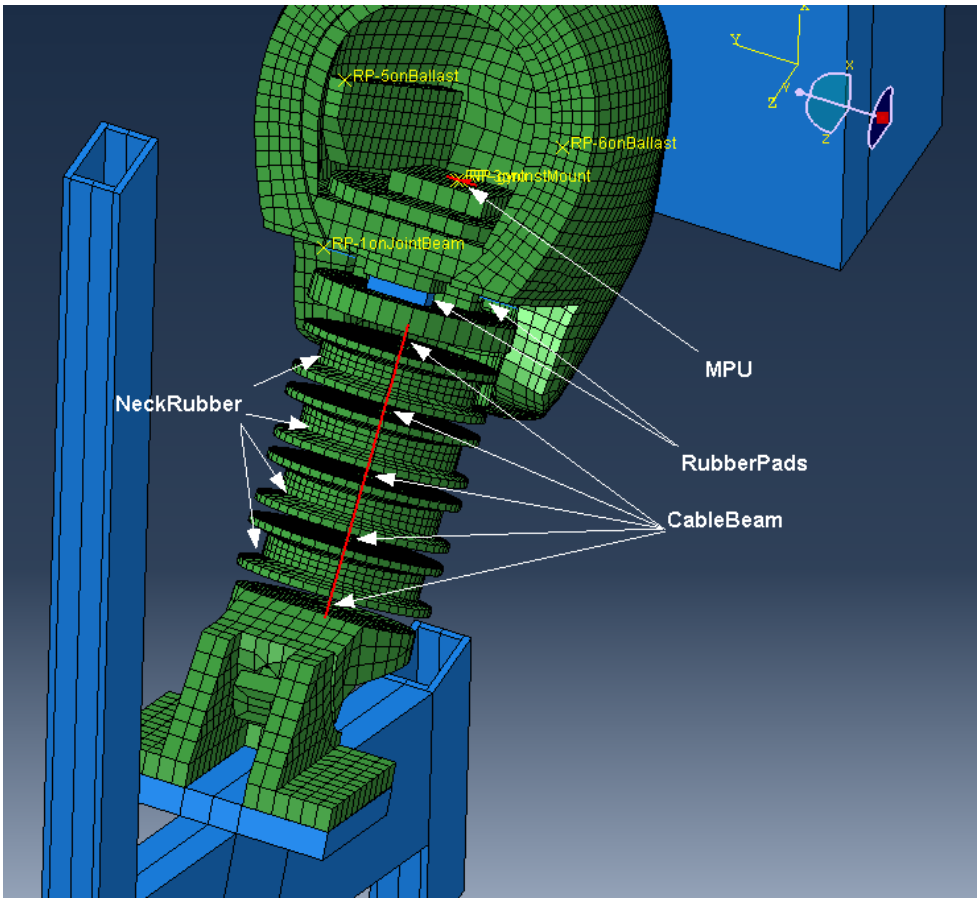

Figure 3.3 Zoomed Picture for CableBeam, MPU, and RubberPad Parts After Hiding Some Other Parts

3.2.1 MEP (Modular Elastomer Programmer) Rubber Pad

The base anvil part (BasePL) consists of two assigned sections, Base-Steel and MEP as shown in Figures 3.2 and 3.4. Base-Steel section is made from steel material, with properties E= 200GPa, ν=0.3, ρ = 7890 kg/m^3, and its dimensions are 25cm by 25cm as a square cross area through a thickness 75mm. Base-Steel section is merged as one part with a 2.54 cm(1inch) thick MEP section. MEP

section is made from MEP-Rubber Mooney material that uses a Mooney-Rivlin hyperelastic material model. The material constants for the MEP-Rubber Mooney material is one of the variants that have studied in this thesis.

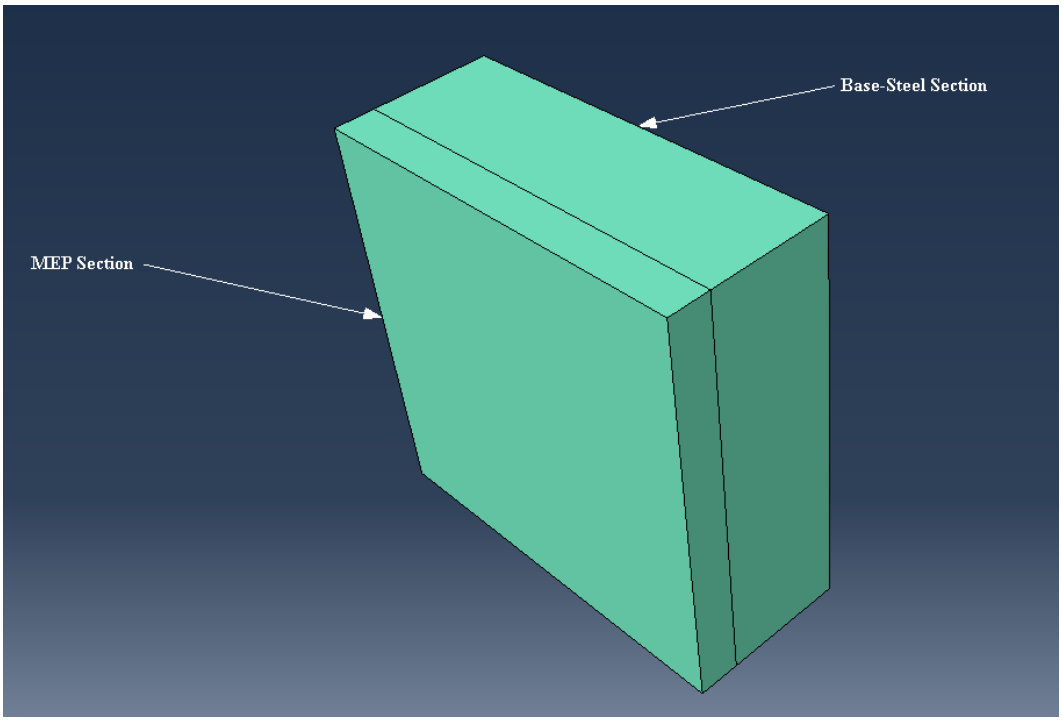

Figure 3.4 BasePL Part

3.2.2 NeckRubber Part

NeckRubber part consists of four pieces modeled as a hyperelastic material. Each piece looks like a pully shape with the main hole through it as shown in Figure 3.5. NeckRubber part is appropriately contacted with NeckDisk-1 Part as shown in Figure 3.6 A. The hyperelastic material is studied here is Neck Rubber-Mooney material that has Mooney-Rivlin hyperelastic properties as described later. The

neck is also made from the CableBeam and NeckCableDisk-1,2,3, and 4 Parts as shown in Figures 3.6 B and 3.7 that are located through the main hole of the NeckRubber part.

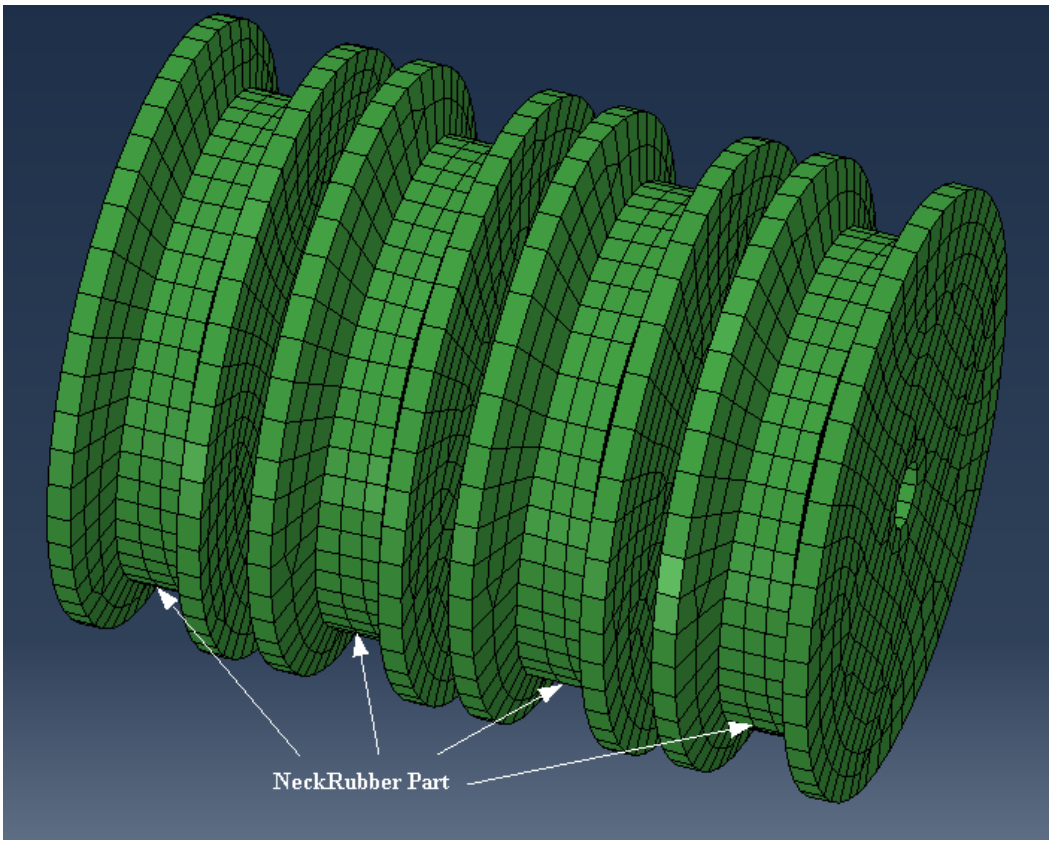

Figure 3.5 NeckRubber Part

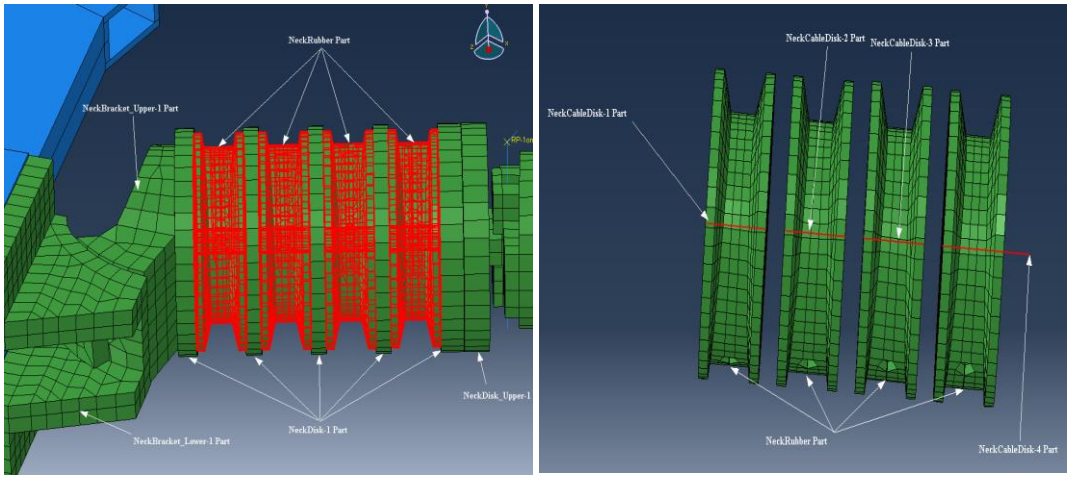

A) NeckRubber Part Position B) NeckCableDisk-1,2,3 and4 Parts

Figure 3.6 NeckRubber Part Position and how the NeckCableDisk-1,2,3, and 4 Parts are Located Through It

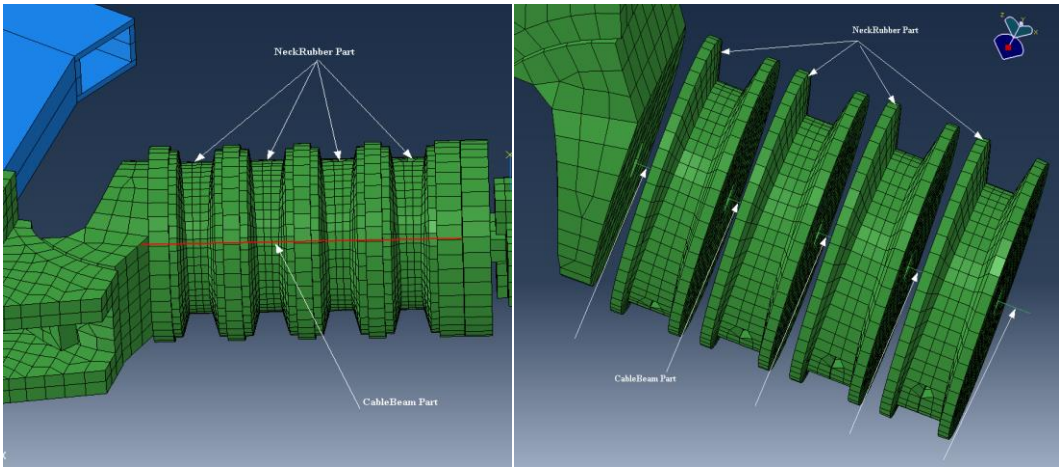

Figure 3.7 Two Views for Location of the CableBeam Part through the Main Hole of NeckRubber Part

3.2.3 RubberPad Parts

Two RubberPad parts are used in the model as shown in Figures 3.3 and 3.9. Each part is designed as parallel rectangular shapes as shown in Figure 3.8, and with dimensions, 9 mm width, 5.9 mm depth, and 26.25 mm length. The RubberPad parts are made from RubberPad material with a various elastic stiffness as studied herein. The rubber pad is in contact and becomes compressed between the base and the neck disk upper during a frontal impact.

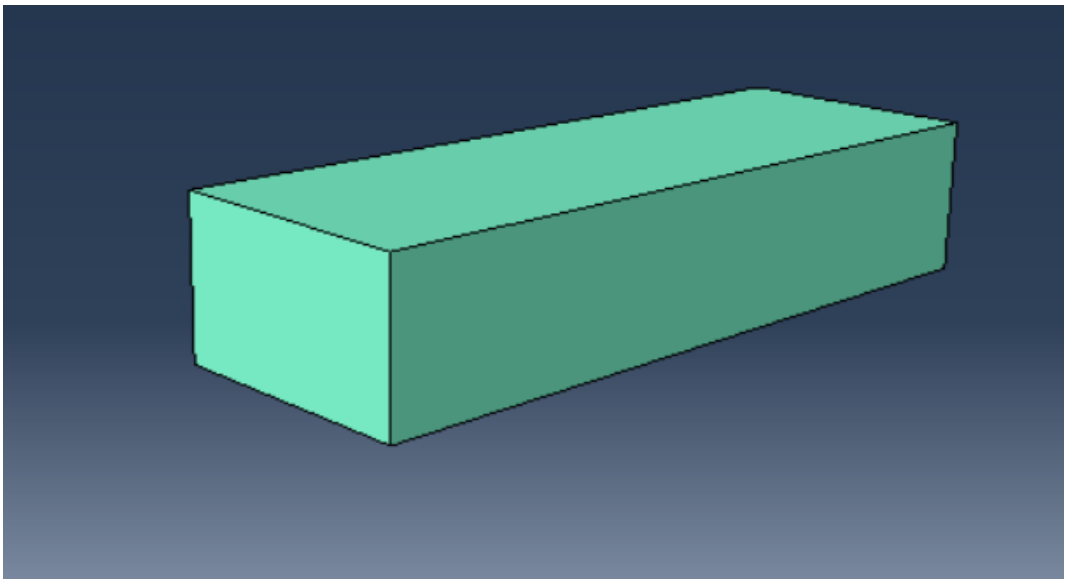

Figure 3.8 RubberPad Part

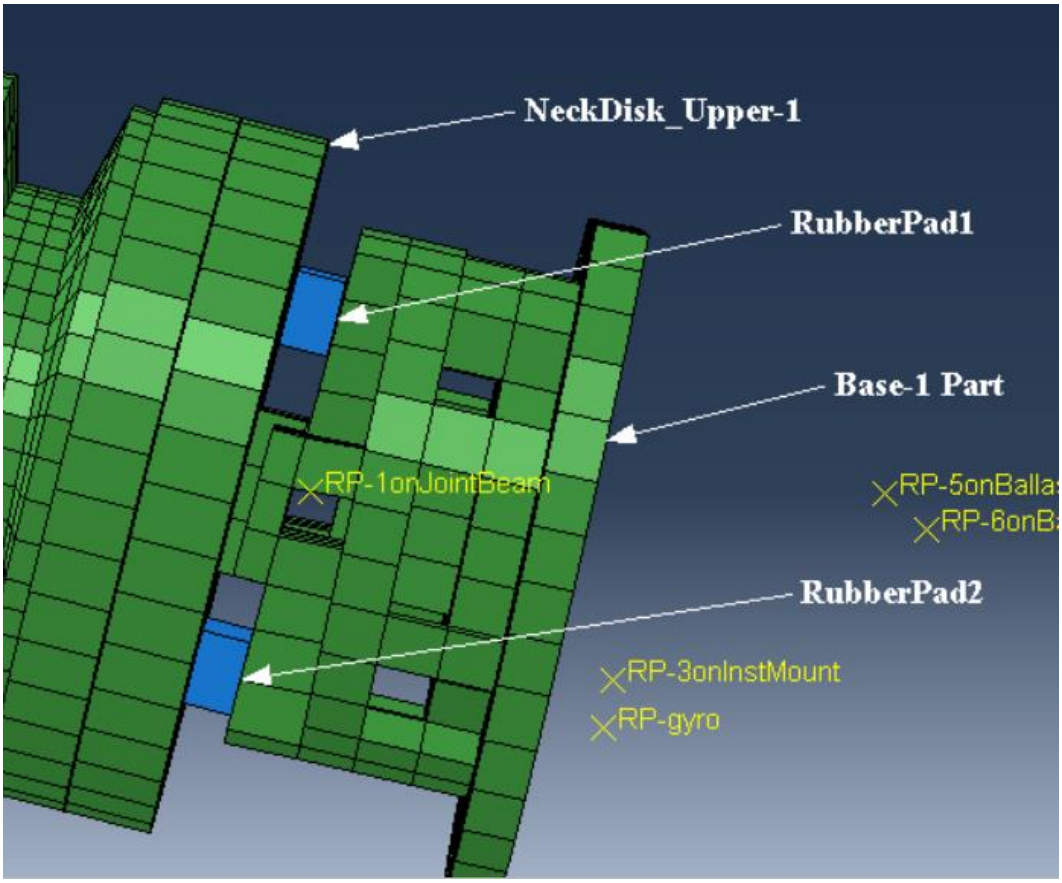

Figure 3.9 Zoomed Section Shows Where RubberPad1 and RubberPad2 Are Located

3.2.4 Skin and SkinCap

Skin and SkinCap parts are made as a solid homogenous with Skin-Rubber-Mooney material that uses a Mooney-Rivlin hyperelastic material model. The Skin part as shown in Figures 3.2 and 3.10 covers aluminum Skull part. SkinCap as shown in Figures 3.2 and 3.11 also covers aluminum SkullCup part. Skin part contacts with the MEP part during the impact test. In this case, analysis is sensitive

to the coefficient of friction between their surfaces. The aluminum Skull and SkullCup parts was made from an elastic isotropic material with modulus of elastisity 70 GPa, 0.33 Poisions's ratio and density of 2700 kg/m^3.

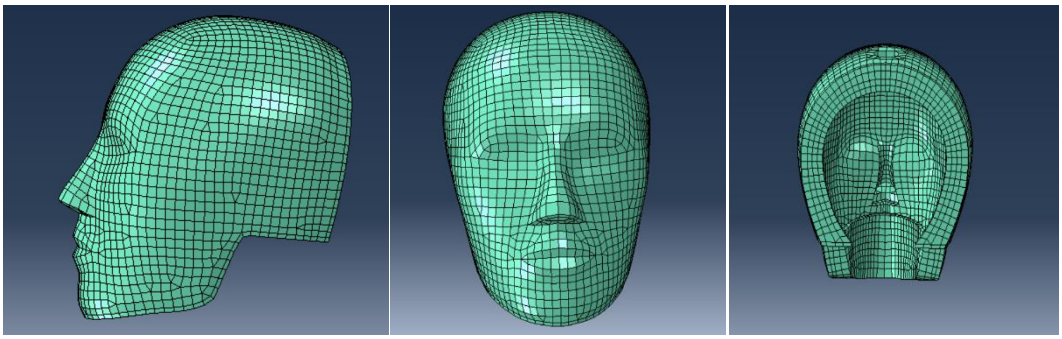

Figure 3.10 Three Views for Skin Part

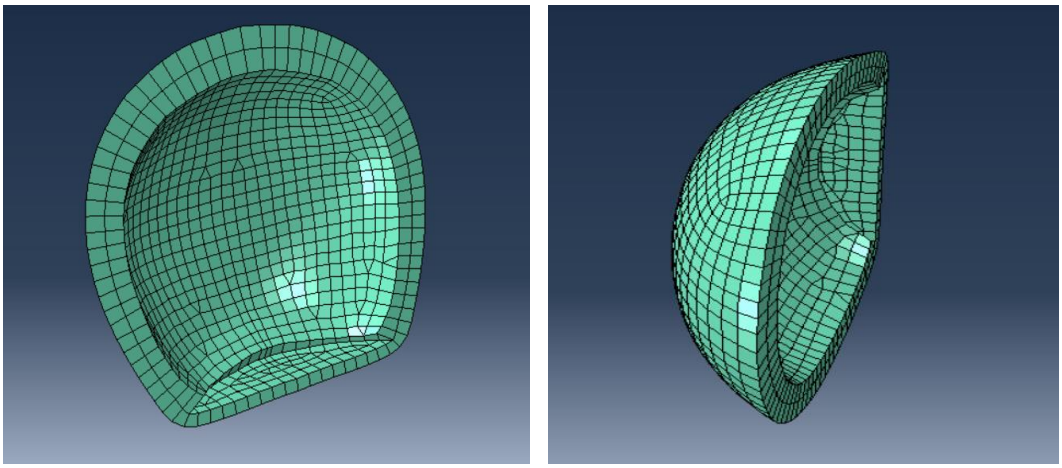

Figure 3.11 SkinCap Part

3.2.5 CableBeam and MPU

CableBeam and MPU parts are made from CableBeam material. This material is an elastic isotropic material with various modulus which is studied here as shown in Section 3.6.8. The section area shape of CableBeam part is also studied in this thesis. CableBeam part has 12.56 cm length, passes throughout the main hole of the NeckRubber part as shown in Figures 3.2, 3.3, and 3.7. The MPU part is clearly shown in Figure 3.13 how is located, and its dimensions are 13.56 mm and 11.75 mm as shown in Figure 3.12 C. the Centroid point of MPU part uses as a reference position of the impact test results. The section type of both is set up as a beam. Figures 3.2, 3.3, 3.7 and 3.12 show more details about them.

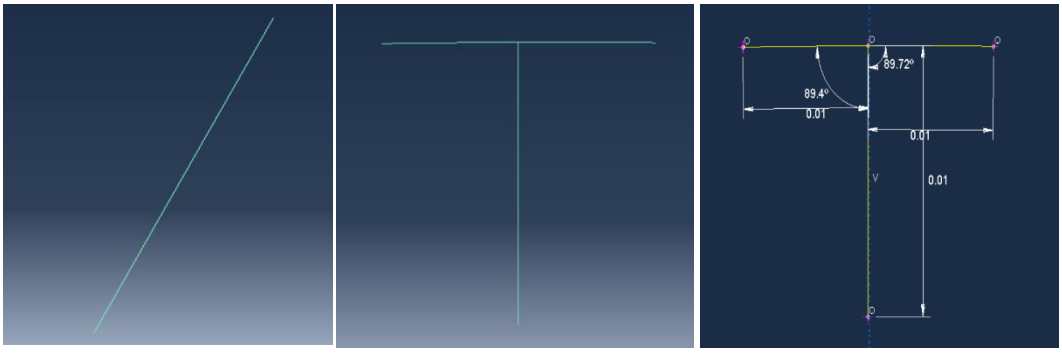

A) CableBeam Part B) MPU Part C) MPU Section Sketch

Figure 3.12 CableBeam and MPU Parts

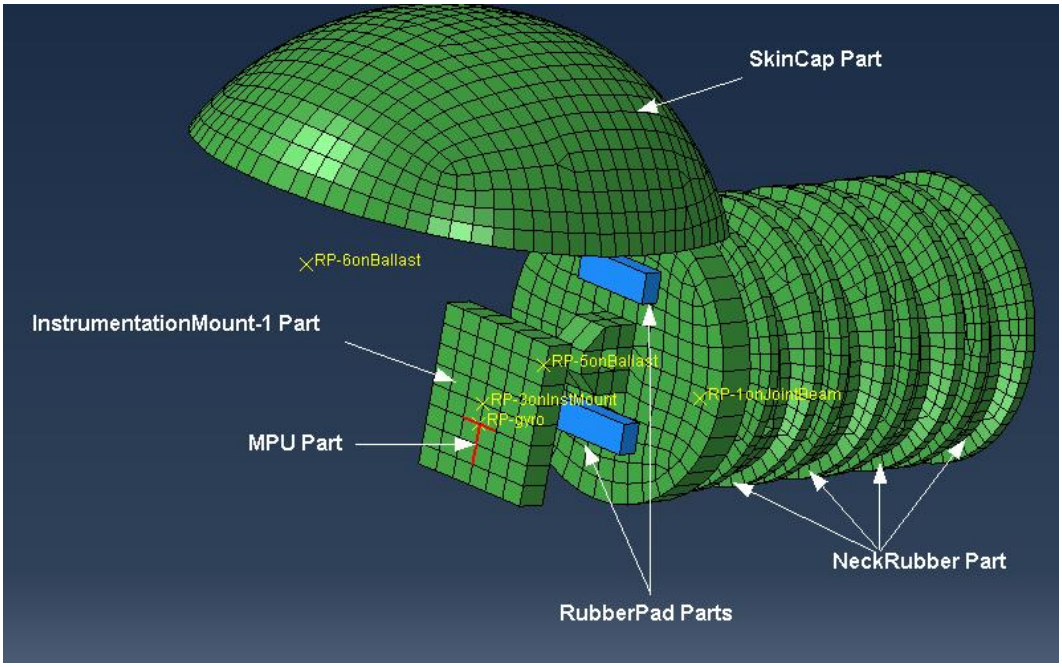

Figure 3.13 MPU Part Location

3.2.6 Applied Loads and Boundary Conditions Description

The impact velocity is used as an initial condition that caused the impact to occur. The impact velocity of the Head-Neck drop tower assembly can be theoretically related to the drop height of the assembly as shown in following calculations: In the standard test, the dropped height of the Head-Neck Assembly is equal to 0.4 meter, and the assembly is released as a free body (i.e. release with zero velocity). The fallen body will move downward according to the gravity effect. That means the kinetic energy of the dropped body should be equal to its potential energy at the impact moment. According to that, we have evaluated the impact velocity as shown here,

$$Potential\ Energy = m * g * H \quad (3.1)$$

$$Kinetic\ Energy = \frac{1}{2} * m * v^2 \quad (3.2)$$

At the impact moment, equation (3.1) = equation (3.2)

Thus,

$$V_{impact} = \sqrt{2 * g * H} \quad (3.3)$$

Where,

m is a mass of the dropped body in kg

g is gravity acceleration, equal to 9.81 m/s^2

H is dropped height in m

V_{impact} is impact velocity in m/s

Equation (3.3) is used for any dropped height case. The baseline conformance test is such that the impact velocity is equal to 2.8 m/s when the dropped height is 0.4 meter. The model has been set up accordingly. The Figures 3.14, 3.15, and 3.16 show the initial velocity being applied to all the components of the drop arm assembly while the base plate anvil if fixed.

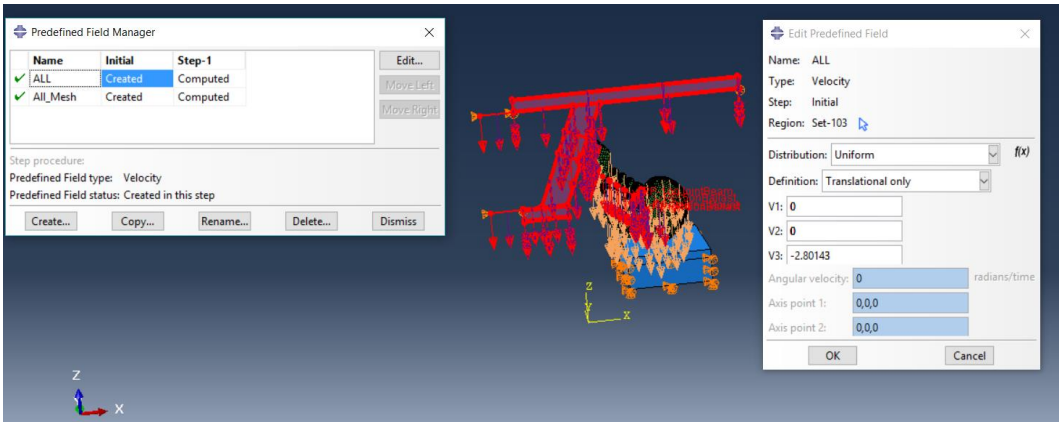

Figure 3.14 A- How to Set up the Applied Load

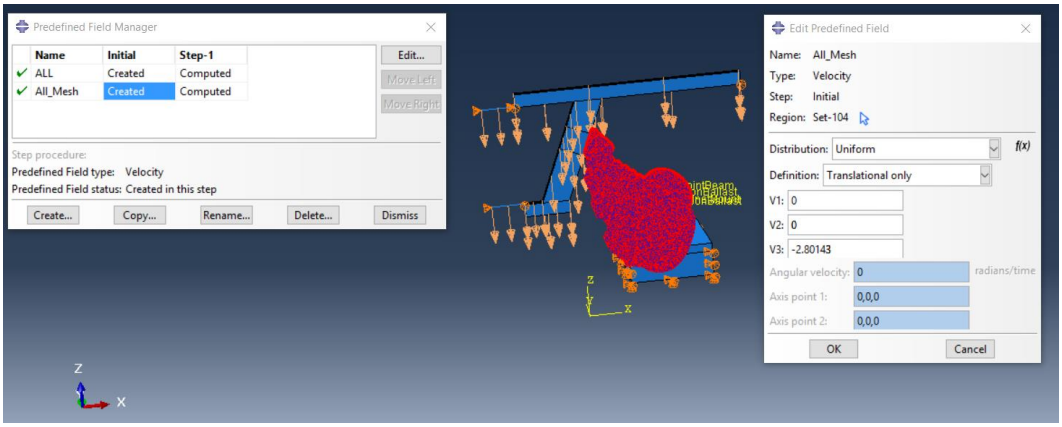

Figure 3.15 B- How to Set up the Applied Load

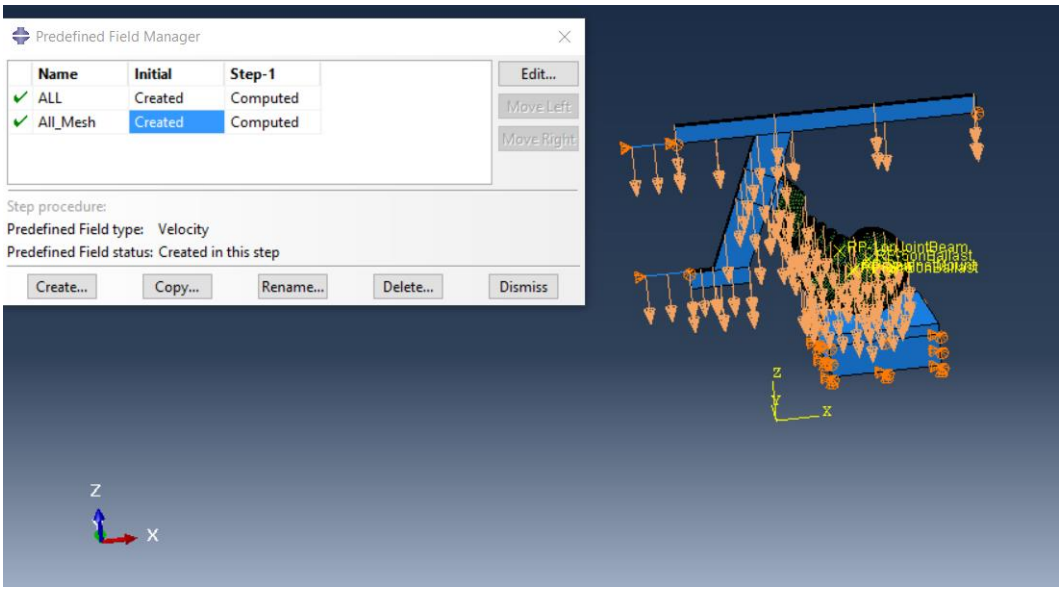

Figure 3.16 General View for Applied Load

Displacement and rotations are also set in the model. The BC1 designation is used for the study of the boundary conditions change effect later as shown in Section 3.6.6. BC1 Settings of BC1 are clearly shown in the six following steps:

1. Set the bottom section of BasePL part, especially Steel-Section, as shown in Figure 3.17. While, displacements are fixed in three directions.

2. Set the side section of BasePL part, especially Steel-Section, as shown in Figure 3.18. While, displacements are fixed in X-direction only.

3. Set the other side section of BasePL part, especially Steel-Section, as shown in Figure 3.19. While, displacements are fixed in Y-direction only.

4. Set a topped point of FlyArm part that is used as a guide for the model motion in the X-axis as shown in Figure 3.20. While, displacements are fixed in X-direction.

5. Set three tipped points of FlyArm part that are used as a guide for the model motion in the Y-axis as shown in Figure 3.21. While, displacements are fixed in Y-direction.

6. Set two points of SpringSupport parts that are used as a guide for the model motion in the X-axis as shown in Figure 3.22. While, displacements are fixed in X-direction.

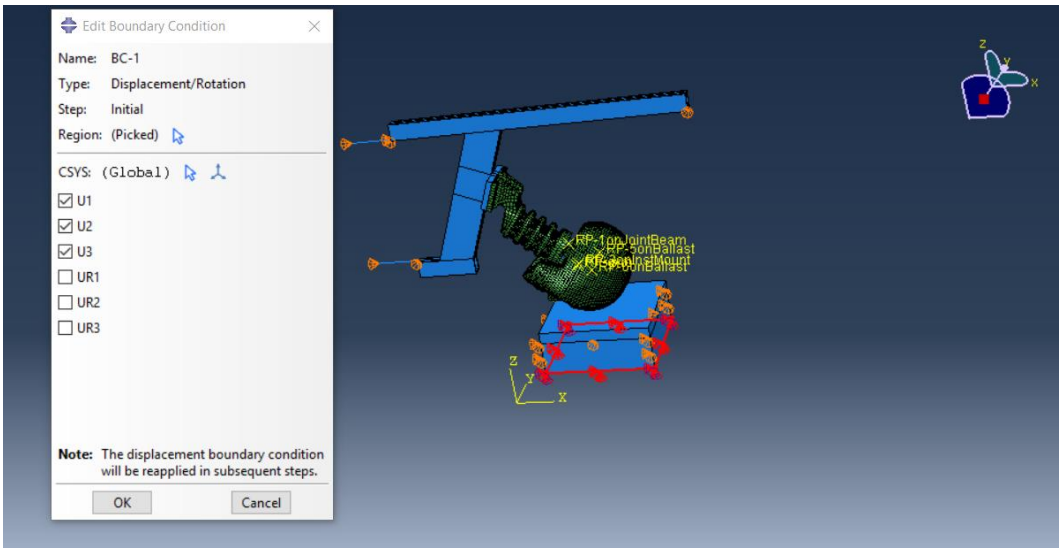

Figure 3.17 First Setting up Picture of BC1

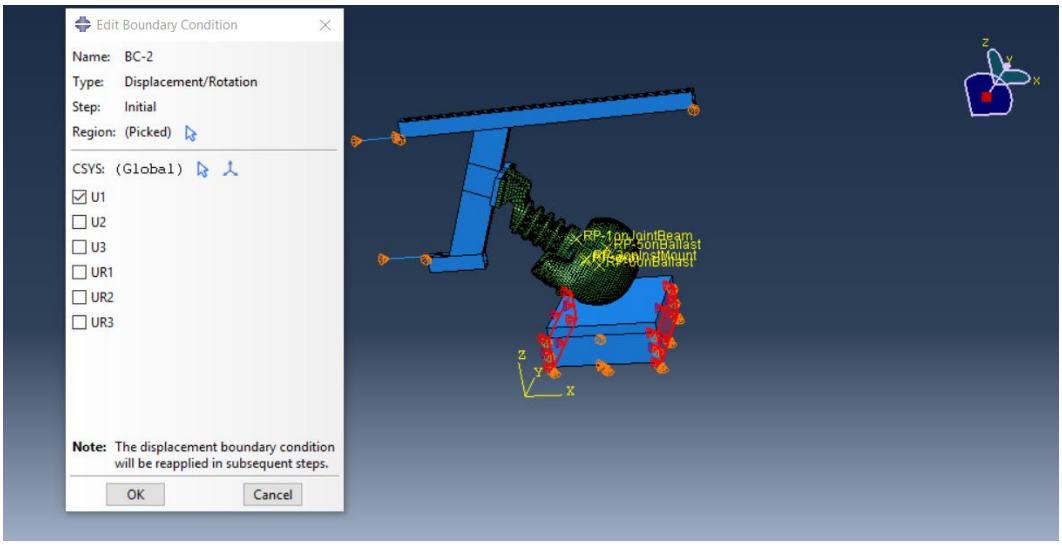

Figure 3.18 Second Setting up Picture of BC1

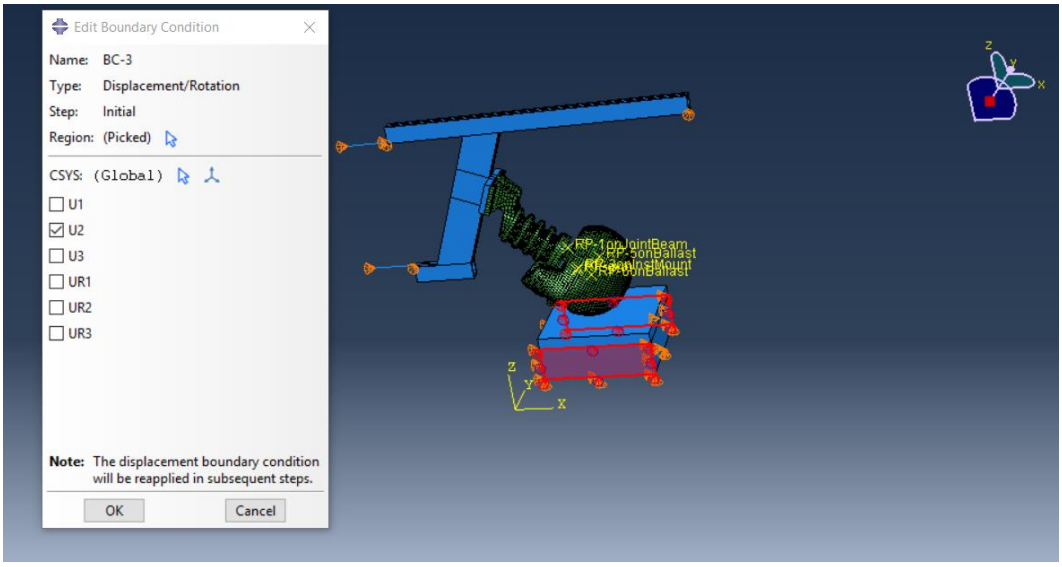

Figure 3.19 Third Setting up Picture of BC1

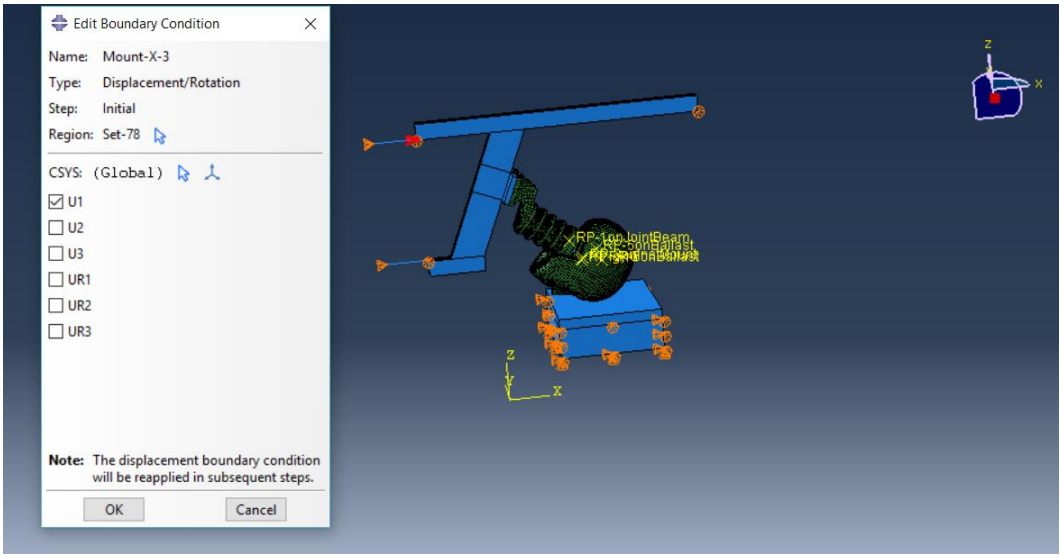

Figure 3.20 Fourth Setting up Picture of BC1

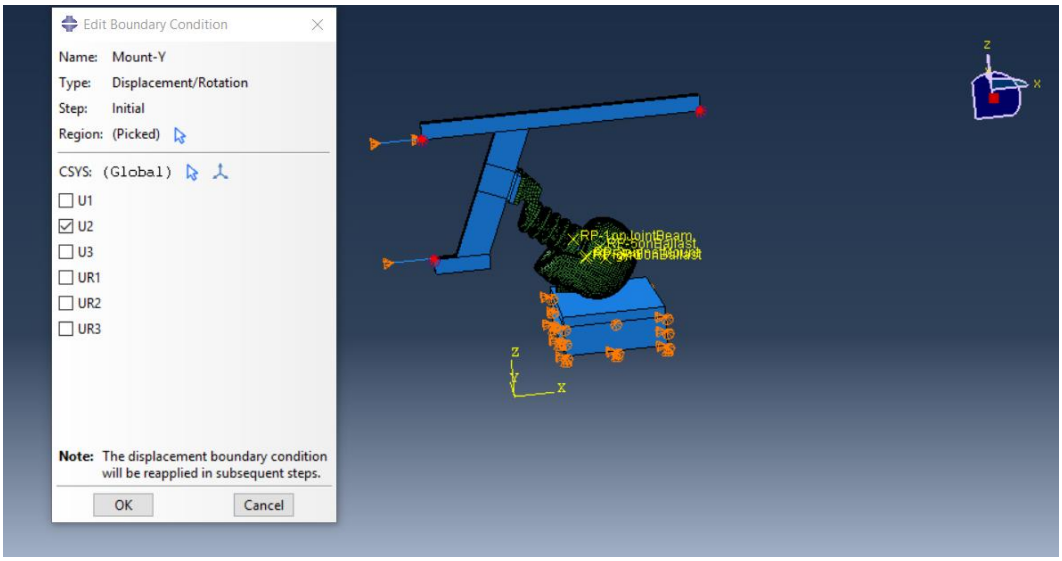

Figure 3.21 Fifth Setting up Picture of BC1

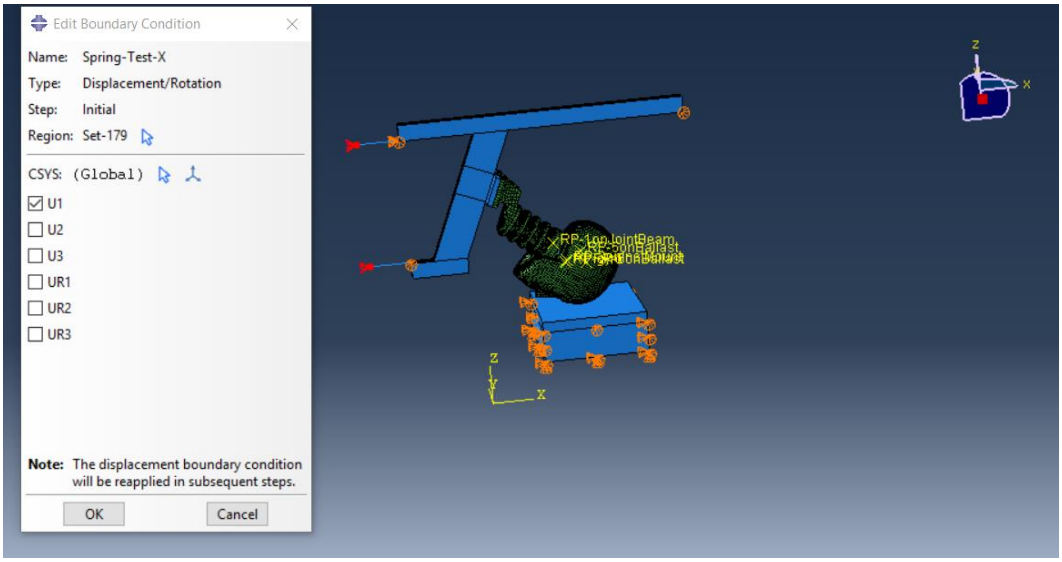

Figure 3.22 Sixth Setting up Picture of BC1

3.3 Materials

Several material models are used in Hybrid III Head-Neck Assembly model. They include the isotropic elastic and hyperelastic materials such as Modular Elastomer Programmer MEP-Mooney, and others are simply elastic such as RubberPad. The material models used for the primary elements are described below.

3.3.1 MEP-Mooney

MEP-Mooney is defined as a hyperelastic material, with 1100 kg/m^3 uniform density and $1*10^{-12}$ Beta damping ratio, and it is used for forming MEP section at the BasePL part as stated in Section 3.2.1. The stiffness of MEP-Mooney is studied here so that its durometer (H) is changed until the coefficients of the

material are evaluated. In addition, Mooney-Rivlin strain energy theory is assumed for the material. Figure 3.23 shows setting the MEP-Mooney coefficients.

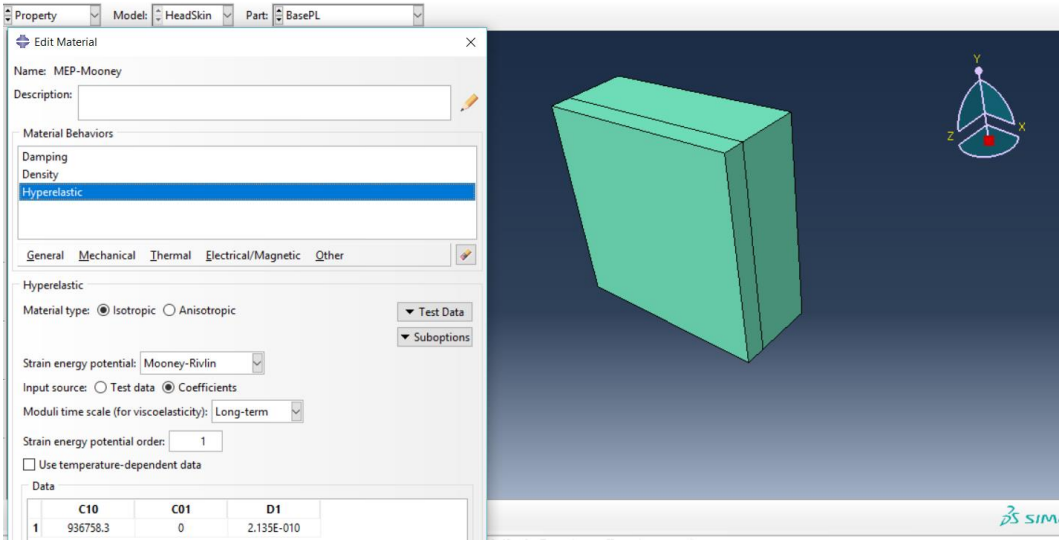

Figure 3.23 How to Set Up MEP-Mooney Stiffness

3.3.2 RubberPad

RubberPad is set up as an isotropic elastic material in the model with 1100 kg/m^3 uniform density and $1*10^{-12}$ Beta damping ratio. Both properties, modulus of elasticity and Poisson's ratio, are studied in this thesis. RubberPad parts are formed from this material as shown in Figures 3.8 and 3.9. Figure 3.24 explains how to set it up.

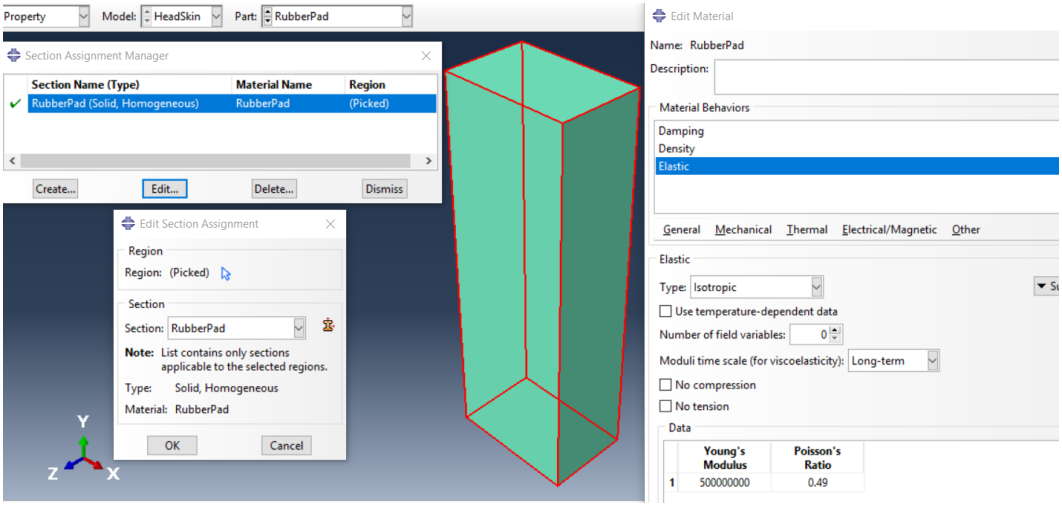

Figure 3.24 Setting up the RubberPad Stiffness

3.3.3 NeckRubber-Mooney

NeckRubber-Mooney material is used in forming the NeckRubber part as explained in Section 3.2.2. It is a hyperelastic material, with 1100 kg/m^3 uniform density and 1*10^{-12} Beta damping ratio, being a various durometer(H) as has studied in this thesis so that the coefficients of the material have been evaluated. Additionally, Mooney-Rivlin theory is assumed for this material. The setting up of different values is shown in Figure 3.25.

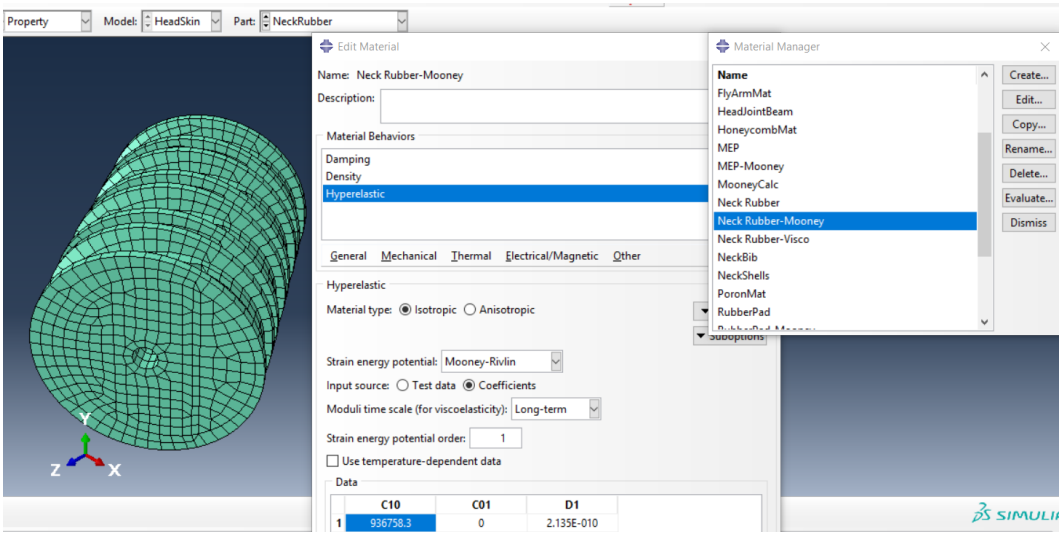

Figure 3.25 NeckRubber-Mooney Material Setting Up

3.3.4 Skin-Rubber-Mooney

Skin-Rubber-Mooney is a hyperelastic material with 1200 kg/m^3 uniform density and 1*10^{-12} Beta damping ratio. Mooney-Rivlin strain energy theory is also assumed for this material. Thus, the invariant coefficients as shown in Figure 3.26 are studied in this thesis. Skin and SkinCap parts are made from this material as observed in Section 3.2.4.

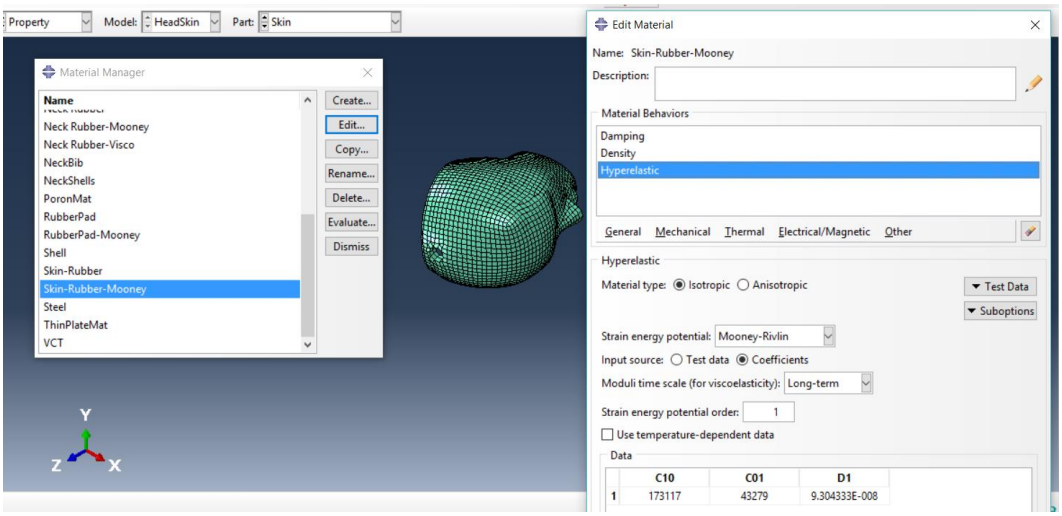

Figure 3.26 Setting of Skin-Rubber-Mooney Material

3.3.5 CableBeam

CableBeam is an isotropic elastic material with 7890 kg/m^3 uniform density and 1*10^{-12} Beta damping ratio. It is used in forming beam parts, especially CableBeam and MPU parts that are studied in this thesis as explained in Section 3.2.5. Figure 3.27 shows how to set up the CableBeam stiffness in MPU part.

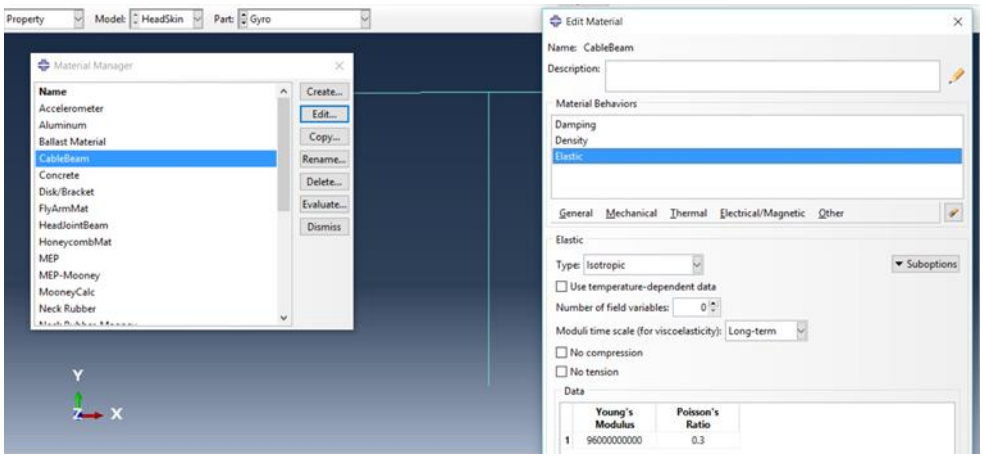

Figure 3.27 MPU Part Stiffness Setting

3.4 Contact Model

In the Hybrid III Head-Neck Assembly model there are numerous contact locations used and the important locations shall only be focused and explained herein. One of them is the frictional surface between the head, especially Skin part surface, and the top surface of the impacted MEP Rubber pad as explained in Section 3.4.2. Another important contact is the behavior of the four NeckRubber parts surfaces against NeckDisk-1 part as shown in Section 3.4.3.

3.4.1 Details for Setting up the Contact Model

The following steps were undertaken for setting up the contact model:

1. Go to Interaction Manager then click on Create to create a new interaction such as General contact (Explicit), Surface-to-surface contact (Explicit). Figure 3.28 shows how to set up the general contact in the model.

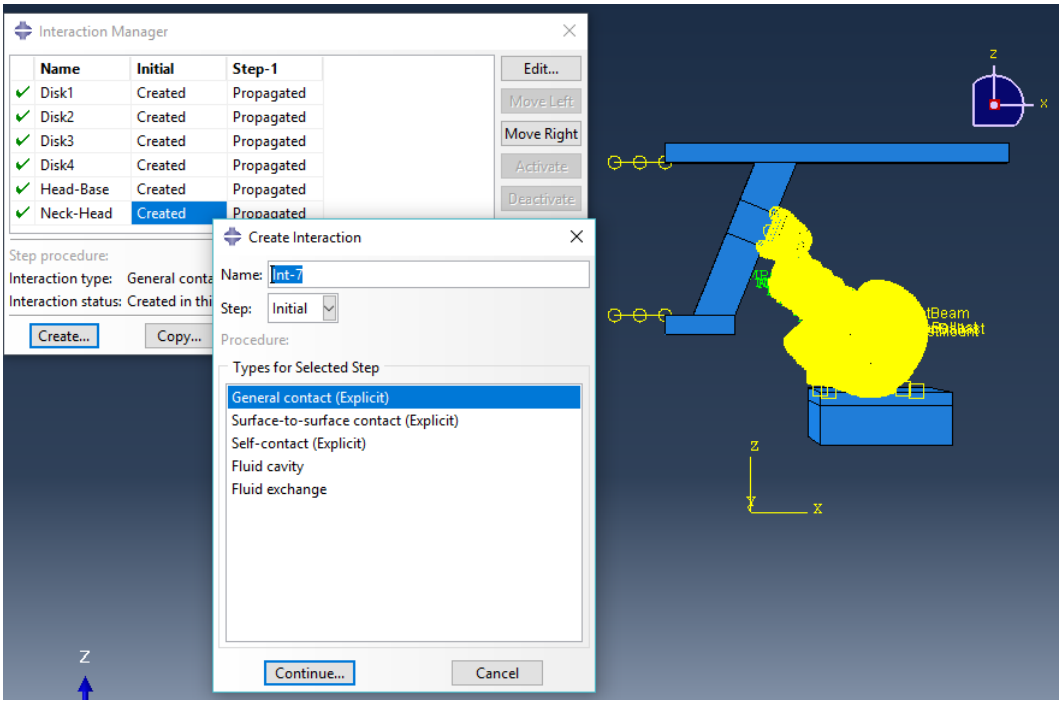

Figure 3.28 How to Create a New Interaction

2. Add a new interaction property that describes the interaction behavior of the model, and it will be used in the first analysis step. Figure 3.29 shows how to set up a new contact property in the model.

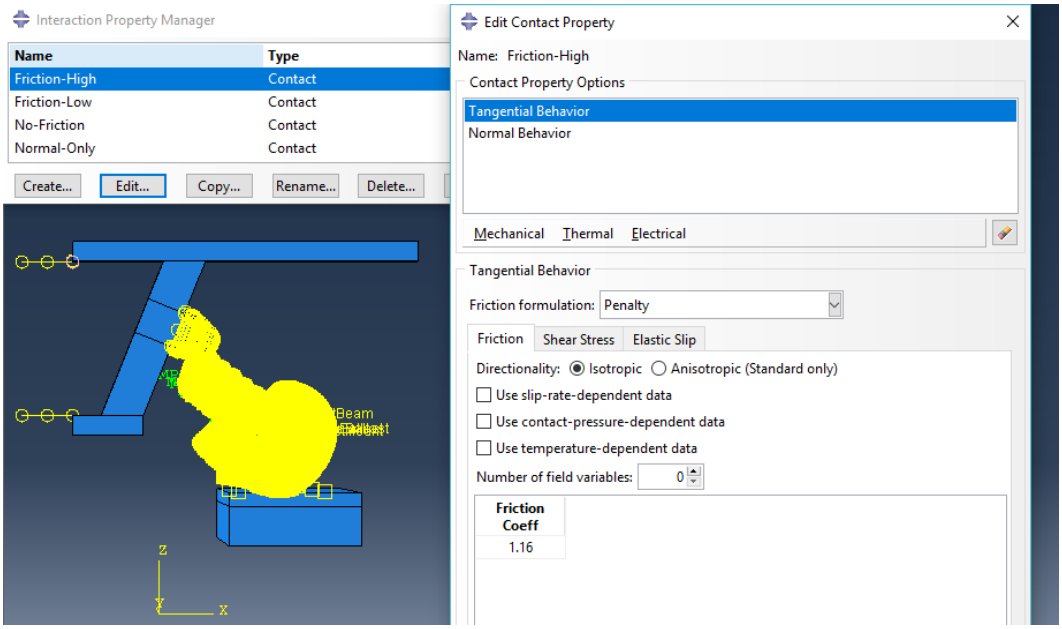

Figure 3.29 How to Set up the Interaction Property

3. Add the constraint properties as needed by using Constraint Manager as shown in Figures 3.30 and 3.31. In this step, we can use the desired behavior in the model such as Tie, Rigid Body, Coupling, etc. as shown clearly in Figure 3.30. Additionally, the Figure 3.32 shows the general contact (Explicit) for the whole model.

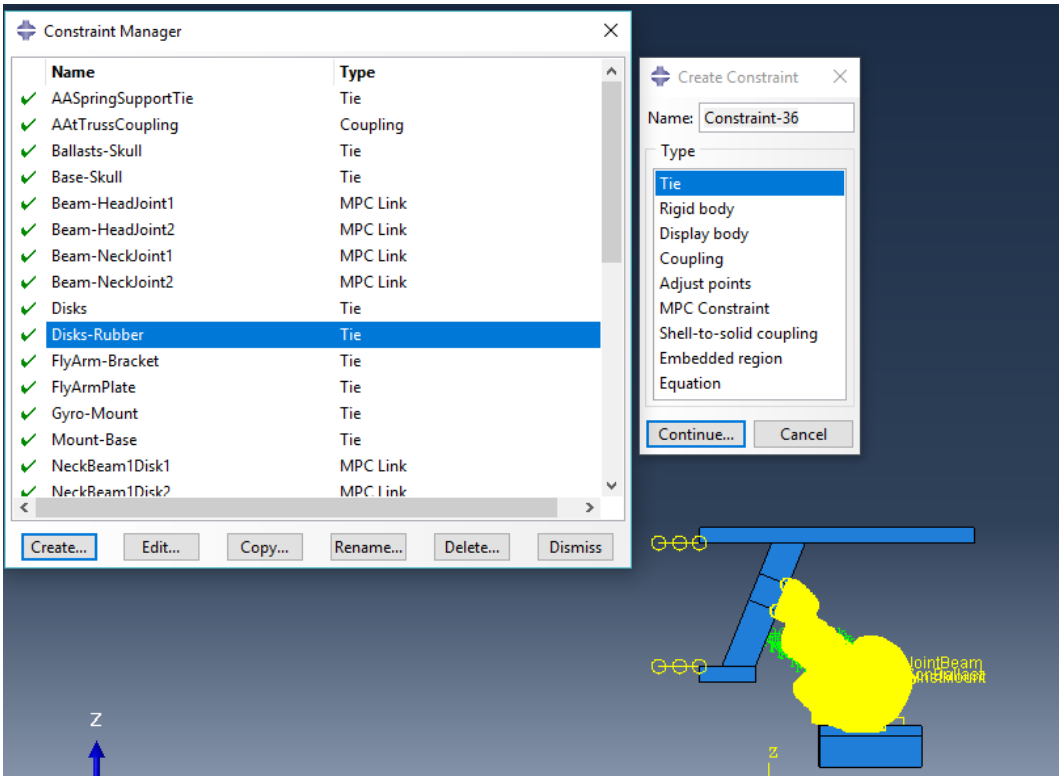

Figure 3.30 How to Create a Constraint Property

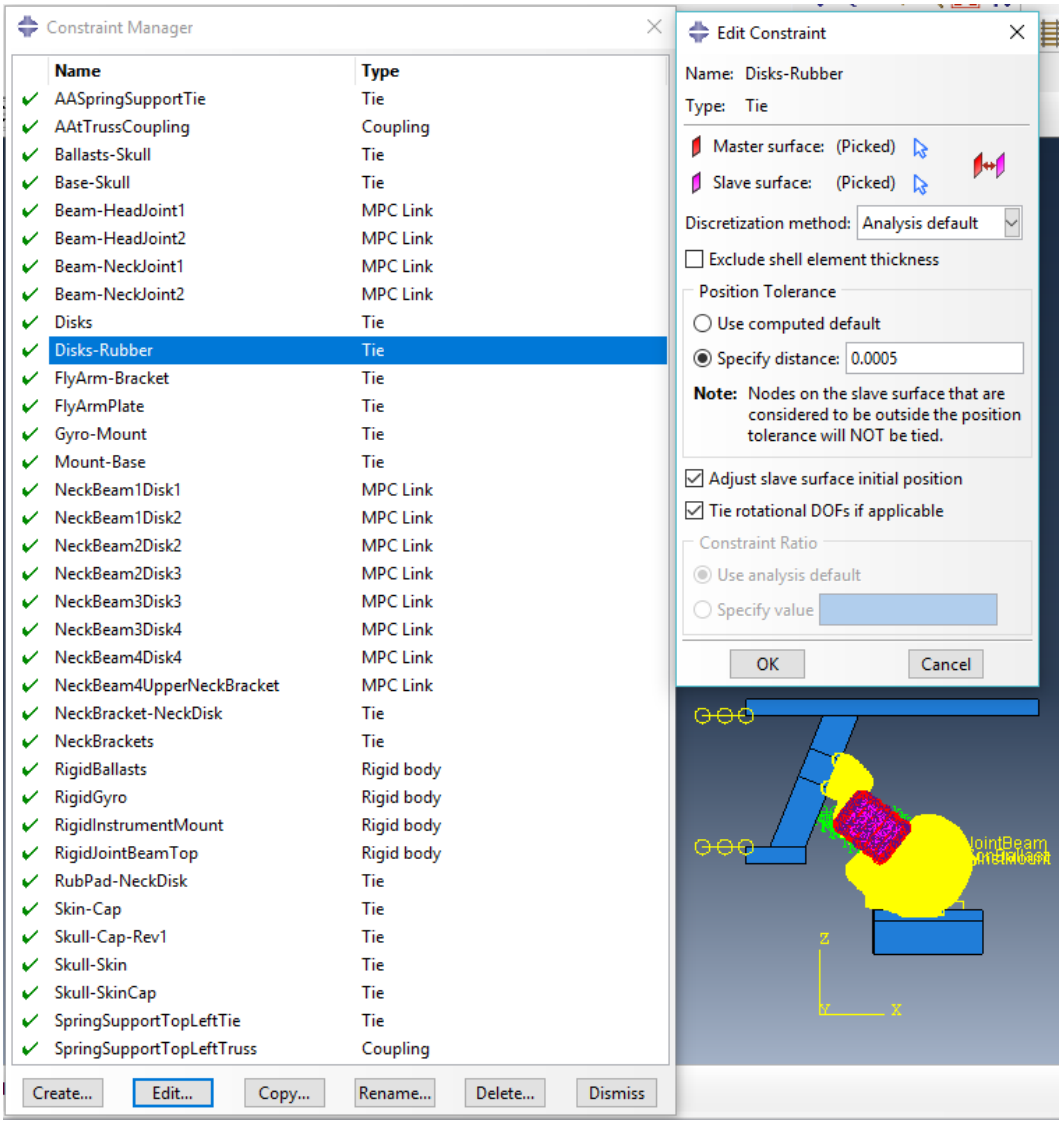

Figure 3.31 How to Set up a Constraint Property

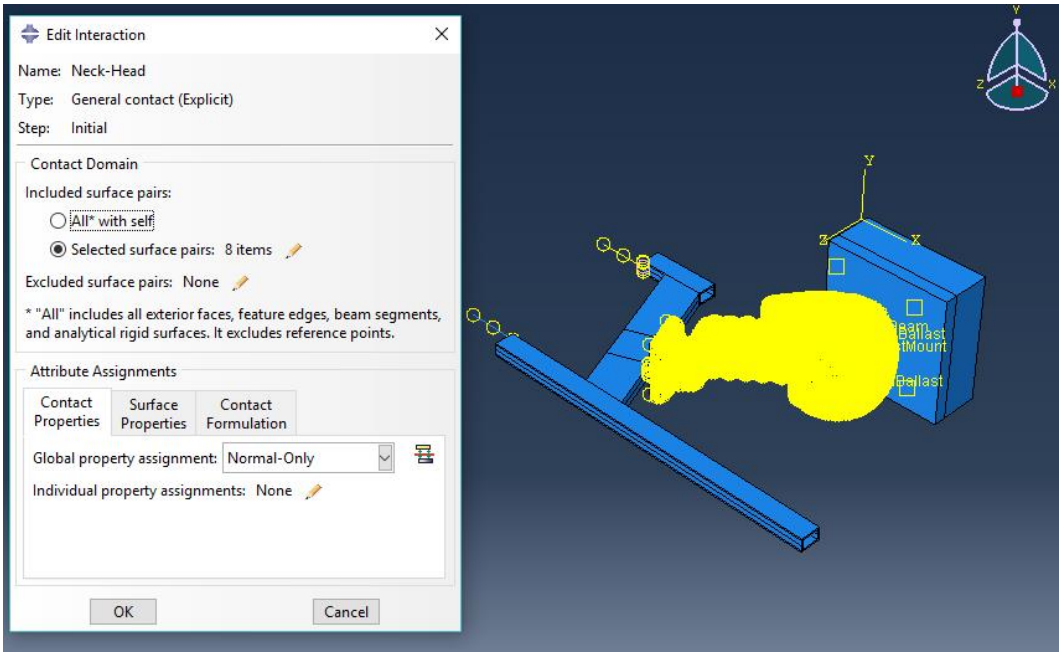

Figure 3.32 Picture of General Contact (Explicit) for the Model

3.4.2 Head-Base Surfaces Contact

The contact interaction of the Head-Base surfaces describes the general behavior of the model during the impact test so that the coefficient of friction between the contact surfaces should be studied and selected to optimize the verification process. The contact surfaces are in two parts, Skin part and BasePl part (it is in contact with the upper MEP Section) as shown in Figure 3.32. In addition, the interaction contact property is set up with mechanical normal behavior as “Hard” Contact and with a constant number of COF (One of the variants of the Model that have studied, for more details, see Section 3.6) for mechanical tangential behavior.

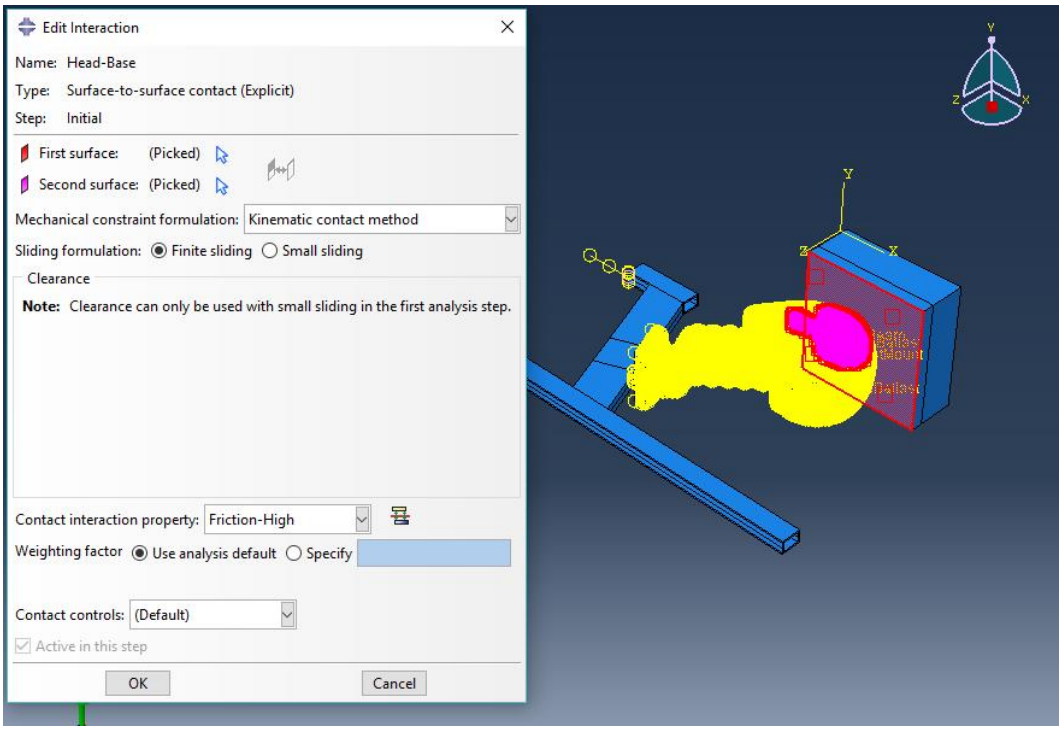

Figure 3.33 Head-Base Contact

3.4.3 NeckRubber-NeckDisk-1 Parts Contact

There are 16 contact surfaces between NeckRubber and NeckDisk-1 parts: slave and master surfaces. Eight are set as slave surfaces (purple) in the NeckRubber part. Otherwise, the master surfaces (red) are set in the NeckDisk-1 part. The constraint property for this interaction is Tie with distance of 0.0005 m specified to trigger the interaction. Figures 3.34 and 3.35 show neck rubber, neck disks and the contact surfaces.

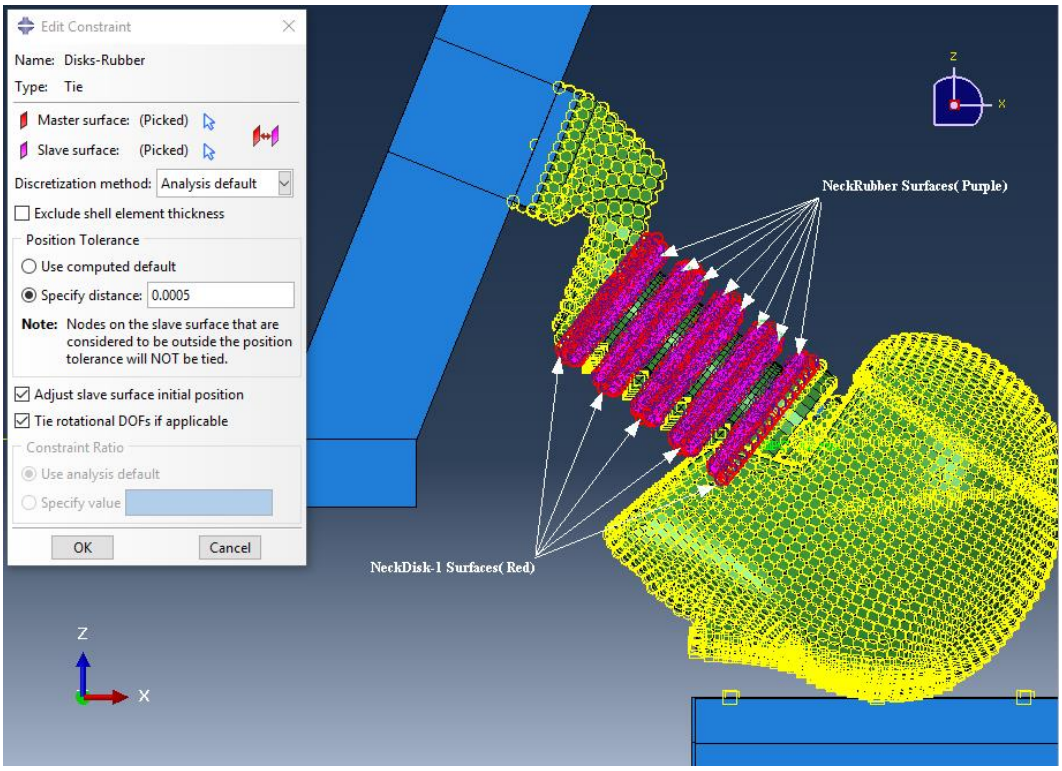

Figure 3.34 NeckRubber-NeckDisk-1 Surfaces Contact

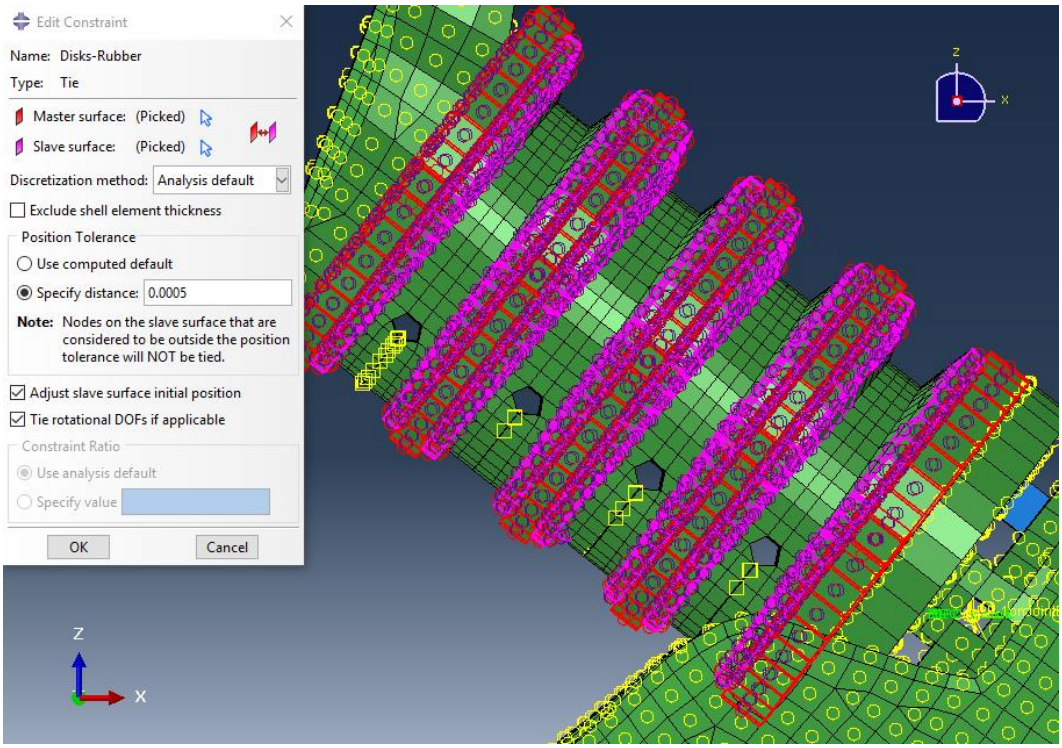

Figure 3.35 Zoomed View of NeckRubber-NeckDisk-1 Surfaces Contact

3.4.4 RubberPad Parts- Contact

RubberPad Parts are directly contacted as shown in Figure 3.9 with two parts, the Base-1 and NeckDisk_Upper-1 parts. The constraint property of this interaction is Tie, and its distance is 0.005 m. Figure 3.36 and 3.37 show more details.

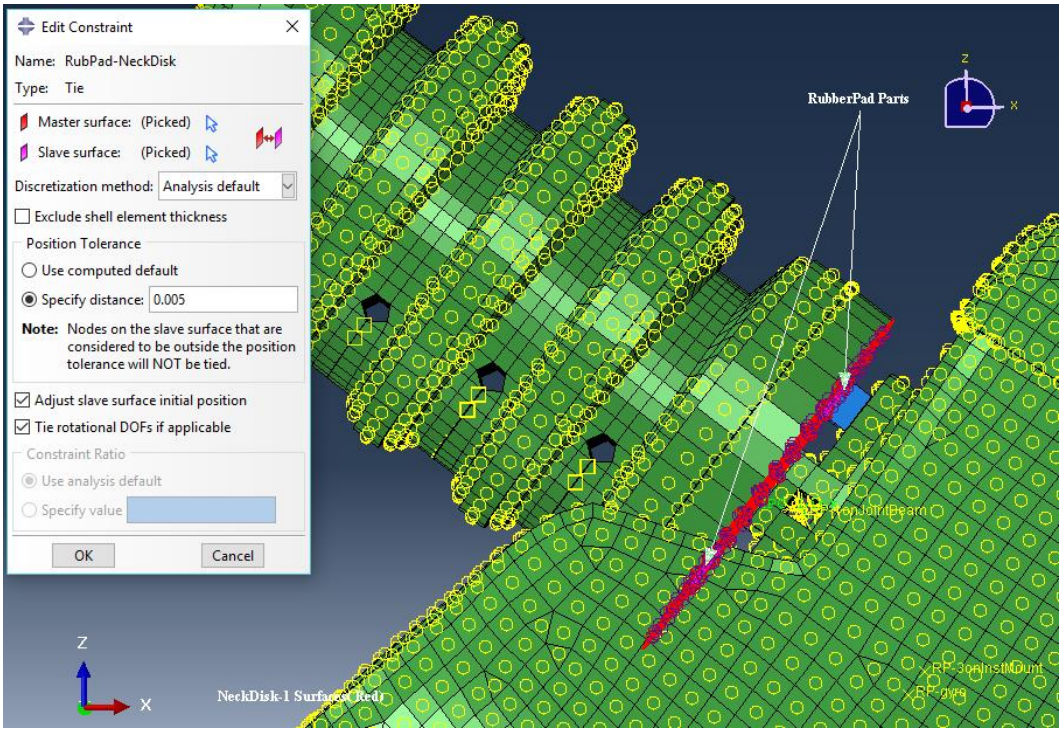

Figure 3.36 RubberPad-NeckDisk_Upper-1 Parts Interaction

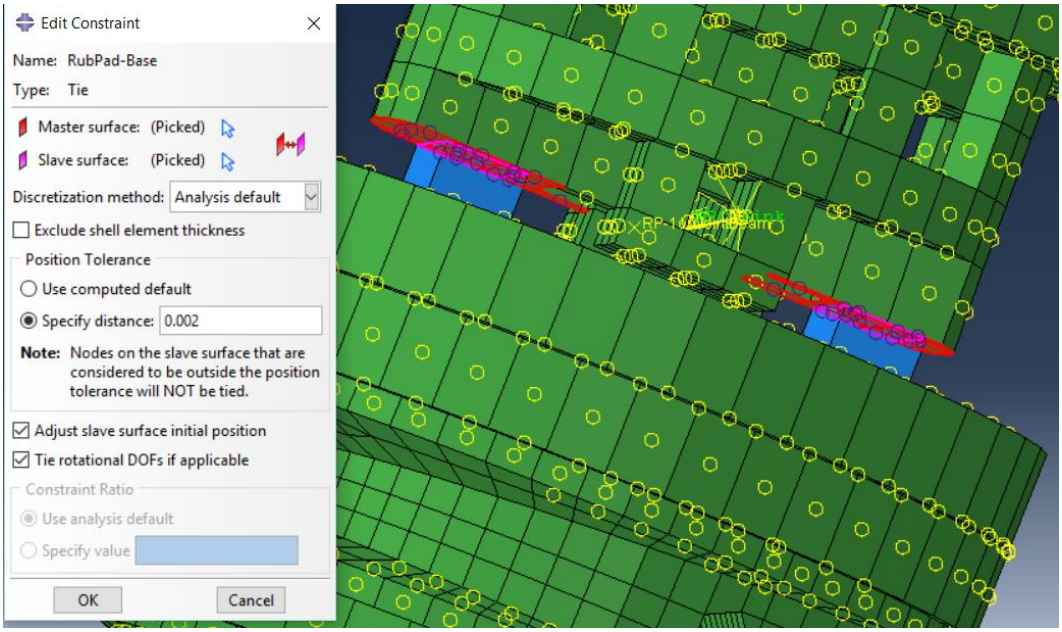

Figure 3.37 RubberPad-Base-1 Parts Interaction

3.5 Explicit Analysis Type

3.5.1 Explicit Time Step Settings

The setting of the output data interval very important in the analysis type so that the following instructions should be pursued in the analysis:

1. Create a new Step to analyze the model, and specify the analysis procedure type by using Step Manager selecting the Dynamic, Explicit type as shown in Figure 3.38. In addition, a 0.01s Time Period is used and the nonlinear geometry option NIgeom is turned on, and automatic increment is selected in this step.

2. Select the output variables and the setting of the domain, frequency, and data output times. Output Field Manager is used for this purpose as shown in Figure 3.39. We have chosen displacement, velocity, and acceleration variables in the model. The model is set to output data exactly at every 1e-5s unit of time.
3. Choose the History Output Requests variables for the analysis history that will be shown in the job file results monitor later. We have selected Energy output variables with 200 intervals as shown in Figure 3.40.
4. Select automatic time step.

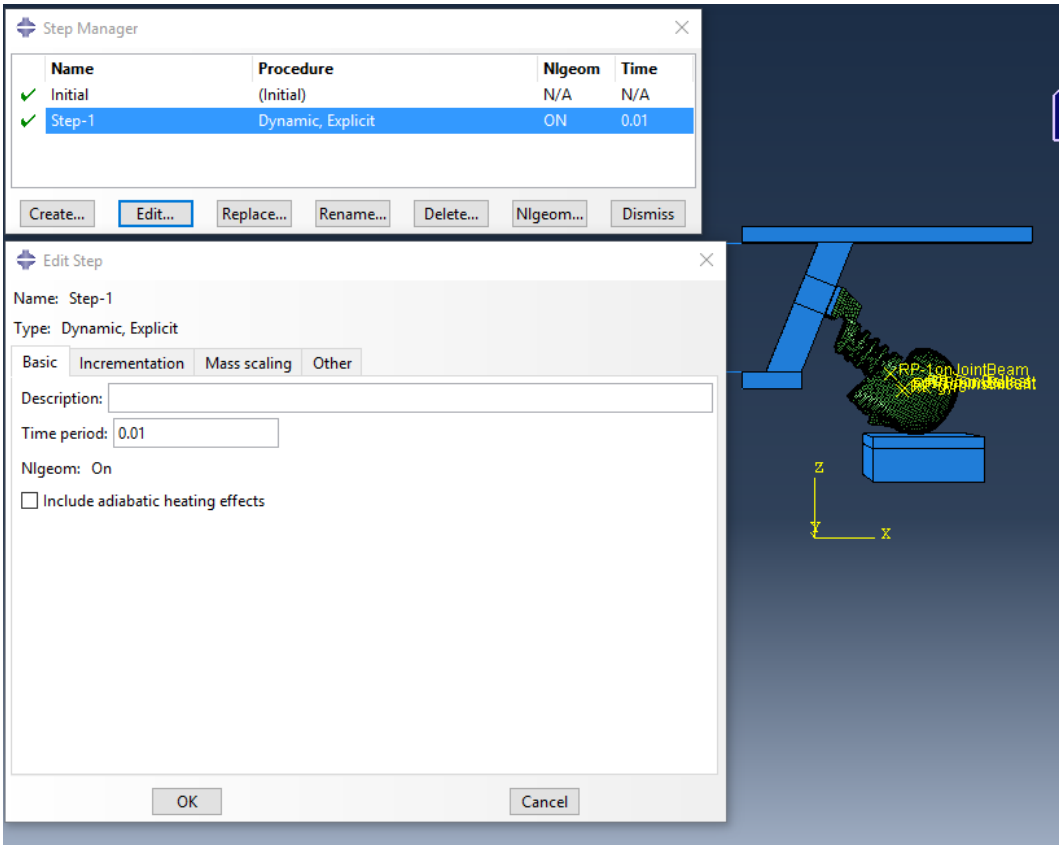

Figure 3.38 Step Manager Setting up

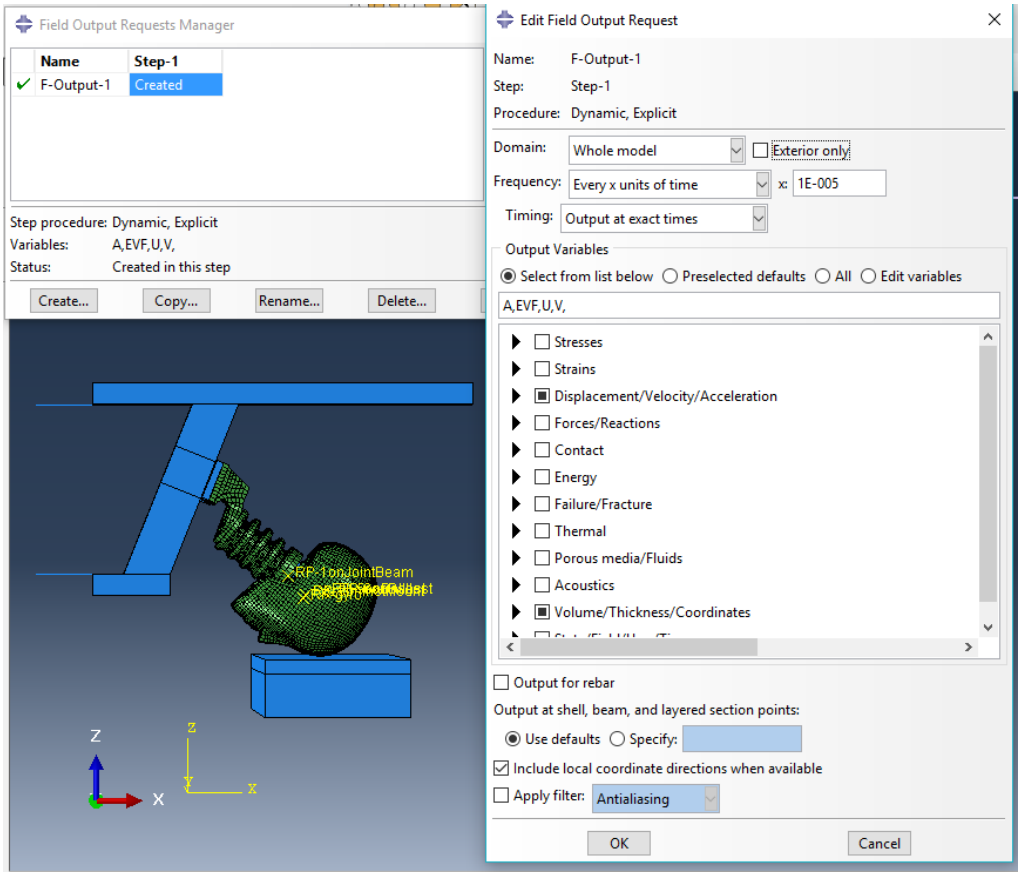

Figure 3.39 Field Output Requests Manager

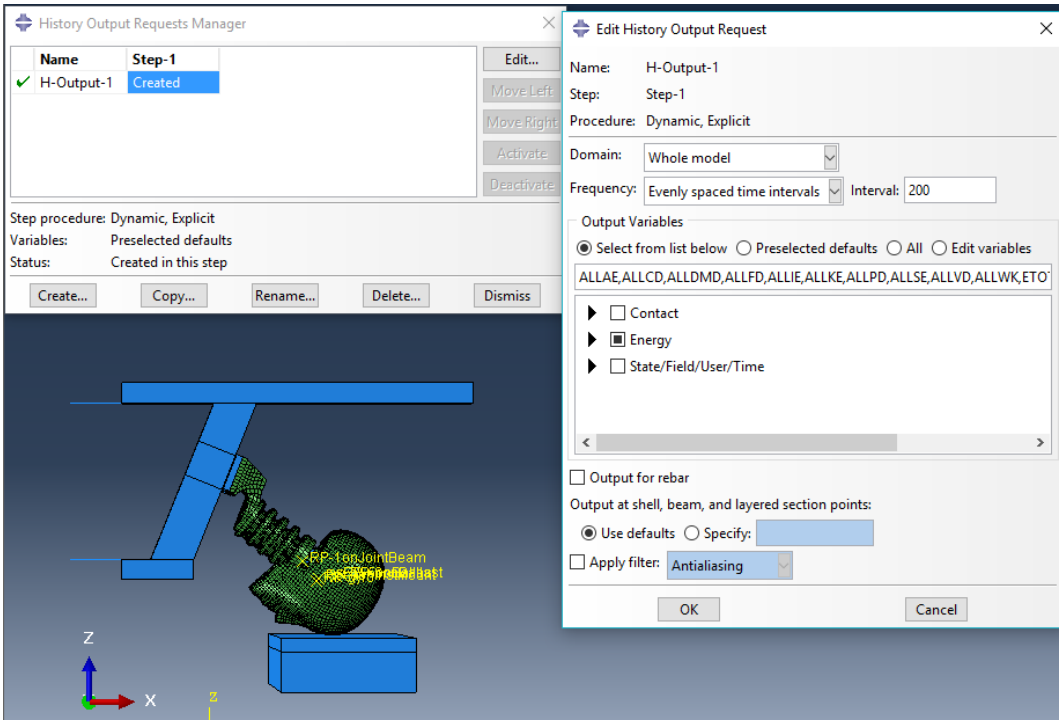

Figure 3.40 History Output Requests Manager

3.5.2 Meshing of Model

Element types, shapes, and procedures of meshing should be compliantly used in the model. For example, we have used Hex-Reduced integration shape, Linear Geometric Order, and Explicit element 3D Stress Element type for meshing control of Skin and SkinCap parts. Another example in the model, Beam Explicit element type with linear order analysis is used in the meshing of MPU and CableBeam parts. Figures 3.41 and 3.42 show more details for meshing some parts that have studied in the model.

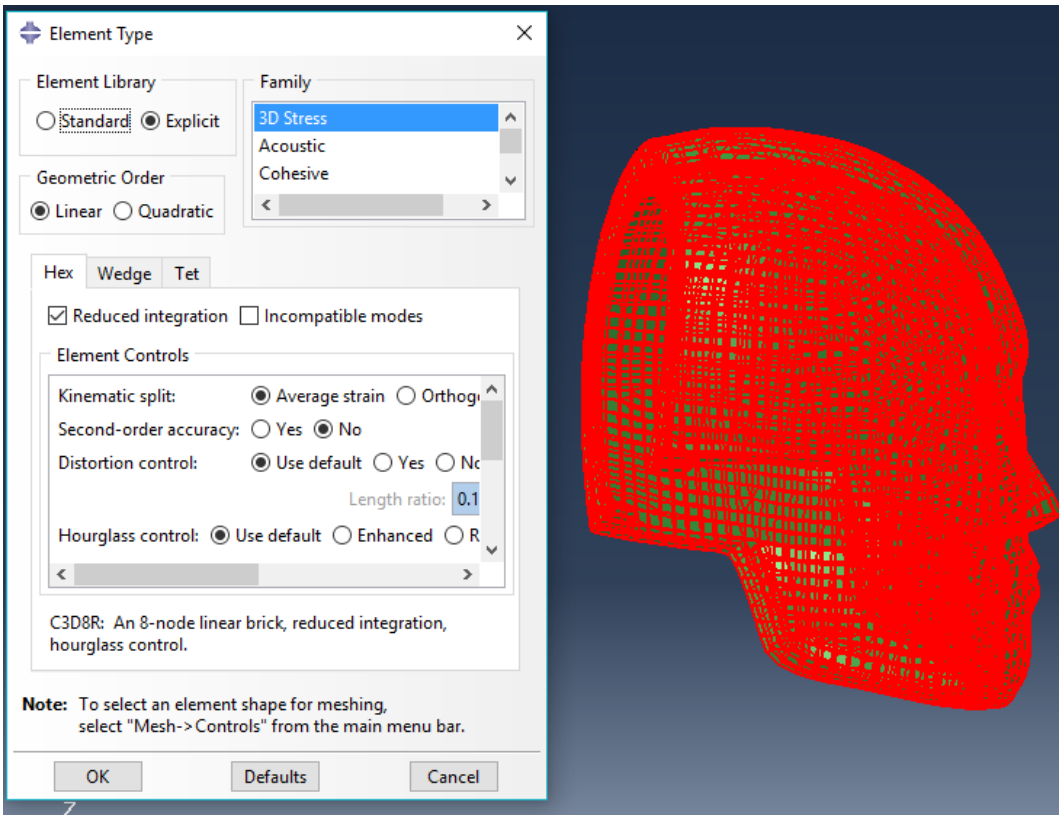

Figure 3.41 Skin Part Meshing

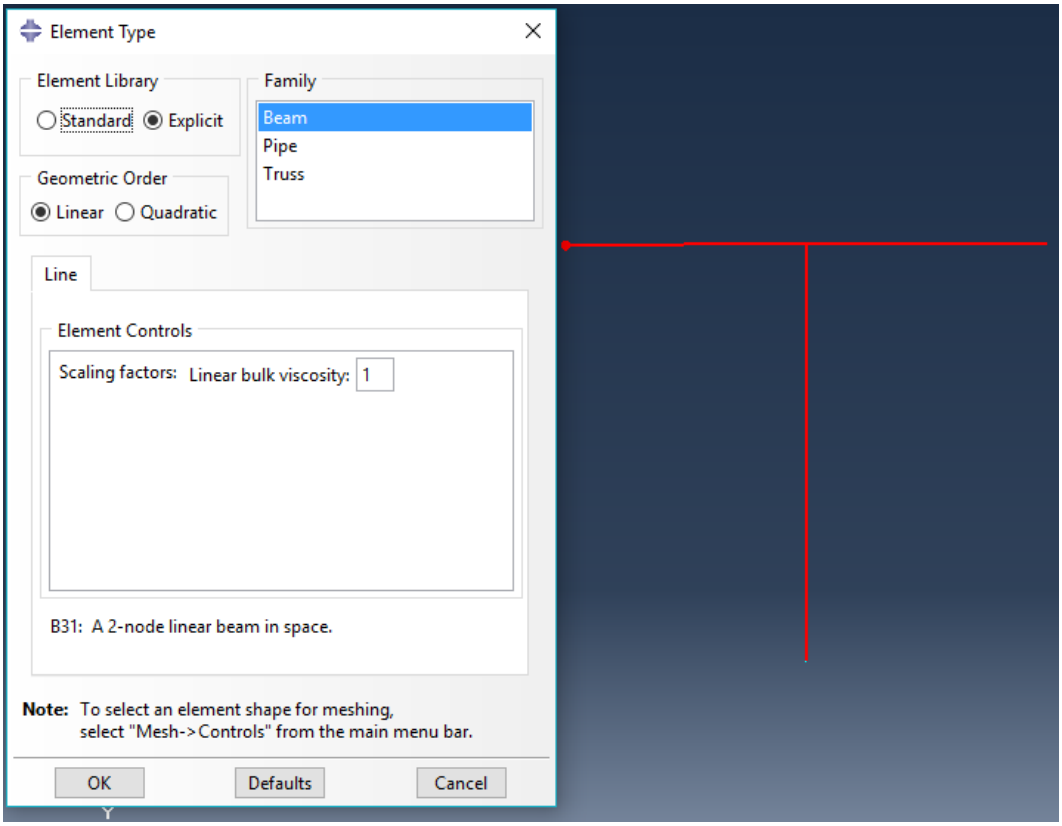

Figure 3.42 MPU Part Meshing

3.5.3 Stable Time Increments

The analysis time of jobs in the model depends on the specification of the computer (Hardware, Processor, etc.) and the server requirements so that we have seen long time for some jobs and short time for other. In the other hand, the performed time also depends on the model analysis setup. The stable Time increment is the primary criterion that controls run time. Some estimated run times are given in the following table. These data are summarized for the parametric studies performed.

Table 3.1 Performed Time and Stable Time Increment for the model

Variant Name	Variant Quantity	Performed Time, Minutes	Stable Time Increment, Seconds
CableBeam	1GPa Section 3.6.8	155	2.29E-08
	10GPa Section 3.6.8	157	2.29E-08
	36.71GPa Section 3.6.8	151	2.29E-08
	50GPa Section 3.6.8	147	2.11E-08
	80GPa Section 3.6.8	197	1.67E-08
	210GPa Section 3.6.8	245	1.03E-08
	294.61GPa Section 3.6.8	248	8.68E-08
	80GPa, COF0.35 Section 3.6.8	246	1.67 E-08
COF	1 See Section 3.6.4	232	1.52E-08
	0.8 See Section 3.6.4	230	1.52E-08
	0.5 See Section 3.6.4	410	1.52E-08
	Zero See Section 3.6.8	260	1.52E-08
	0.25 See Section 3.6.8	235	1.52E-08
	0.5 See Section 3.6.8	226	1.51E-08
	0.75 See Section 3.6.8	269	1.52E-08
BC	BC2 See Section 3.6.6	281	1.52E-08
	BC3 See Section 3.6.6	184	1.52E-08
	BC4 See Section 3.6.6	229	1.52E-08
	BC5 See Section 3.6.6	303	1.52E-08
Skin-Rubber-Mooney	67.61GPa See Section 3.6.7	222	1.52E-08
	48 GPa See Section 3.6.7	231	1.52E-08
Neck Rubber-Mooney	60 GPa See Section 3.6.5	220	1.53E-08
	65 GPa See Section 3.6.5	210	1.53E-08
	67.61 GPa See Section 3.6.5	250	1.54E-08
	70 GPa See Section 3.6.5	230	1.52E-08
RubberPad and MEP Mooeny	55.5 E500 v0.49 See Table 3.5	208	1.52E-08
	55.5 E450 v0.45 See Table 3.5	210	1.52E-08
	55.5 E400 v0.45 See Table 3.5	215	1.52E-08
	56 E450 v0.45 See Table 3.5	229	1.52E-08
	60 E450 v0.45 See Table 3.5	219	1.52E-08
	60 E400v0.45 See Table 3.5	211	1.52E-08
	65.5 E500v0.49 See Table 3.5	227	1.52E-08
	65.5 E450v0.45 See Table 3.5	217	1.52E-08
	65.5 E400v0.45 See Table 3.5	212	1.52E-08

3.6 Analysis Results

The results from the Finite Element Analysis FEA for Hybrid Head-Neck Assembly consisted of mainly the translational and angular accelerations of the headform caused by the impact. Due to the noise in the acceleration output results, both accelerations are evaluated by two ways. The first way is directly computed from equation (3.4) using the output acceleration data file. The other way is by taking square root of the sum of the squares of the time derivative of linear velocity and angular velocity outputs to evaluate translational and angular acceleration respectively as shown in equation (3.5).

$$a(t) = \sqrt{a_1^2 + a_2^2 + a_3^2} \tag{3.4}$$

$$a(t) = \sqrt{\frac{dv_1}{dt}^2 + \frac{dv_2}{dt}^2 + \frac{dv_3}{dt}^2} \tag{3.5}$$

Where: a = resultant translational acceleration in g's or resultant angular acceleration in rad/s^2

a_1, a_2, and a_3 = components of the translational in g's or angular acceleration in rad/s^2 respect to x, y, and z-axis respectively

$\frac{dv_1}{dt}$, $\frac{dv_2}{dt}$, and $\frac{dv_3}{dt}$ = derivative with respect to time of the components of the translational velocity in g's or angular velocity in rad/s^2 respect to x, y, and z-axis respectively

t = impact duration in seconds

According to equations (3.4) and (3.5), four accelerations are calculated: two translational accelerations and two angular accelerations. For translational acceleration, usually, there are little differences between the two methods used for evaluation, especially the peak acceleration. Thus, the resultant that obeys to the first equation (3.4) has been taken for the given results. The following Figures and the table are shown that.

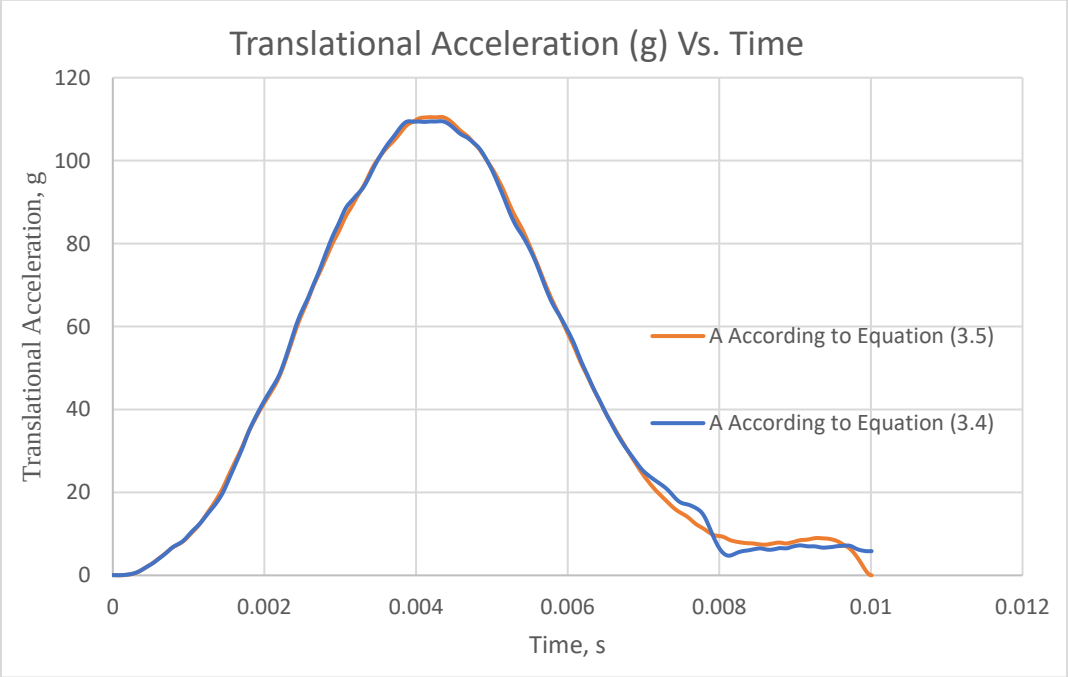

Figure 3.43 Sample Figure of the Differences Between Translational Acceleration Calculations According to the Equations (3.4) and (3.5)

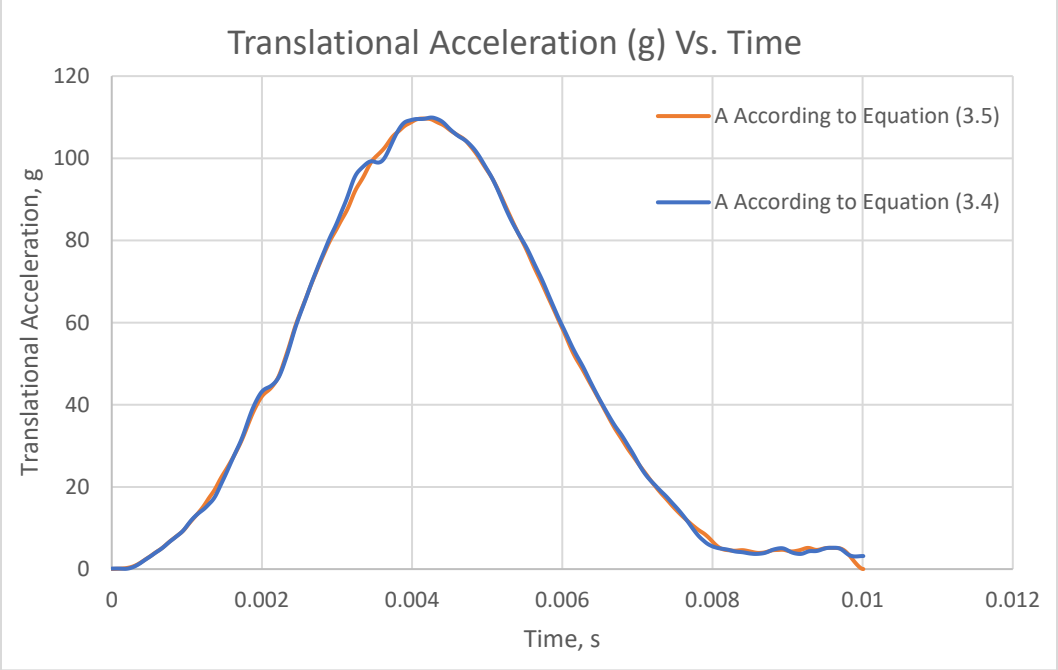

Figure 3.44 Another Sample Figure Shows the Differences Between the Two Ways that Calculate the Translational Acceleration

Table 3.2 Sample Table Shows the Differences Between the Two Ways Calculations

Study of E Beam(Gpa) Changing	**Translational $A_{according\ to\ Equation\ (3.4)}$**	**Translational $A_{according\ to\ Equation\ (3.5)}$**	**Angular $A_{according\ to\ Equation\ (3.4)}$**	**Angular $A_{according\ to\ Equation\ (3.5)}$**
1	109.51	110.52	5143.97	3598.44
10	111.48	112.02	6385.98	4390.15
36.71	110.73	111.02	5488.77	3597.13
50	111.3	111.7	5574.77	4391.06
80	109.92	109.67	6400.07	3576.79
96	109.29	109.76	4901.82	3722.12
210	113.47	111.92	5739.79	4384.49
294.61	112.76	107.91	5079.81	3839.8
80	111.8	110.27	4395.13	3701.1

For angular acceleration calculations, there is considerably more noise in the acceleration output, the difference between the two methods is significant, particularly the peak angular acceleration resultant. Table 3.2 and Figure 3.46 shows clearly the noise on the output data set.

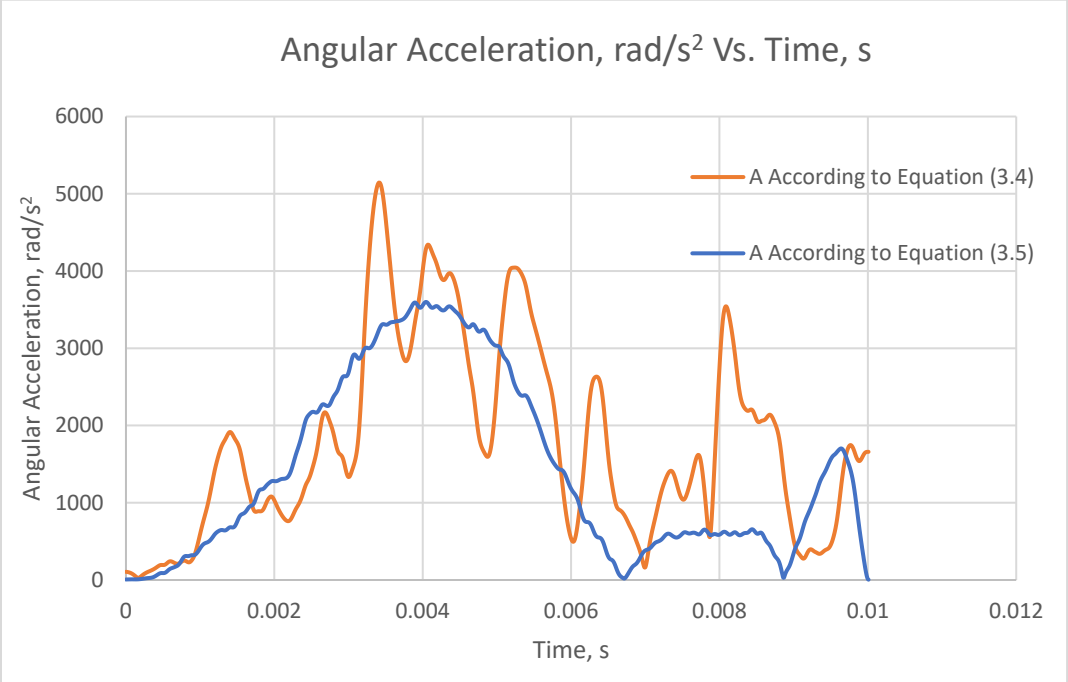

Figure 3.45 Sample Figure Shows the Differences Between the Two Ways Angular Acceleration Calculations

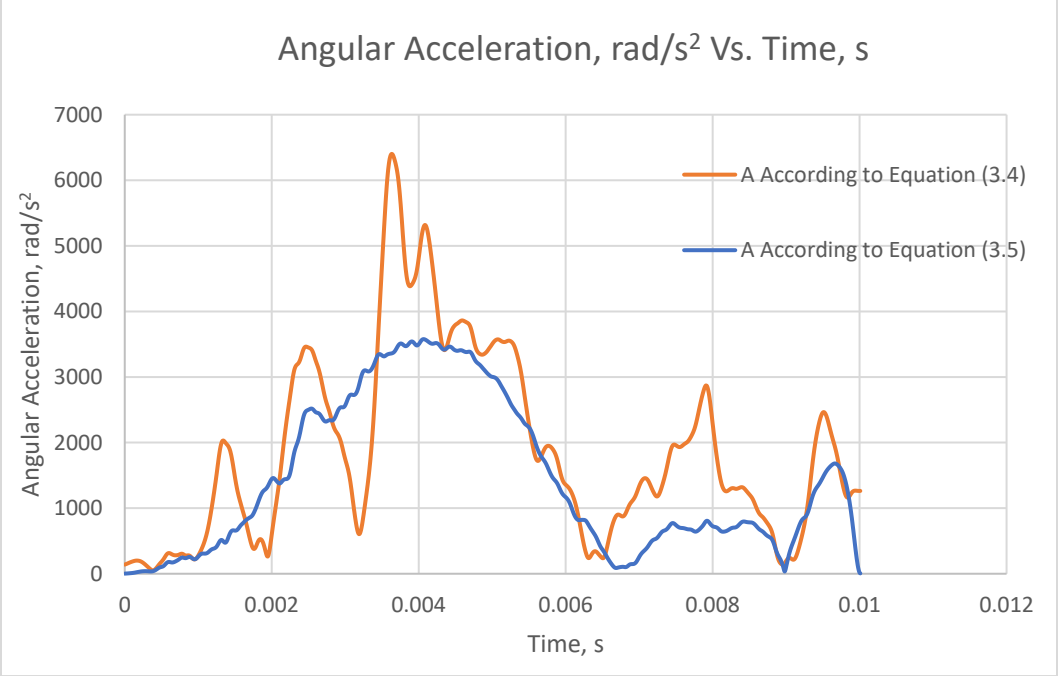

Figure 3.46 Another Sample Figure Shows the Two Ways to Calculate the Angular Acceleration

3.6.1 Analysis Variants

The results for the head neck assembly impact are dependant on the changing of essential variants of Hybrid Head-Neck Assembly model. These variants are summarized in the following table.

Table 3.3 Initial Properties Used as a Baseline for the Variants

Name of Variant	Quantity of Variant	Variant Related with
MEP-Mooney Material Stiffness	C_{10}= 0.503 MPa	MEP-BasePL Part
	C_{01}= 0.126 MPa	
	D_1= 32.037 GPa^{-1}	
Modulus of Elasticity for RubberPad material, Mpa	500	RubberPad Part
Poisson's Ratio for RubberPad Material	0.49	RubberPad Part
Coefficient of Friction	1.16	Head-Base Contact Surfaces
Neck Rubber-Mooney Material Stiffness	C_{10}= 0.503 MPa	NeckRubber Part
	C_{01}= 0.126 MPa	
	D_1= 32.037 GPa^{-1}	
Boundary Conditions	BC1	See Section 3.2.6
Skin-Rubber-Mooney Material Stiffness	C_{10}= 0.329 MPa	Skin and SkinCap Parts
	C_{01}= 0 MPa	
	D_1= 0.607 GPa^{-1}	
Shape of Cross-Sectional Area for Cable Beam Part	Squared, 30 mm^2	CableBeam and MPU Parts
Modulus of Elasticity for Cable Beam Material, Gpa	96	CableBeam and MPU Parts

3.6.2 MEP-Mooney Material Stiffness

For study of the MEP pad stiffness the Hybrid III Head-Neck Assembly properties are set up as shown in Table 3.4. The invariants of the MEP- Mooney material has been taken from the MEP-Rubber Pad study, and then the durometer was changed by changing the variants respectively as shown in the results table.

3.6.3 RubberPad Material Stiffness

RubberPad material stiffness and its Poisson's ratio are studied combined with MEP- Mooney stiffness as shown in the following table. As mentioned above, the model should set up with the data at the following table, and the study would start up.

Table 3.4 Setting up the Hybrid III Head- Neck Assembly Model Tests For MEP-Mooney and RubberPad Materials Study

Name of Variant	Quantity of Variant	Variant Related with
MEP-Mooney Material Stiffness	C_{10}= Varies	MEP-BasePL Part
	C_{01}= 0	
	D_1= Varies	
Modulus of Elasticity for RubberPad material, Mpa	Varies	RubberPad Part
Poisson's Ratio for RubberPad Material	Varies	RubberPad Part
Coefficient of Friction	1.16	Head-Base Contact Surfaces
Neck Rubber-Mooney Material Stiffness	C_{10}= 0.503 MPa	NeckRubber Part
	C_{01}= 0.126 MPa	
	D_1= 32.037 GPa^{-1}	
Boundary Conditions	BC1	See Section 3.2.6
Skin-Rubber-Mooney Material Stiffness	C_{10}= 0.329 MPa	Skin and SkinCap Parts
	C_{01}= 0 MPa	
	D_1= 0.607 GPa^{-1}	
Shape of Cross Sectional Area for Cable Beam Part	Squared, 30 mm^2	CableBeam and MPU Parts
Modulus of Elasticity for Cable Beam Material, Gpa	96	CableBeam and MPU Parts

The study for MEP-Mooney stiffness and RubberPad material has been done with the following results at this table.

Table 3.5 MEP-Mooney Stiffness and RubberPad Material Results

$E_{RubberPad}$, Mpa	Poisson 's Ratio	MEP Mooney Durometer (H), GPa	C_{10}, MPa	D_1, GPa^{-1}	Translational Acceleration, g	Angular Acceleration, rad/s^2
500	0.49	55.5	0.491	0.407	97.24	3249
450	0.45	55.5	0.491	0.407	98.30	3374
400	0.45	55.5	0.491	0.407	96.91	3254
450	0.45	56	0.504	0.397	98.37	3278
450	0.45	60	0.624	0.32	102.47	3393
400	0.45	60	0.624	0.32	102.69	3442
500	0.49	65	0.815	0.245	108.42	3725
450	0.45	65	0.815	0.245	109.49	3737
400	0.45	65	0.815	0.245	106.86	3656

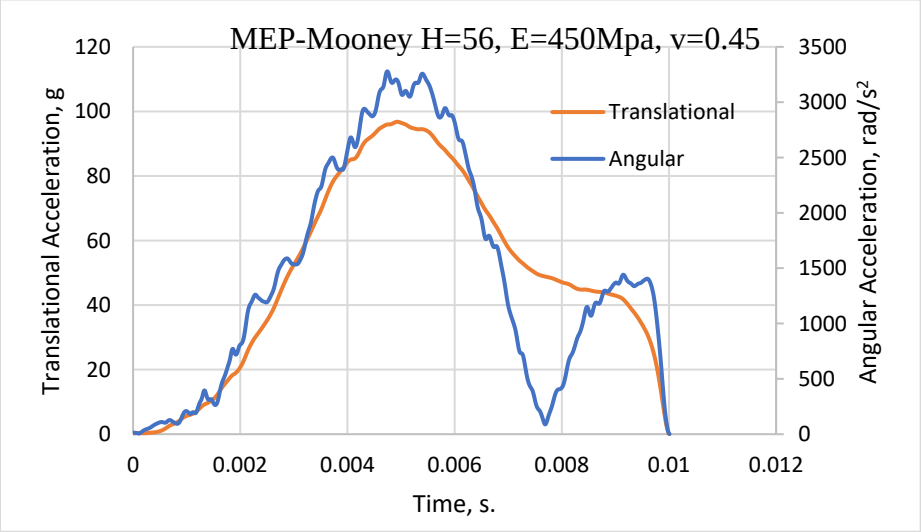

Figure 3.47 Acceleration Versus Time Results for First Case MEP-Mooney Durometer H = 56, E = 450Mpa, v = 0.45

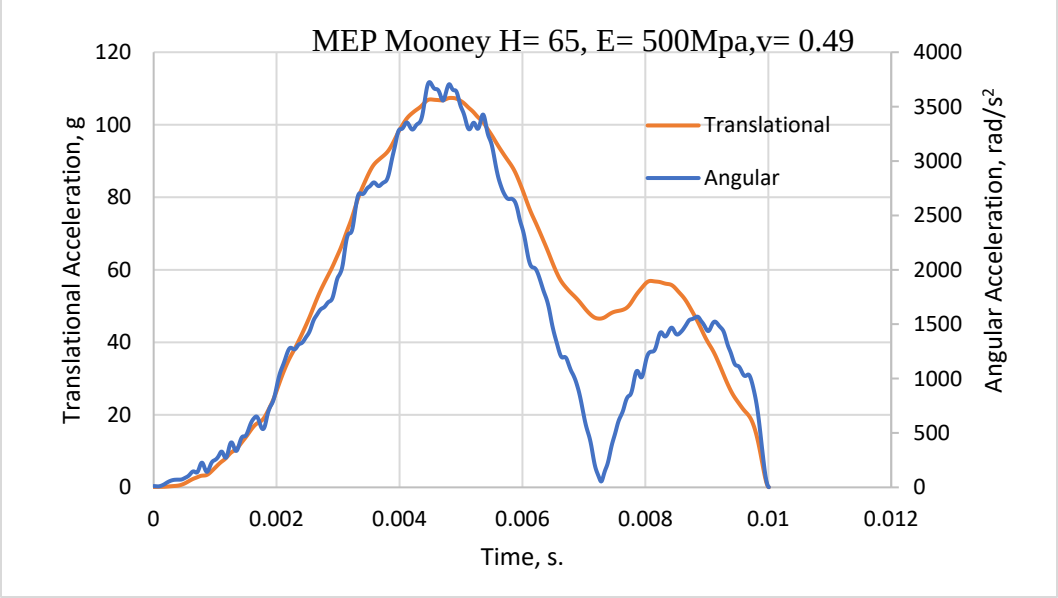

Figure 3.48 Acceleration Versus Time for Last Case MEP-Mooney Durometer

H = 65, E = 500Mpa, v = 0.49

3.6.4 Coefficient of Friction

The Coefficient of Friction (COF) effect study was set up as shown in Table 3.6. The results are shown in Table 3.7 and Figures 3.50 and 3.51. In addition to this study, we have studied the coefficient of friction effects again in Section 3.6.8 in relation to the cable beam properties.

Table 3.6 The Setup for the COF Study

Name of Variant	**Quantity of Variant**	**Variant Related with**
MEP-Mooney Material Stiffness	C_{10}= 0.815 MPa	MEP-BasePL Part
	C_{01}= 0	
	D_1= 0.245 GPa^{-1}	
Modulus of Elasticity for RubberPad material, Mpa	500	RubberPad Part
Poisson's Ratio for RubberPad Material	0.49	RubberPad Part
Coefficient of Friction	Varies	Head-Base Contact Surfaces
Neck Rubber-Mooney Material Stiffness	C_{10}= 0.503 MPa	NeckRubber Part
	C_{01}= 0.126 MPa	
	D_1= 32.037 GPa^{-1}	
Boundary Conditions	BC1	See Section 3.2.6
Skin-Rubber-Mooney Material Stiffness	C_{10}= 0.33 MPa	Skin and SkinCap Parts
	C_{01}= 0 MPa	
	D_1= 0.607 GPa^{-1}	
Shape of Cross-Sectional Area for Cable Beam Part	Square, 30 mm^2	CableBeam and MPU Parts
Modulus of Elasticity for Cable Beam Material, GPa	96	CableBeam and MPU Parts

Table 3.7 Results of Coefficient of Friction Study

Coefficient of Friction COF	Translational Acceleration, g	Angular Acceleration, rad/s^2
1.16	108.42	3725
1	108.59	3698
0.8	109.12	3721
0.5	108.09	3807

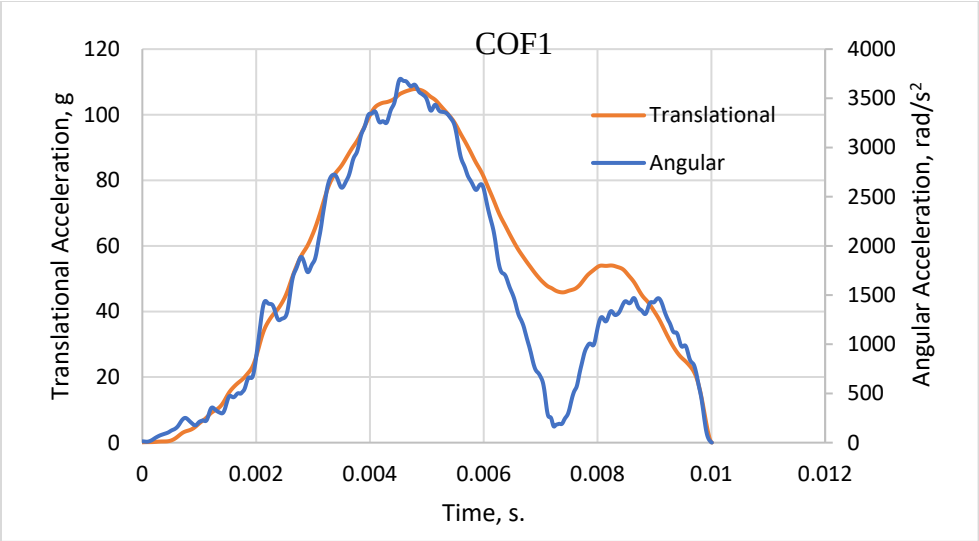

Figure 3.49 Acceleration Versus Time for COF Equal to 1 Testing

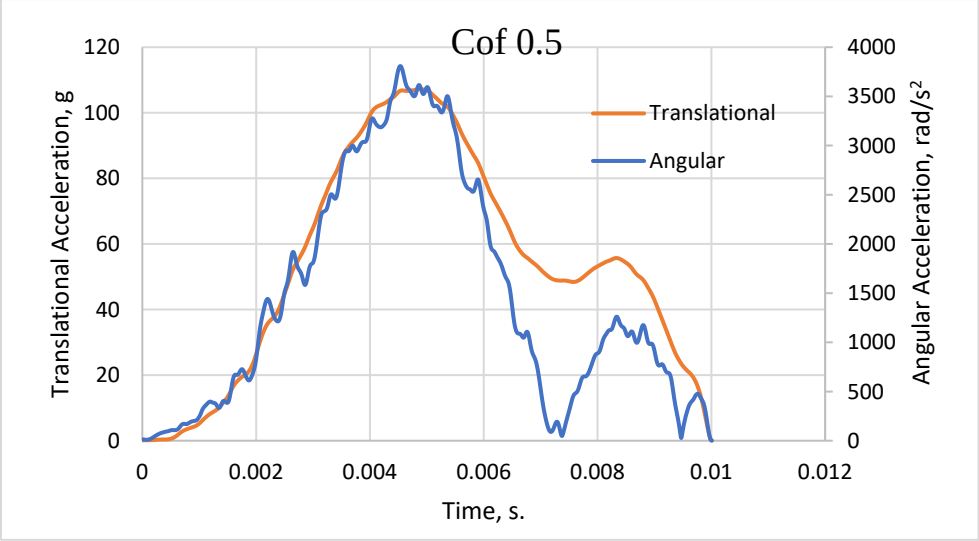

Figure 3.50 Acceleration Versus Time for COF Equal to 0.5 Testing

3.6.5 Neck Rubber-Mooney Material

In this study, the properties of the neck rubber are varied and we have set up the Hybrid III Head- Neck Assembly model by the variants data as shown in Table 3.8. The Neck Rubber-Mooney invariants and MEP Mooney invariants are changed for each test as they were given the same value during each run based upon the selected durometer value. The results of this study are shown in Figures 3.52,3.53, and 3.54 and Table 3.9.

Table 3.8 Setting up Neck Rubber-Mooney Study

Name of Variant	Quantity of Variant	Variant Related with
MEP-Mooney Material Stiffness	C_{10}= Varies	MEP-BasePL Part
	C_{01}= 0	
	D_1= Varies	
Modulus of Elasticity for RubberPad Material, Mpa	500	RubberPad Part
Poisson's Ratio for RubberPad Material	0.49	RubberPad Part
Coefficient of Friction	1	Head-Base Contact Surfaces
Neck Rubber-Mooney Material Stiffness	C_{10}= Varies	NeckRubber Part
	C_{01}= 0	
	D_1= Varies	
Boundary Conditions	BC1	See Section 3.2.6
Skin-Rubber-Mooney Material Stiffness	C_{10}= 0.33 MPa	Skin and SkinCap Parts
	C_{01}= 0 MPa	
	D_1= 0.607 GPa^{-1}	
Shape of Cross Sectional Area for Cable Beam Part	Squared, 30 mm^2	CableBeam and MPU Parts
Modulus of Elasticity for Cable Beam Material, Gpa	96	CableBeam and MPU Parts

Table 3.9 Neck Rubber Mooney Study Results

Durometer of Neck Rubber-Mooney and MEP Mooney, MPa	C_{10}, MPa	D_1, GPa^{-1}	Translational Acceleration, g	Angular Acceleration, rad/s^2
60	0.624	0.32	101.39	3517
65	0.815	0.245	105.52	3647
67.61	0.937	0.214	109.02	3840
70	1.064	0.188	111.96	3953

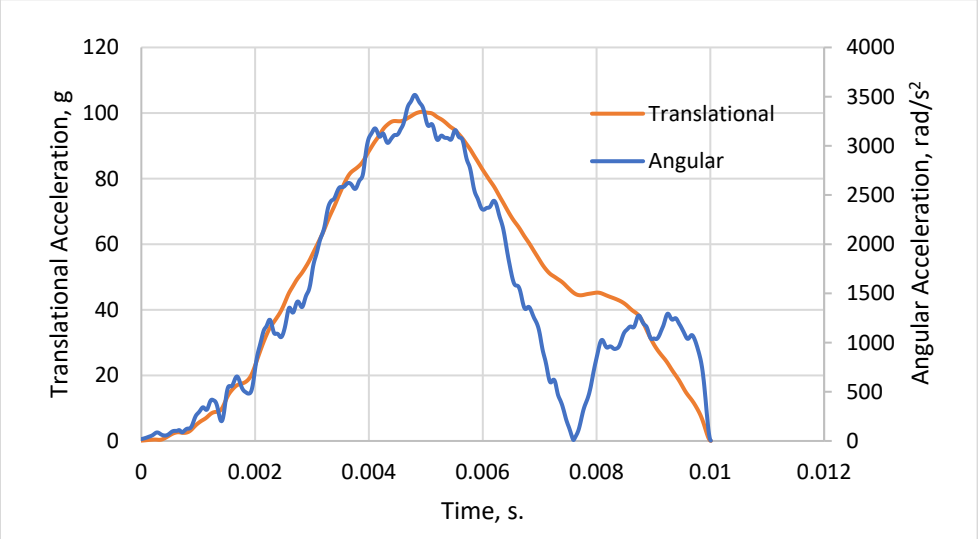

Figure 3.51 Acceleration Versus Time for Neck Rubber-Mooney and MEP Durometer Equal to 60 MPa

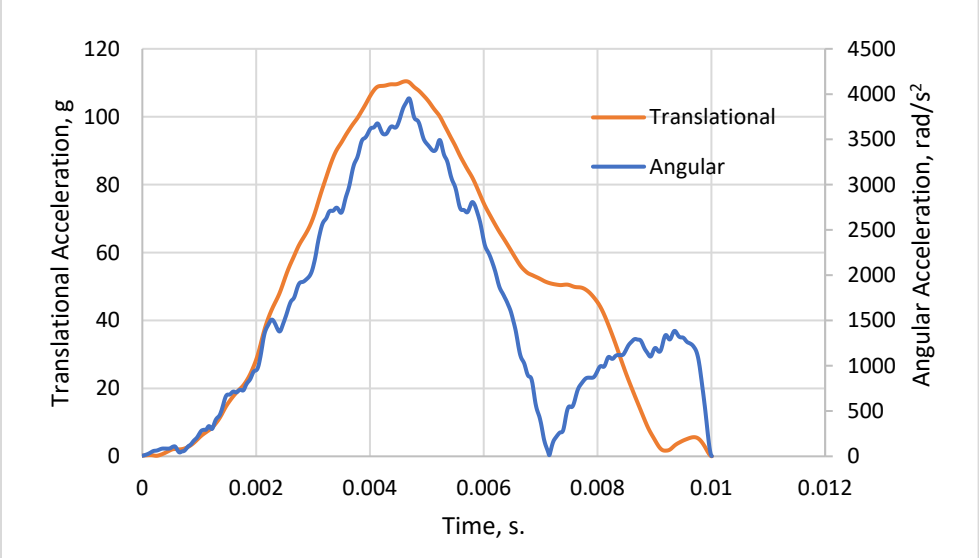

Figure 3.52 Acceleration Versus Time for Neck Rubber-Mooney and MEP Durometer Equal to 70 MPa

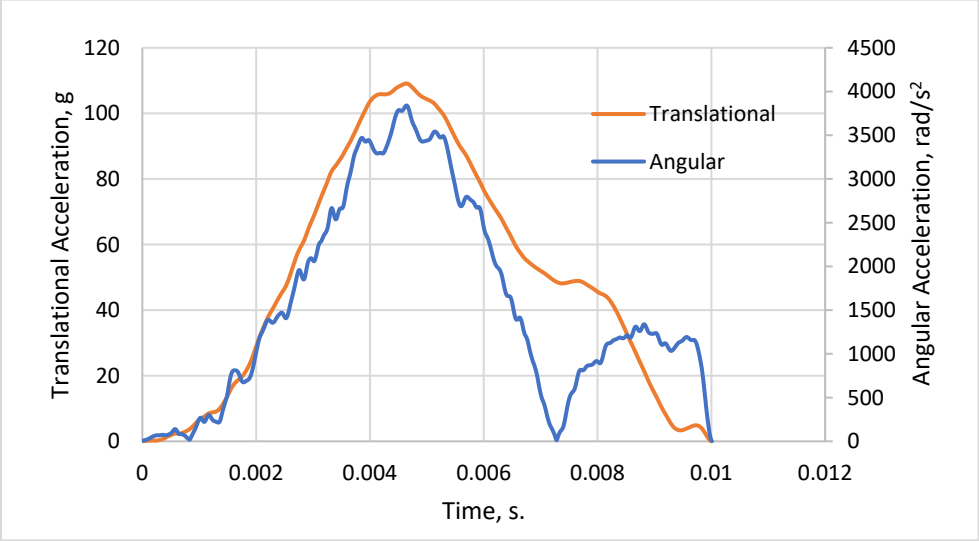

Figure 3.53 Acceleration Versus Time for Neck Rubber-Mooney and MEP Durometer E qual to 67.61 MPa

3.6.6 Boundary Conditions

The various boundary condition designations were presented in Section 3.2.6. Each boundary condition change was studied herein according to case designation. Table 3.10 shows the study cases and the pertinent section where the boundary condition details are described.

Table 3.10 Boundary Conditions Study Cases with Designation

Number of case	Case Designation	Details
1	BC2	See Section 3.6.5.1
2	BC3	See Section 3.6.5.2
3	BC4	See Section 3.6.5.3
4	BC5	See Section 3.6.5.4

3.6.6.1 BC2

In this case, we have set up the boundary for four conditions only. Where, we have kept in the model the last three boundary conditions for BC1 (See Section 3.2.6), and we have added new boundary conditions where, the bottom section of BasePL part displacements only were fixed in three directions as shown in Figure 3.55.

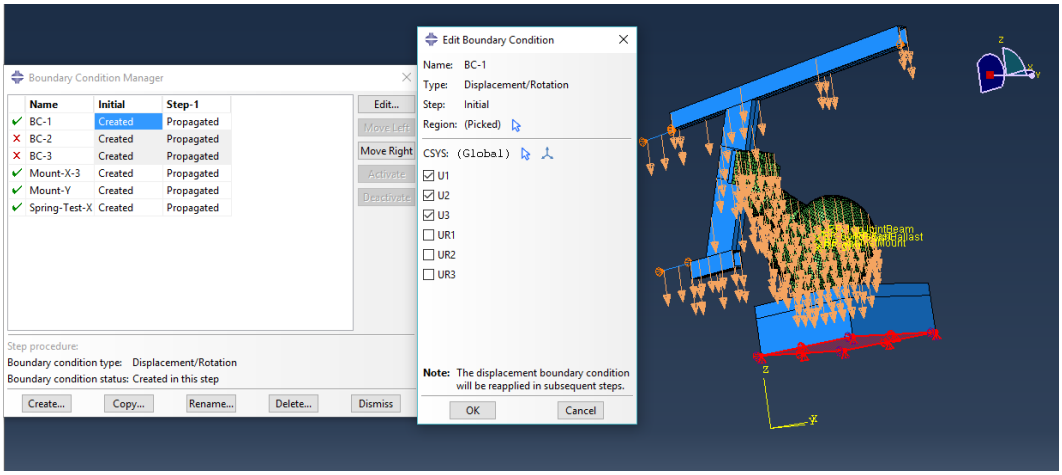

Figure 3.54 New Boundary conditions of BC2

3.6.6.2 BC3

In this case, we have set up the boundary for four conditions only. Where, we have kept in the model the last three boundary conditions for BC1 (See Section 3.2.6), and we have added new boundary conditions where, the bottom section of BasePL part displacements and rotations were fixed in three directions as shown in Figure 3.56.

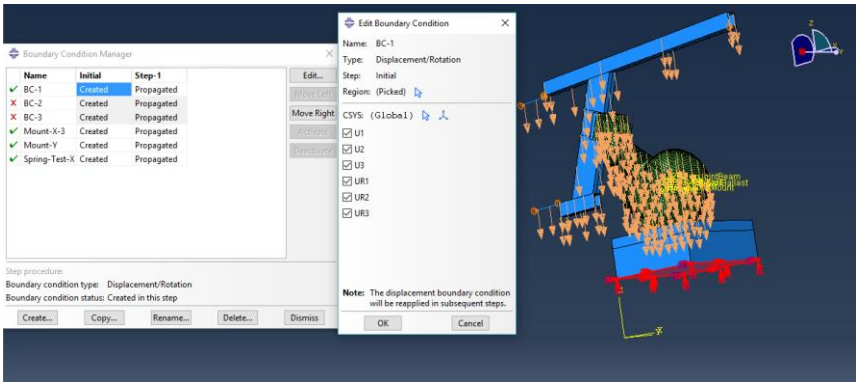

Figure 3.55 New Boundary conditions of BC3

3.6.6.3 BC4

In this case, we have set up the boundary for six conditions. Where, we have kept in the model the last three boundary conditions for BC1 (See Section 3.2.6), and we have added new three boundary conditions where, the bottom section and the other four surfaces of the BasePL part displacements and rotations were fixed in three directions as shown in Figure 3.57.

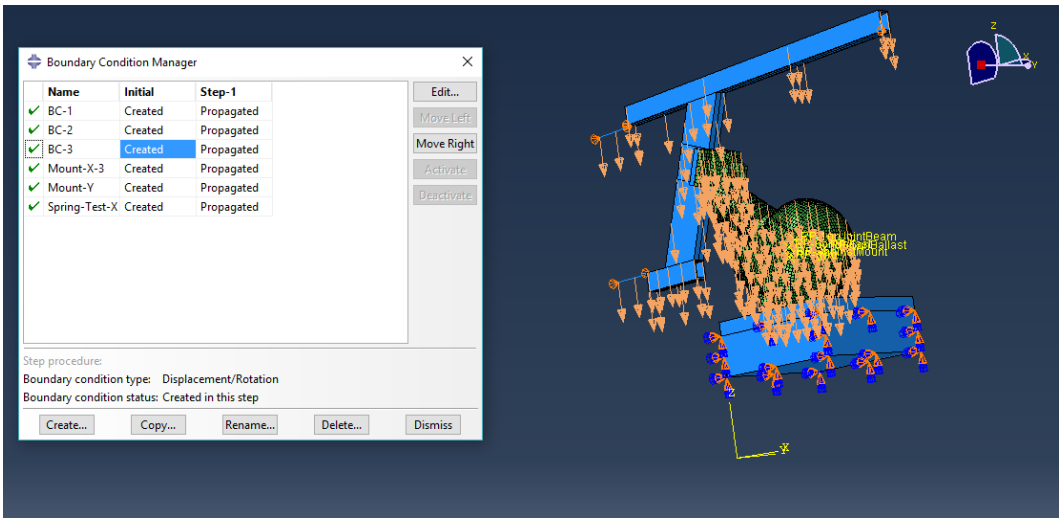

Figure 3.56 BC4 Description

3.6.6.4 BC5

In this case, we have set up the boundary for six conditions. Where, we have kept in the model the last three boundary conditions for BC1 (See Section 3.2.6), and we have added new three boundary conditions as showing below:

1. The bottom section of BasePL part displacements and rotations were fixed in three directions as shown in Figure 3.58.

2. Fix the two side sections of BasePL part displacements and rotations were fixed in three directions as shown in Figure 3.59.
3. Fix the other two side sections of BasePL part displacements and rotations were fixed in three directions as shown in Figure 3.60.

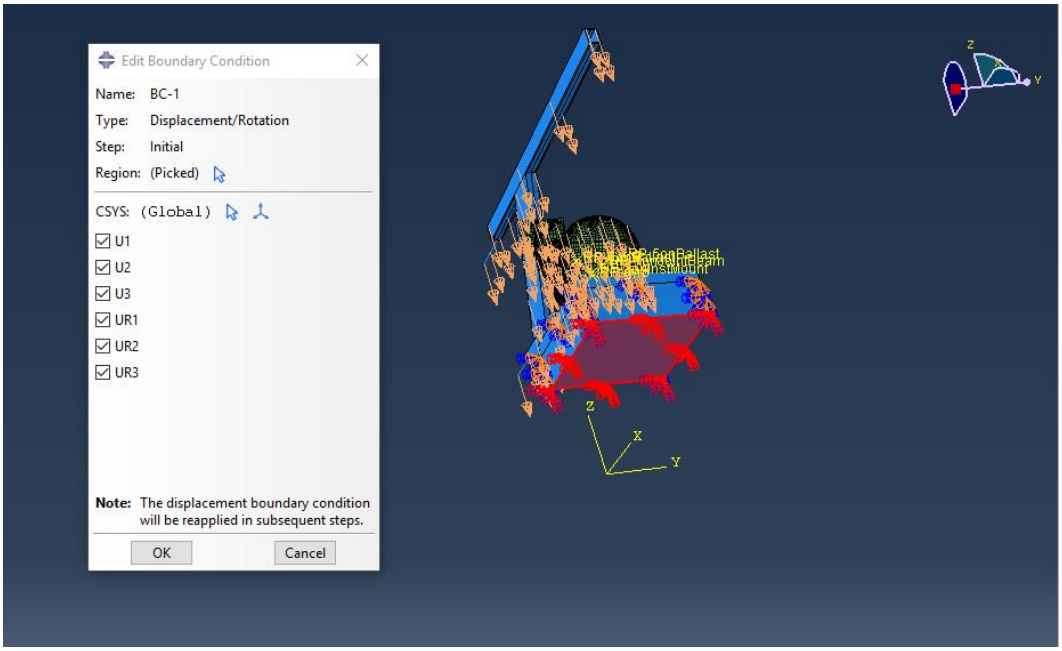

Figure 3.57 First Setting Up of New Boundary conditions of BC5

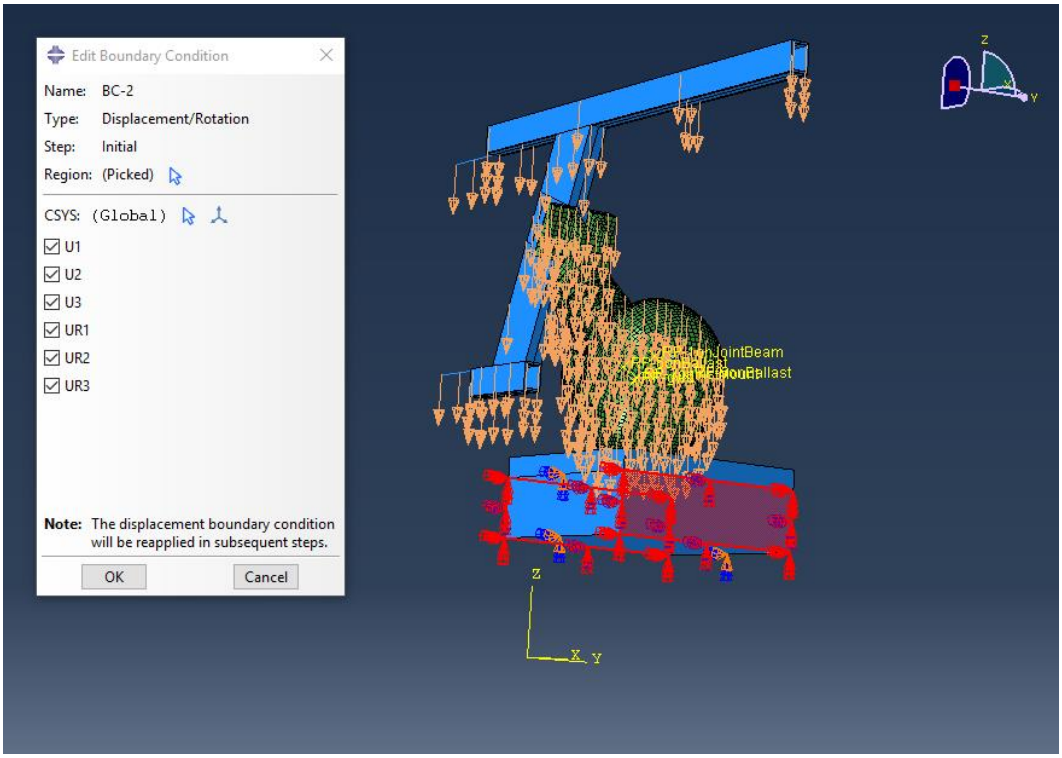

Figure 3.58 Second Setting Up of New Boundary conditions of BC5

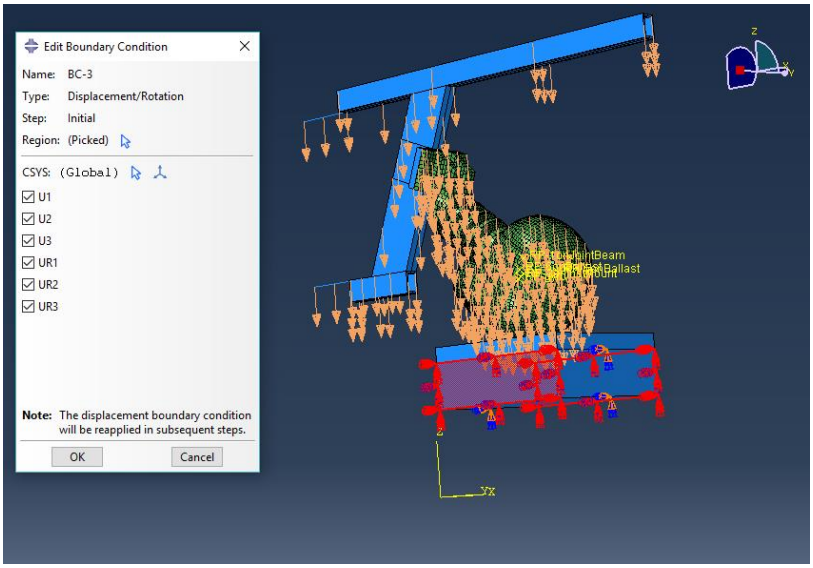

Figure 3.59 Third Setting Up of New Boundary conditions of BC5

Table 3.11 give a summary of the parameters used in the boundary condition study.

Table 3.11 Boundary Conditions Study Setting Up

Name of Variant	Quantity of Variant	Variant Related with
MEP-Mooney Material Stiffness	C_{10}= 0.937 MPa C_{01}= 0 D_1= 0.214 GPa^{-1}	MEP-BasePL Part
Modulus of Elasticity for RubberPad Material, Mpa	500	RubberPad Part
Poisson's Ratio for RubberPad Material	0.49	RubberPad Part
Coefficient of Friction	1	Head-Base Contact Surfaces
Neck Rubber-Mooney Material Stiffness	C_{10}= 0.937 MPa C_{01}= 0 D_1= 0.214 GPa^{-1}	NeckRubber Part
Boundary Conditions	Varies	Varies
Skin-Rubber-Mooney Material Stiffness	C_{10}= 0.329 MPa C_{01}= 0 MPa D_1= 0.607 GPa^{-1}	Skin and SkinCap Parts
Shape of Cross Sectional Area for Cable Beam Part	Square, 30 mm^2	CableBeam and MPU Parts
Modulus of Elasticity for Cable Beam Material, Gpa	96	CableBeam and MPU Parts

After we have done with these cases, the following table shows the results. Figures also show the acceleration versus time curves.

Table 3.12 Boundary Conditions Study Results

Case of BC's	Translational Acceleration, g	Angular Acceleration, rad/s^2
BC2	109.02	3840
BC3	109.02	3840
BC4	109.68	3730
BC5	110.20	3823

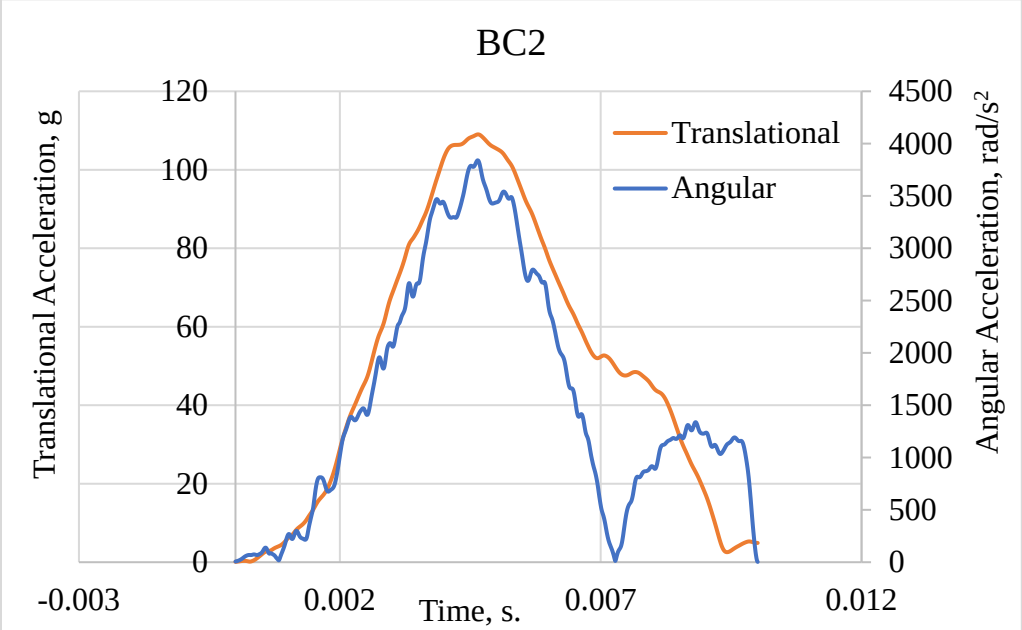

Figure 3.60 Acceleration Versus Time for BC2 Case

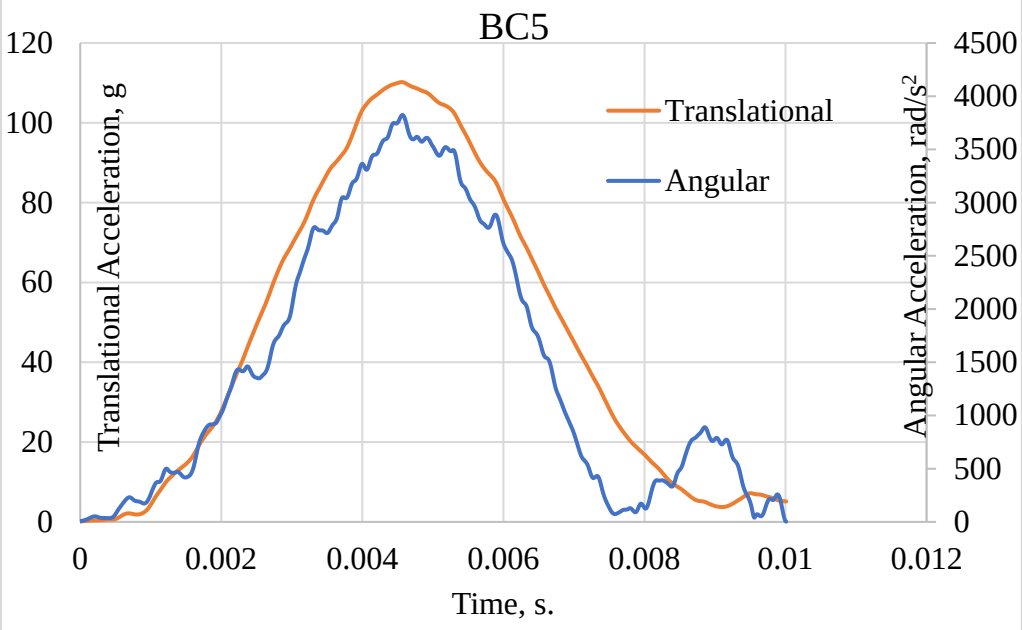

Figure 3.61 Acceleration Versus Time for BC5 Case

3.6.7 Skin -Rubber-Mooney Material

The parameters used for the skin rubber material study are given in Table 3.13 for setting the model up with these following data. The results also are submitted below in the Table 3.14 and the Figures 3.63 and 3.64.

Table 3.13 Skin-Rubber -MooneyMaterial Study Setting up

Name of Variant	Quantity of Variant	Variant Related with
MEP-Mooney Material Stiffness	C_{10}= 0.937 MPa C_{01}= 0 D_1= 0.214 GPa^{-1}	MEP-BasePL Part
Modulus of Elasticity for RubberPad Material, Mpa	500	RubberPad Part
Poisson's Ratio for RubberPad Material	0.49	RubberPad Part
Coefficient of Friction	1	Head-Base Contact Surfaces
Neck Rubber-Mooney Material Stiffness	C_{10}= 0.937 MPa C_{01}= 0 D_1= 0.214 GPa^{-1}	NeckRubber Part
Boundary Conditions	BC5	See Section 3.6.6
Skin-Rubber-Mooney Material Stiffness	C_{10}= Varies C_{01}= 0 MPa D_1= Varies	Skin and SkinCap Parts
Shape of Cross Sectional Area for Cable Beam Part	Square, 30 mm^2	CableBeam and MPU Parts
Modulus of Elasticity for Cable Beam Material, Gpa	96	CableBeam and MPU Parts

Table 3.14 Results of Skin-Rubber-Mooney Material Study

Durometer of Skin-Rubber-Mooney, MPa	C_{10}, MPa	D_1, GPa^{-1}	Translational Acceleration, g	Angular Acceleration, rad/s^2
67.61	0.937	0.214	122.26	3857
48	0.33	0.607	108.43	3533

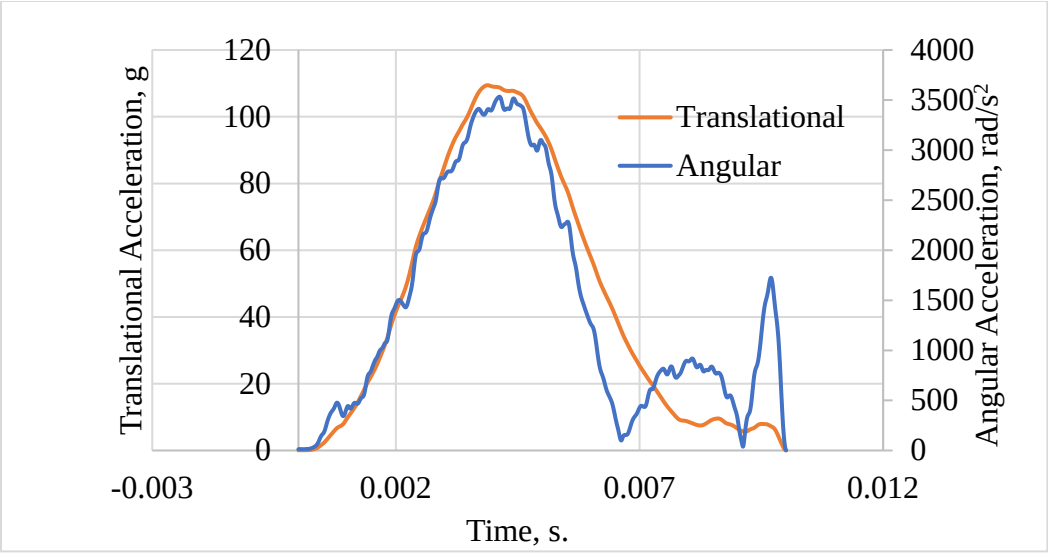

Figure 3.62 Acceleration versus Time for Skin-Rubber-Mooney Material with Durometer Equal to 48

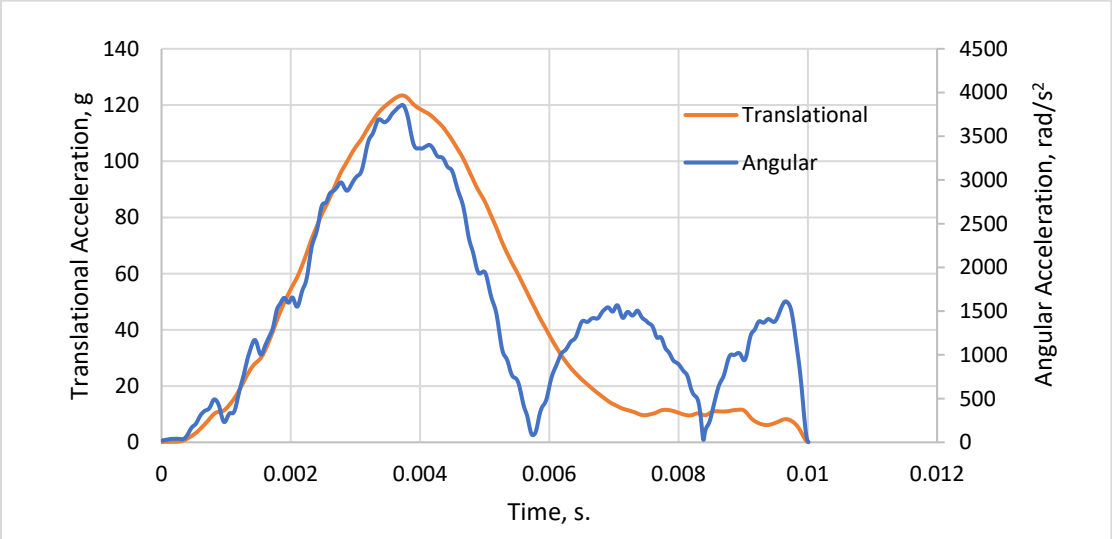

Figure 3.63 Acceleration Versus Time for Skin-Rubber-Mooney Material with Durometer Equal to 67.61MPa

3.6.8 CableBeam Material with Changing COF

The cable beam cross-sectional area was changed from square to circular shape in this study with keeping the same area for the new circular area since $A_{\text{Cross-sectional area}} = 30\ mm^2$. The first step used all same previous variants values as given in Table 3.13 with new values for Skin-Rubber-Mooney durometer (H= 48 Mpa). Table 3.15 and Figure 3.65 provide the results for this case:

Table 3.15 CableBeam Part, Results for Changing Cross-Sectional Shape

Shape of Cross-Sectional Area for CableBeam Part	Translational Acceleration, g	Angular Acceleration, rad/s^2	COF
Square, 5.477mm	108.43	3533	1
Circular, D= 6.18mm	110.55	3648	1

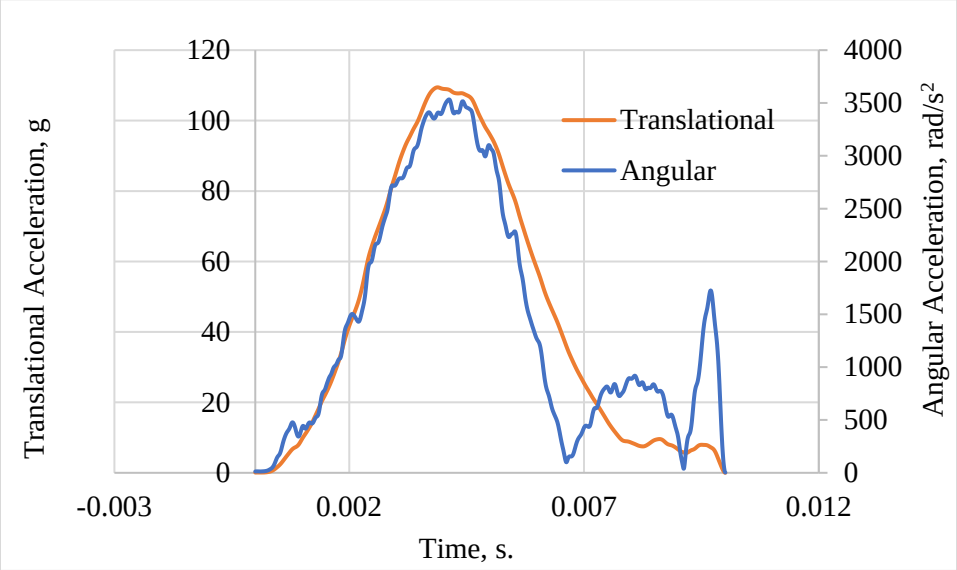

Figure 3.64 Acceleration Versus Time for Changing Only the Shape of CableBeam Cross-Sectional Area to Circular Shape

In addition, the COF values are changed in the study with the model setup according to Table 3.16. The results are provided in Table 3.17.

Table 3.16 Setting up the Hybrid III Head-Neck Assembly to Study COF Effects with Changing the Cross-Sectional Area Shape for CableBeam Part

Name of Variant	Quantity of Variant	Variant Related with
MEP-Mooney Material Stiffness	C_{10}= 0.937 MPa	MEP-BasePL Part
	C_{01}= 0	
	D_1= 0.214 GPa^{-1}	
Modulus of Elasticity for RubberPad Material, Mpa	500	RubberPad Part
Poisson's Ratio for RubberPad Material	0.49	RubberPad Part
Coefficient of Friction	Varies	Head-Base Contact Surfaces
Neck Rubber-Mooney Material Stiffness	C_{10}= 0.937 MPa	NeckRubber Part
	C_{01}= 0	
	D_1= 0.214 GPa^{-1}	
Boundary Conditions	BC5	See Section 3.6.6
Skin-Rubber-Mooney Material Stiffness	C_{10}= 0.329 MPa	Skin and SkinCap Parts
	C_{01}= 0 MPa	
	D_1= 0.607 GPa^{-1}	
Shape of Cross Sectional Area for Cable Beam Part	Circular, 30 mm^2	CableBeam and MPU Parts
Modulus of Elasticity for Cable Beam Material, Gpa	96	CableBeam and MPU Parts

Table 3.17 COF Study Results

COF	Translational Acceleration, g	Angular Acceleration, rad/s^2
1	110.55	3648
0.75	109.29	3722
0.5	111.28	3587
0.25	113.41	3767
0	110.54	4393

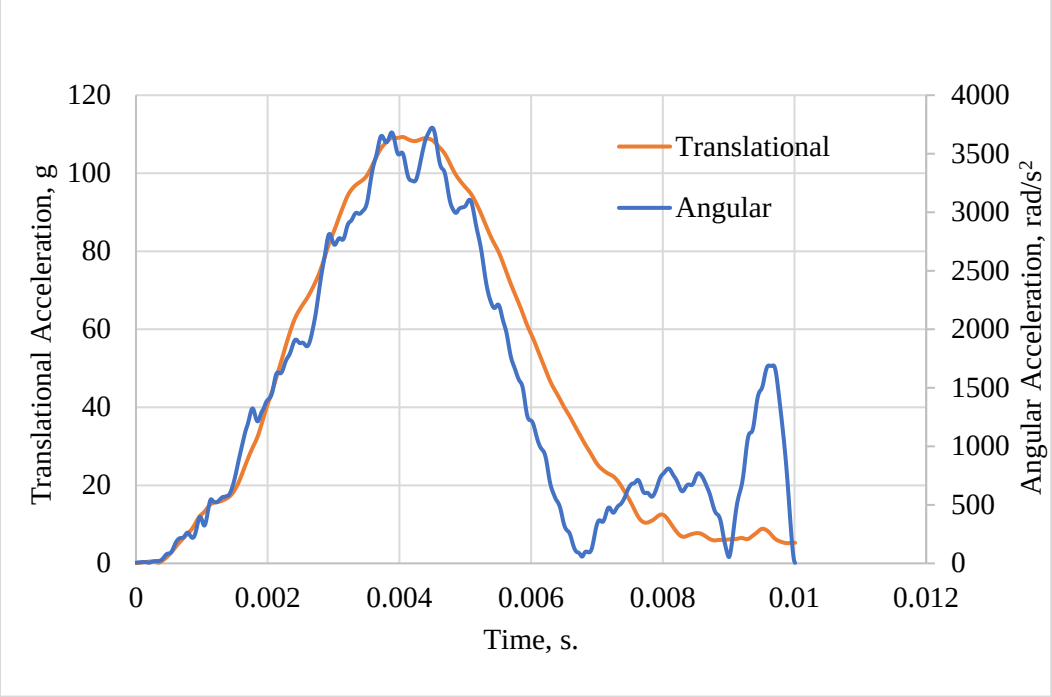

Figure 3.65 Acceleration Versus Time for the COF Equal to 0.75 Results

In addition, the modulus of elasticity of Cablebeam material part (E) was investigated. The Hybrid III Head-Neck Assembly model should essentially be set up with following data as shown in the Table 3.18. The results of these analysis are shown in the Table 3.19 and Figures 3.67,3.68, and 3.69.

Table 3.18 Setting Up Data for CableBeam E Study

Name of Variant	Quantity of Variant	Variant Related with
MEP-Mooney Material Stiffness	C_{10}= 0.937 MPa	MEP-BasePL Part
	C_{01}= 0	
	D_1= 0.214 GPa^{-1}	
Modulus of Elasticity for RubberPad Material, Mpa	500	RubberPad Part
Poisson's Ratio for RubberPad Material	0.49	RubberPad Part
Coefficient of Friction	0.75	Head-Base Contact Surfaces
Neck Rubber-Mooney Material Stiffness	C_{10}= 0.937 MPa	NeckRubber Part
	C_{01}= 0	
	D_1= 0.214 GPa^{-1}	
Boundary Conditions	BC5	See Section 3.6.6
Skin-Rubber-Mooney Material Stiffness	C_{10}= 0.33 MPa	Skin and SkinCap Parts
	C_{01}= 0 MPa	
	D_1= 0.607 GPa^{-1}	
Shape of Cross Sectional Area for Cable Beam Part	Circular, 30 mm^2	CableBeam and MPU Parts
Modulus of Elasticity for Cable Beam Material, Gpa	Varies	CableBeam and MPU Parts

Table 3.19 Changing of Modulus of Elasticity (E) for BeamCable Material Part

Results

Modulus of Elasticity(E) for CableBeam Material Part (Gpa)	Translational Acceleration, g	Angular Acceleration, rad/s^2	COF
1	109.51	3598	0.75
10	111.48	4390	0.75
36.71	110.73	3597	0.75
50	111.30	4391	0.75
80	109.92	3577	0.75
96	109.29	3722	0.75
210	113.47	4385	0.75
294.61	112.76	3840	0.75
80	111.80	3701	0.35

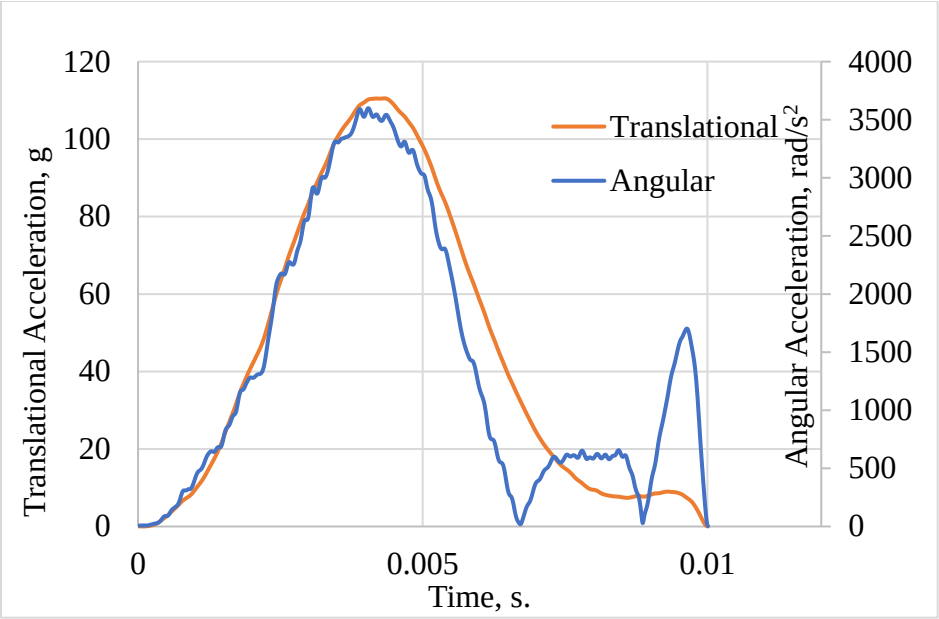

Figure 3.66 Acceleration Versus Time for CableBeam Part E Equal to 1 GPa

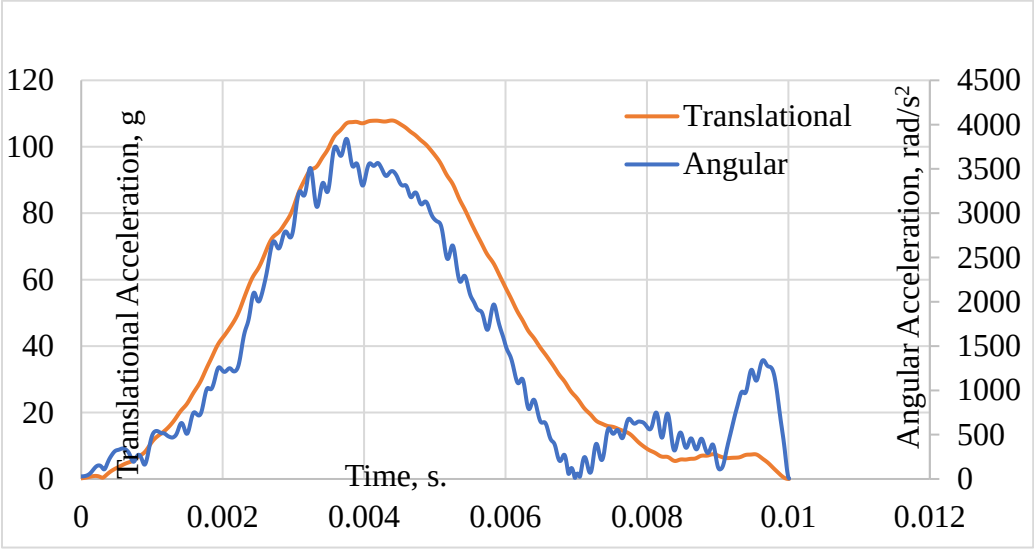

Figure 3.67 Acceleration Versus Time for CableBeam Part E Equal to 294.61 GPa

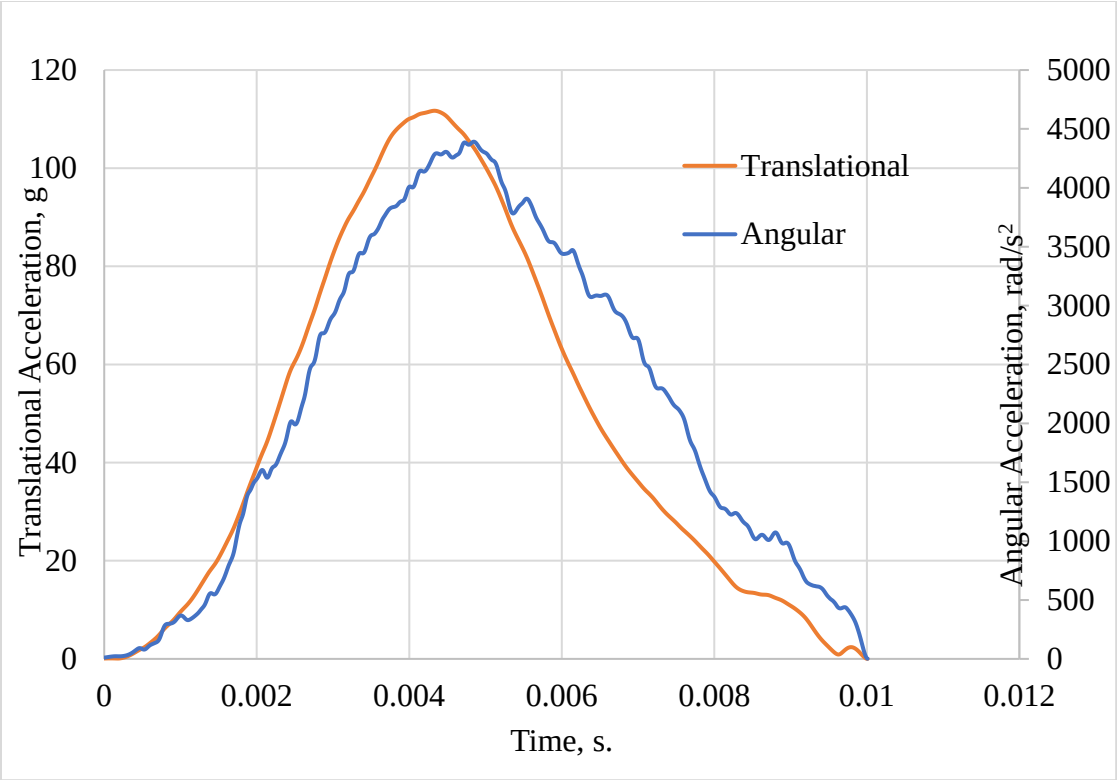

Figure 3.68 Acceleration Versus Time for CableBeam Part E Equal to 50 GPa

CHAPTER 4

THE EXPERIMENTAL RESULTS AND THE RECOMMENDED MODEL

In this chapter, the impact testing apparatus of the Hybrid III Head-Neck Assembly model is described and the experimental results of the head/neck assembly calibration testing using the MEP pad anvil are given. The results of the FEA model are compared the experimental testing and recommendations are given. In addition, the behavior of the Head-Neck assembly during a stepped impact test done at incremental drop heights is summarized.

4.1 Experimental Data

The impact testing apparatus details and set up are important to obtaining accurate results. The obtained experimental data will be more precious and acceptable. In general, the translational and angular accelerations versus the performed time are evaluated as the goal results, especially the peak magnitudes.

4.1.1 Testing Apparatus Description

The apparatus used in these experiments is the same impact test apparatus used for the MEP rubber pad tests summarized in Chapter 2. The primary difference is the impactor assembly type and details. The Hybrid III Head-Neck assembly model will be used as the impactor in this case. It is shown falling toward the impacted pad, MEP Rubber pad in Figure 4.1. The Hybrid III Head-Neck assembly has a mass of 8.25 kg, and it consists of the skull and skull cap, skin and

skin cap, neck and fly arm and its attached parts. An accelerometer array consisting of 4 triaxial accelerometers is placed inside the head form.

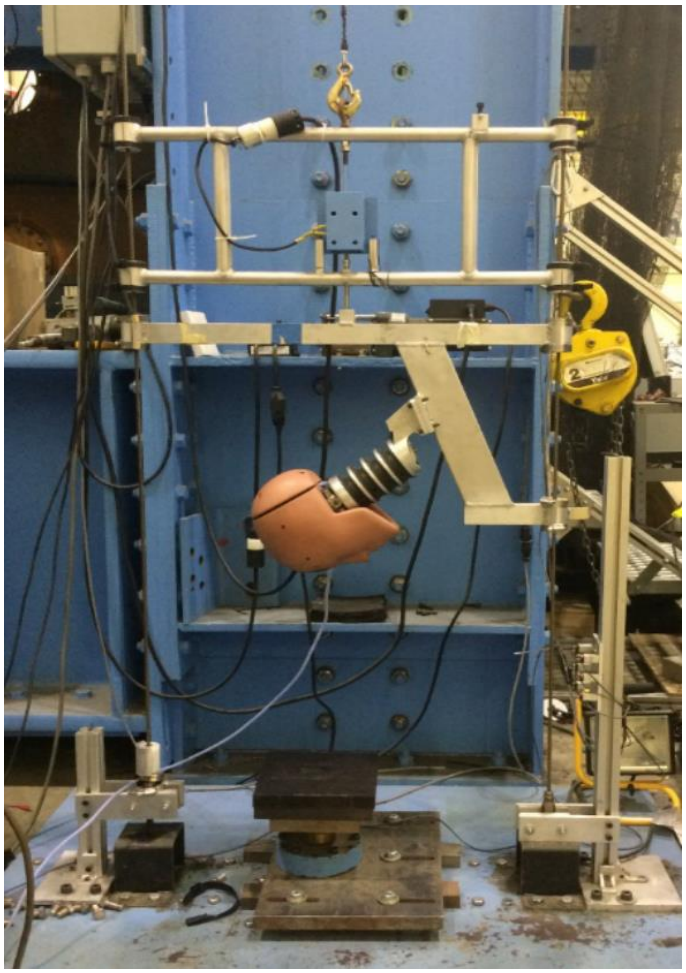

Figure 4.1 Hybrid Head-Neck Assembly

The skull and skullcap parts are made from aluminum, covered by a urethane skin and skin cap materials as shown in Figure 4.2. The skull part has a hole and groves in which the accelerometers are installed inside the head.

Figure 4.2 The Head- Neck Assembly Details: a) Uncapped Hybrid III Head with Neck b) Skull Cap and Skin Cap c) Another View for Skull Cap and Skin Cap d) Skin and Skull Caps Together e) Hybrid III Head

The neck part as shown in Figure 4.2a and 4.3 basically, consists of five neck disks, four neck rubber, two rubber pads and beam parts. Neck disks and beam parts are made of elastic materials such as aluminum. Neck rubber and rubber pads parts are made from rubber materials that are hyperplastic materials. The beam passes through the holes of neck disks and neck rubber parts, and it is tied and

connected by two side (between the head and the adjusted part in the arm) to make the neck assembly.

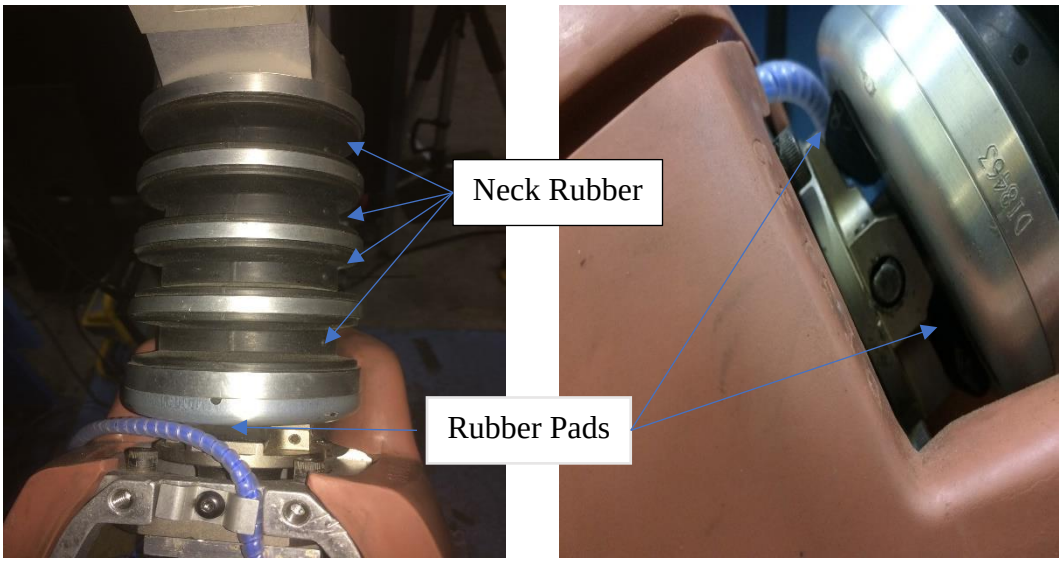

a) b)

Figure 4.3 Examples of the Studied Parts: a) Neck Assembly b) Zoomed Rubber Pads as Pointed

Four accelerometers used in the apparatus as shown in Figure 4.4: Center of Gravity CG, Side, Top, and Back accelerometers. All these accelerometers are in appropriate positions inside the Skull part at the Hybrid III Head-Neck assembly and used for evaluating the translational accelerations during the impact test at these points. The distances between their locations are dependent on the gender of the dummy used. Testing was conducted with a 50^{th} percentile male head as will be

shown later. The accelerometers used were PCB model 356B21 triaxial accelerometer with a peak acceleration magnitude of 500 g (Caccese et al., 2016).

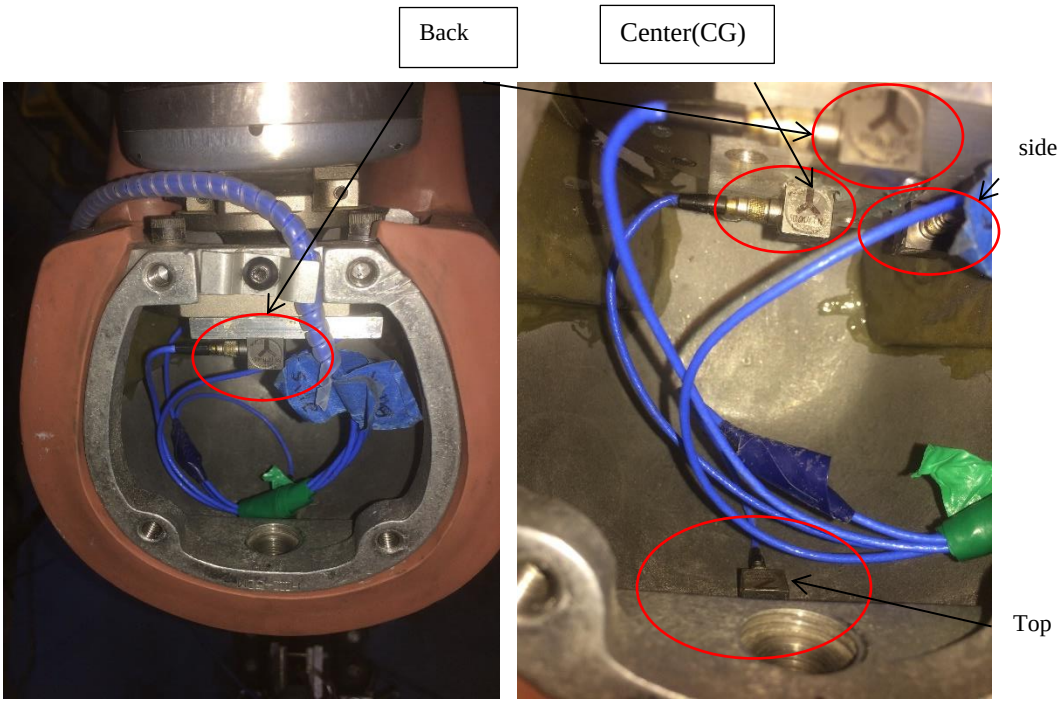

Figure 4.4 Accelerometer Locations As Pointed

The fly arm is an aluminum tube with dimensions shown in Figure 4.5. The Hybrid head-neck assembly can be oriented as required such as in front, rear, or side position depending on the adjustment adapter that can make the connection between the head and fly arm. Figure 4.6 shows the adjustment parts that can be used, in this thesis we have used the front orientation only as shown in Figure 4.7.

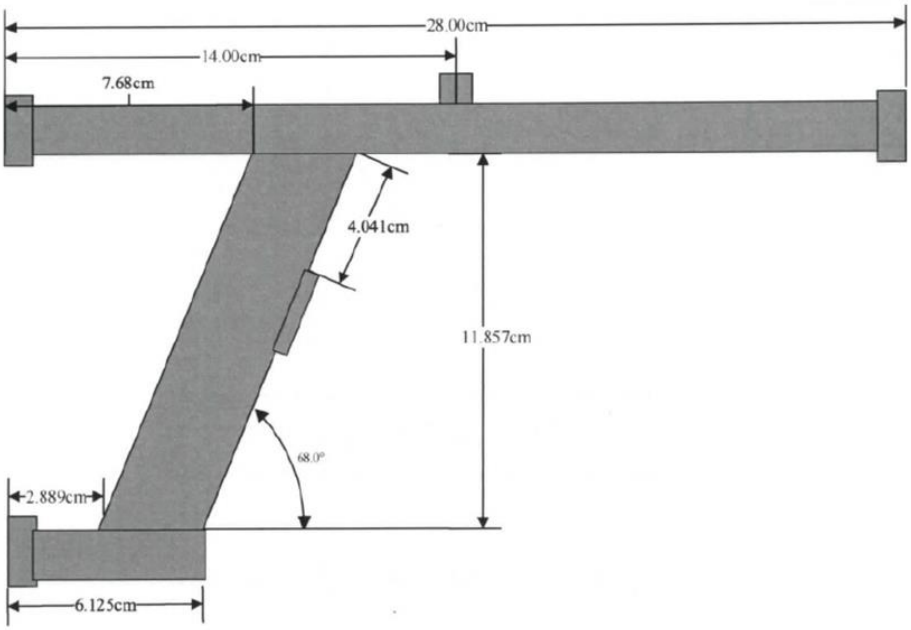

Figure 4.5 Fly arm Dimensions (Seidi, 2015)

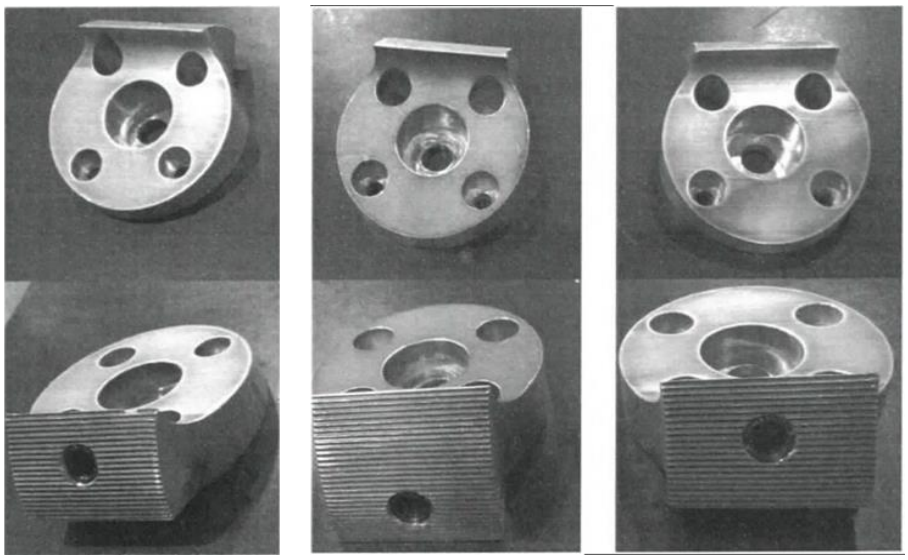

a) front b) rear c) side

Figure 4.6 Adaptors for Mounting Head and Neck Assembly to the Fly Arm

(Seidi, 2015)

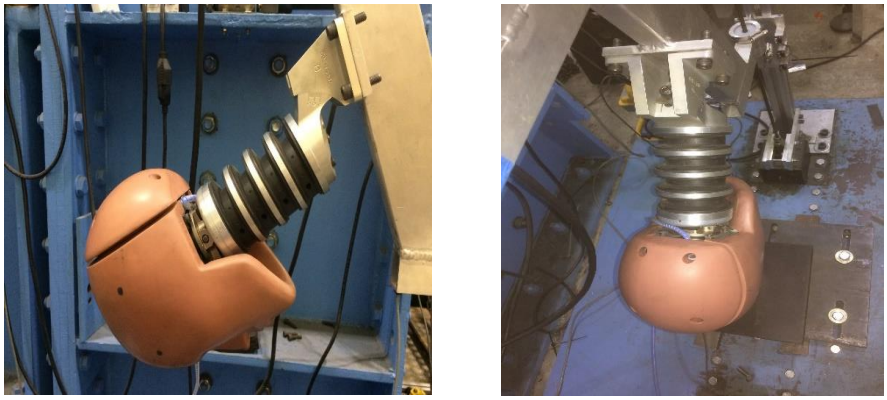

Figure 4.7 Side and Top Views of the Head Neck Assembly

(front orientation type)

4.1.2 Testing Control

The CG accelerometer measures the translational acceleration of the assembly at each 5e-5 second time increment as set by the data acquisition program. The angular acceleration is evaluated according to the resultant of the accelerometer readings, Top, Side, and Back with respect to the CG point accordingly to the equations 4.1, 4.2, 4.3 and 4.4 and the configuration shown in Figure 4.8 According to (Padgaonkar et al., 1975) and (Bussone, Bove, Thomas, Richards, & Prange, 2010).

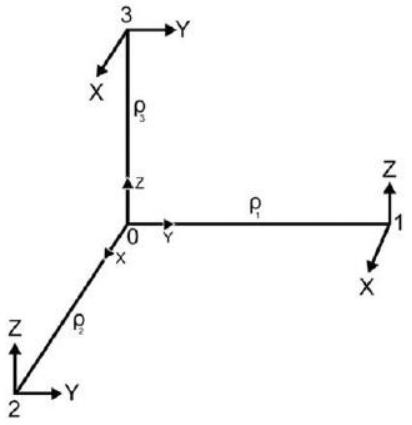

Figure 4.8 Six and Nine- Accelerometer Configurations Adapted from Padgaonkar, Krieger et al. 1975 (Bussone et al. 2010)

$$\dot{\omega}_x = \frac{(A_{z1} - A_{z0})}{2\rho_{y1}} - \frac{(A_{y3} - A_{y0})}{2\rho_{z3}} \tag{4.1}$$

$$\dot{\omega}_y = \frac{(A_{x3} - A_{x0})}{2\rho_{z3}} - \frac{(A_{z2} - A_{z0})}{2\rho_{x2}} \tag{4.2}$$

$$\dot{\omega}_z = \frac{(A_{y3} - A_{y0})}{2\rho_{x2}} - \frac{(A_{x1} - A_{x0})}{2\rho_{y1}} \tag{4.3}$$

$$\boldsymbol{A_{Angular}} = \sqrt{\dot{\omega}_x{}^2 + \dot{\omega}_y{}^2 + \dot{\omega}_z{}^2} \tag{4.4}$$

Where 0, 1, 2 and 3 points as shown in Figure 4.8 are the CG, back, side and top accelerometers positions respectively, ω_x, ω_y and ω_z are the angular acceleration components with respect to x, y, and z axes. ρ_1, ρ_2 and ρ_3 are the distances between back, side and top accelerometers positions and the center of gravity CG

respectively. ρ_{y1}, ρ_{x2} and ρ_{z3} are 88 mm, 26.6 mm 47.3 mm respectively and $A_{Angular}$ is the resultant acceleration of the required test in rad/s^2.

The following procedure was performed to obtain the hybrid head neck assembly impact test results:

1. Place the MEP anvil that consists of MEP Rubber Pad and steel plate on the base of the apparatus as shown in Figure 4.9. The MEP anvil has the dimensions 22.86 cm, 22.86 cm, and 2.54, length, width and thick respectively. Insure that the top surface center of the anvil location is in the center of the front area that will be impacted.

Figure 4.9 Two views of the MEP anvil

2. Move the head neck assembly toward the MEP anvil until the front head touches the top surface of the anvil. Make sure visually that the front head only touches the

anvil without displacing it as shown in Figure 4.10. The impactor (head-neck assembly) position now is in the zero location for the apparatus.

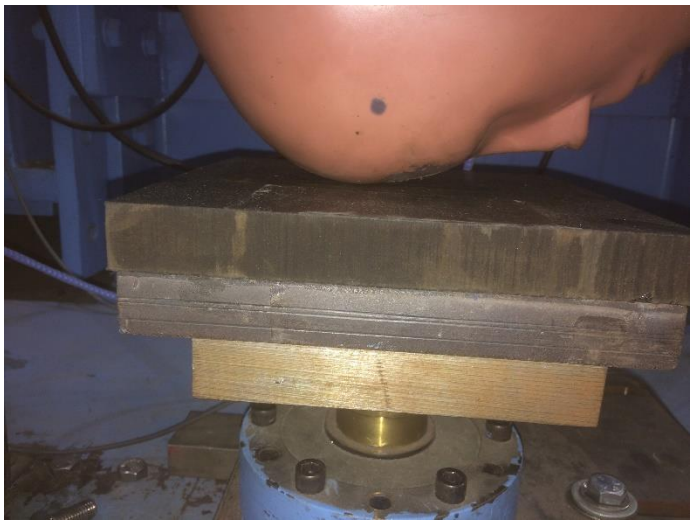

Figure 4.10 Contact Between the Head and the MEP Anvil Without Displacing It

3. Move the velocity photo gate by sliding it down or up until the red bottom light turns off by the drop arm tab as described in Chapter 2. Then, secure the gate to make sure it will not move during the impact.

4. In the controller part of the data acquisition program, reset the apparatus code by inserting and applying the suitable impact configuration file used for head impact testing. Check that the correct calibration factors are loaded. The file activation code should be reset before starting the next impact test step. The drop height should be reset to zero position to insure we will start from zero drop height as we

did in Chapter2. Figures 4.11 and 4.12 show the windows that control the head-neck impact test.

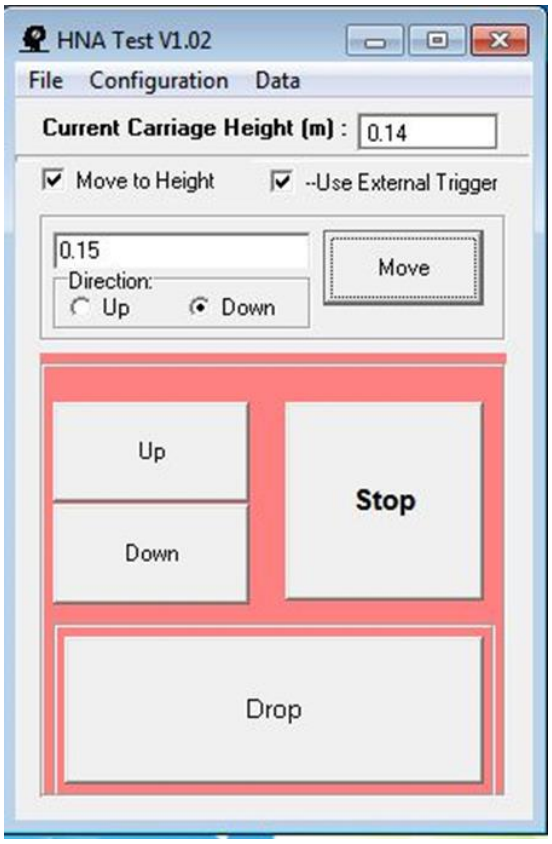

Figure 4.11 Head-Neck Assembly Control Panel

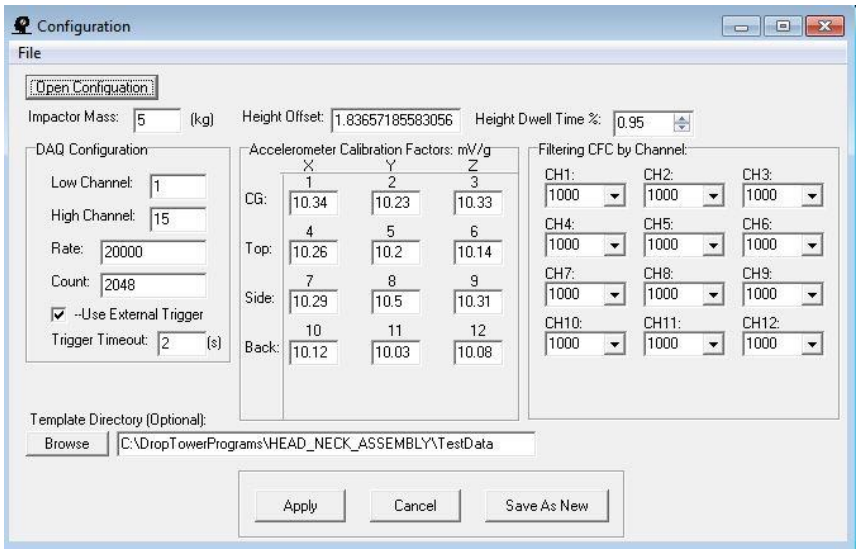

Figure 4.12 Head Neck Impact Test File Code Configuration

5. Insert the required drop height and move the fly arm accordingly to the desired height, and then release the fly arm by clicking on the drop button by using the Figure 4.11. Finally, use the write data button to obtain the test results as shown in the sample test in Figure 4.13. It was for 40 cm drop height test.

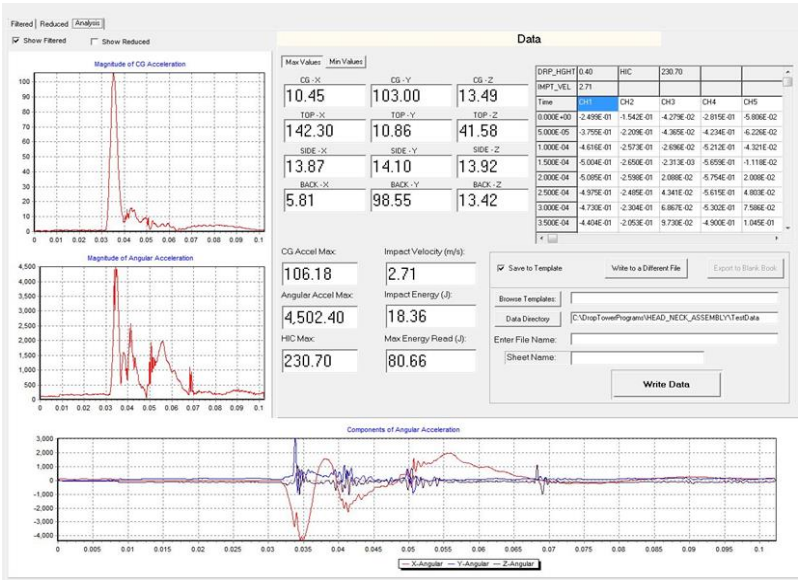

Figure 4.13 Last Step for Head Neck Assembly Drop Test With 40 cm

Drop Height Test

4.1.3 Results of Testing

The results of the Head Neck assembly impact test are shown in Table 4.1 and Figures 4.14 and 4.15. Where, the experimental tests were done 10 times for each drop height and the results are consisted of peak translational and angular accelerations versus various drop heights. HIC_{15} results are evaluated and shown in Figure 4.16. The standard deviation STDEV for the all values are also shown in the Table 4.1.

Table 4.1 Experimental Results for Head- Neck Assembly Test

Impact Velocity	Drop Height	Peak Acceleration		HIC_{15}	Standard Deviation, STDEV				
m/s	m	CG, g	Angular rad/s^2		Impact Velocity	Drop Height	CG	Ang	HIC_{15}
1.52	0.14	52.23	2593.1	51.22	0.04	0	1.13	197.32	2.63
1.88	0.2	67.03	2927.18	86.96	0.01	0	0.5	86.54	1.28
2.33	0.3	88.36	3747.82	158.76	0.01	0	0.75	76.99	2.14
2.56	0.4	109.27	4746.09	246.97	0.02	0	0.81	71.63	2.54
2.85	0.5	128.33	5524.27	349.16	0.82	0	1.23	95.54	4.67
3.41	0.6	146.61	6110.8	457.08	0.02	0	1.12	33.61	5.94
3.7	0.7	164.92	6804.1	589.34	0.02	0.01	1.4	102.66	4.32
3.95	0.8	180.75	7435.2	719.55	0.01	0.01	0.89	52.2	3.98
4.17	0.9	197.09	7935.6	858.18	0.01	0	1.1	114.63	4.91

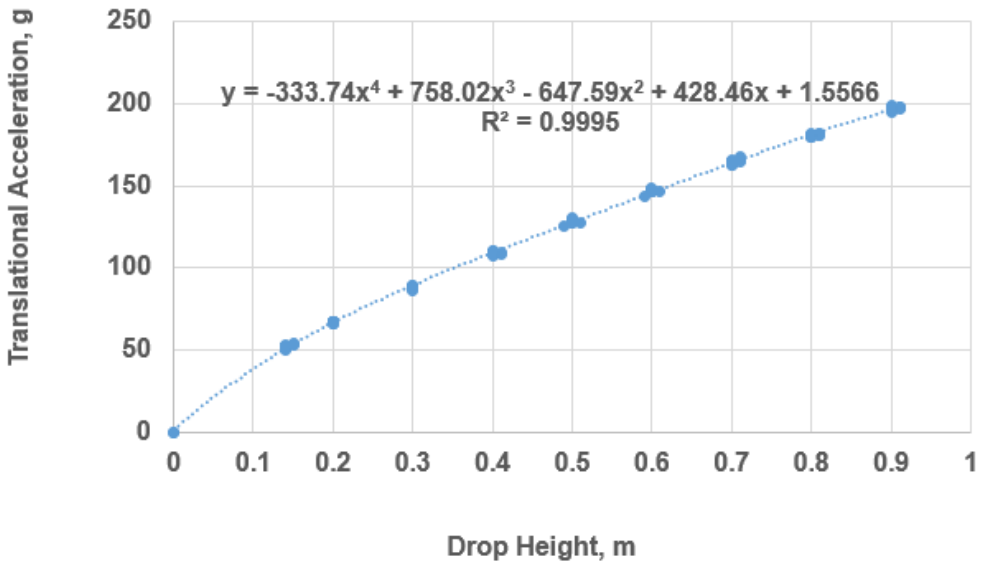

Figure 4.14 Peak Experimental Translational Acceleration Versus Drop Heights

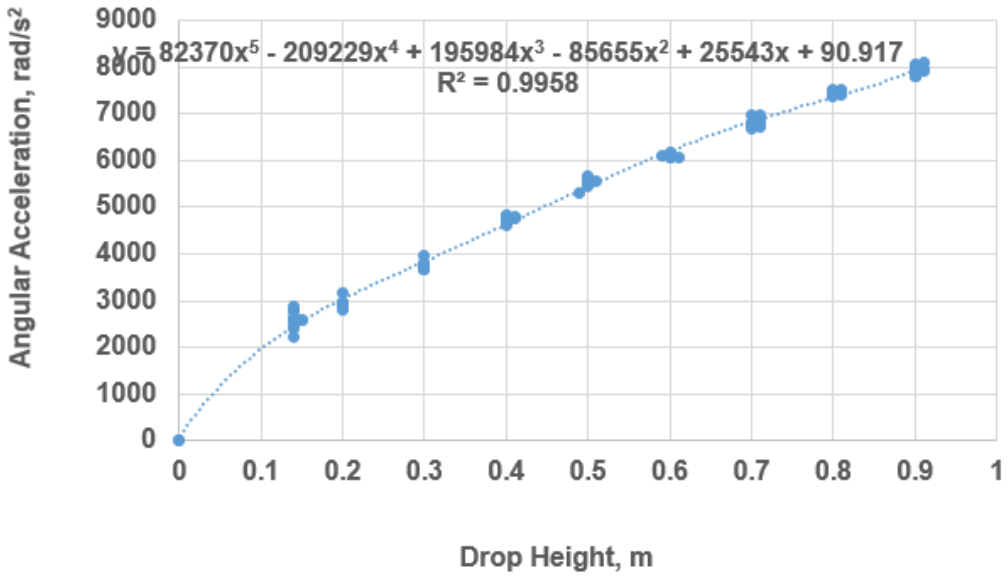

Figure 4.15 Peak Experimental Angular Acceleration Versus Drop Heights

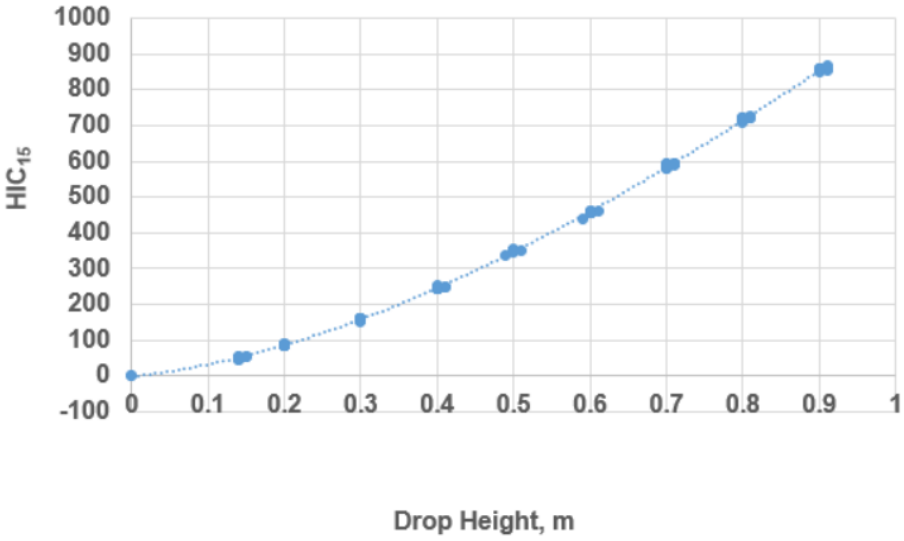

Figure 4.16 Head Injury Criterion HIC_{15} Versus Drop Height

In addition, the head-neck assembly was tested 12 times for drop height 0.4 m to use these results in the comparison with FEA model at Section 4.3.1. This is the nominal height specified in the Soccer headgear specification. The experimental results are shown in Table 4.2 and the standard deviation STDEV for the impact velocity, drop height, peak translational acceleration CG and the peak angular acceleration values are 0.02, 0.01, 1.52 and 274.78 respectively. Thus, the mean translational and angular accelerations are 110.28 ± 1.52 m/s^2, 4722.42 ± 274.78 rad/s^2 respectively.

Table 4.2 Experimental Results of the Head-Neck Assembly Impact Test at 0.4 m Drop Height

Test No.	Impact Velocity, m/s	Dropped Height, m	CG Acceleration, g	Angular Acceleration, rad/s^2
1	**2.78**	**0.41**	**111.3**	**4483**
2	**2.77**	**0.4**	**110.5**	**4488**
3	**2.78**	**0.4**	**113.0**	**4533**
4	**2.74**	**0.4**	**110.5**	**4580**
5	**2.73**	**0.39**	**108.2**	**4753**
6	**2.74**	**0.4**	**109.3**	**4682**
7	**2.73**	**0.4**	**109.9**	**4483**
8	**2.74**	**0.4**	**109.3**	**4530**
9	**2.78**	**0.41**	**113.0**	**5165**
10	**2.74**	**0.4**	**108.7**	**5142**
11	**2.74**	**0.39**	**109.9**	**4671**
12	**2.75**	**0.4**	**109.7**	**5159**
MEAN	**2.75**	**0.4**	**110.28**	**4722**
STDEV	**0.02**	**0.01**	**1.52**	**275**
COV,%	**0.72**	**1.51**	**1.38**	**5.82**

Two following samples of the neck-head assembly drop tests time histories are shown in Figures 4.17, and 4.18 which portray the relationship between translational and angular acceleration versus time for various drop heights

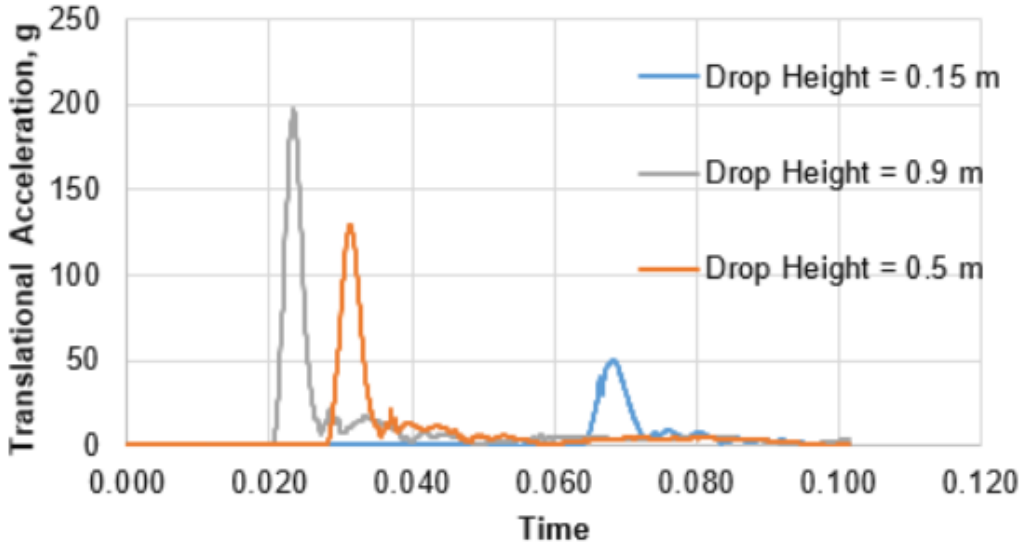

Figure 4.17 Translational Acceleration Versus Time

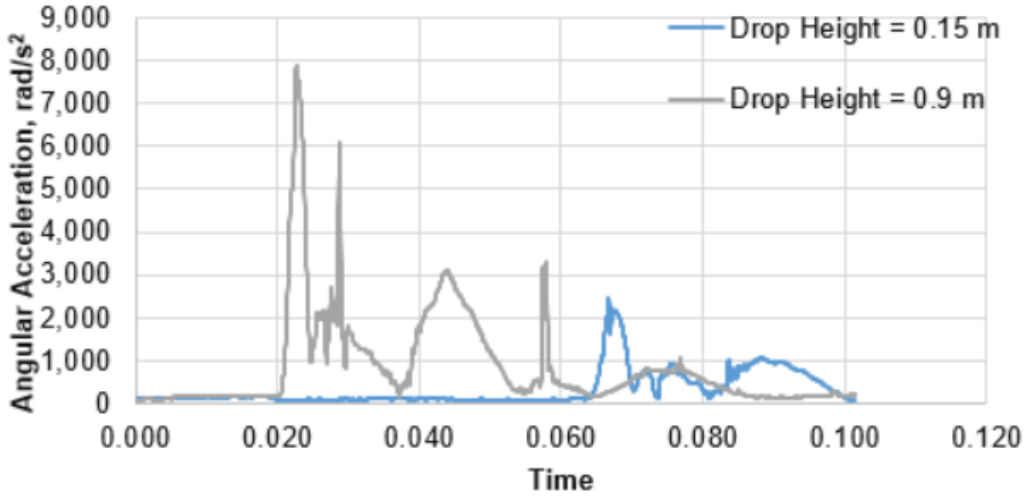

Figure 4.18 Angular Acceleration Versus Time

4.2 FEA Recommended Model for the Head- Neck Assembly

The Finite Element Analysis FEA recommended model of the head-neck assembly was presented in Chapter 3. Table 4.3 shows the recommended values for the studied variants noting the FEA model is applied with Abaqus 2016 version.

Table 4.3 Recommended Quantities of the Studied Variants for Hybrid III Head-Neck Assembly Model

Name of Variant	Quantity of Variant	Variant Related with
MEP-Mooney Material Stiffness	C_{10}= 0.937 MPa C_{01}= 0 D_1= 0.214 GPa^{-1}	MEP-BasePL Part
Modulus of Elasticity for RubberPad Material, Mpa	500	RubberPad Part
Poisson's Ratio for RubberPad Material	0.49	RubberPad Part
Coefficient of Friction	0.75	Head-Base Contact Surfaces
Neck Rubber-Mooney Material Stiffness	C_{10}= 0.937 MPa C_{01}= 0 D_1= 0.214 GPa^{-1}	NeckRubber Part
Boundary Conditions	BC5	See Section 3.6.5
Skin-Rubber-Mooney Material Stiffness	C_{10}= 0.329 MPa C_{01}= 0 MPa D_1= 0.607 GPa^{-1}	Skin and SkinCap Parts
Shape of Cross Sectional Area for Cable Beam Part	Circular 30 mm^2	CableBeam and MPU Parts
Modulus of Elasticity for Cable Beam Material, Gpa	50	CableBeam and MPU Parts

4.3 Comparison Between the Experimental and Model Results

The comparison between experimental results and the FEA head neck assembly model will described be in two parts: 1) using the results for a drop height

of 0.4 m that done with Abaqus 2016 version and 2) using various drop heights which done with Abaqus version 2017.

4.3.1 Comparison Between the Experimental and Model Results for one Dropped Height (0.4m)

The FEA model results are evaluated using Abaqus 2016 based on the values that were shown in Table 4.3. The FEA results are: peak translational and angular acceleration 111.3 m/s^2 and 4391.06 rad/s^2 respectively. However, the experimental results as shown in Section 4.1.3 are peak translational and angular accelerations 110.28 ± 1.52 m/s^2 and 4722.42 ± 274.78 rad/s^2 respectively. Figure 4.19 and 4.20 show the translational and angular acceleration versus time respectively with comparison between the FEA and experimental results.

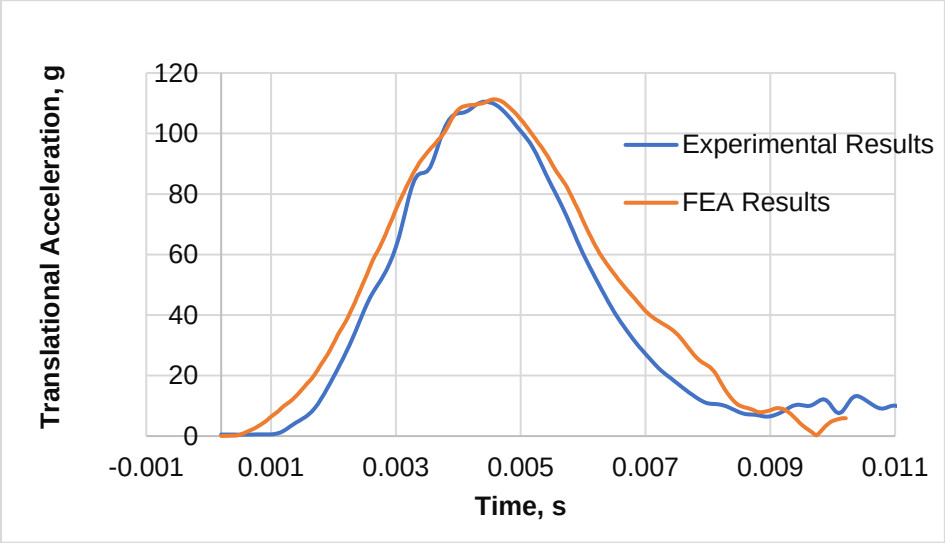

Figure 4.19 Experimental and FEA Translational Acceleration Results Versus Time at Drop Height 0.4m

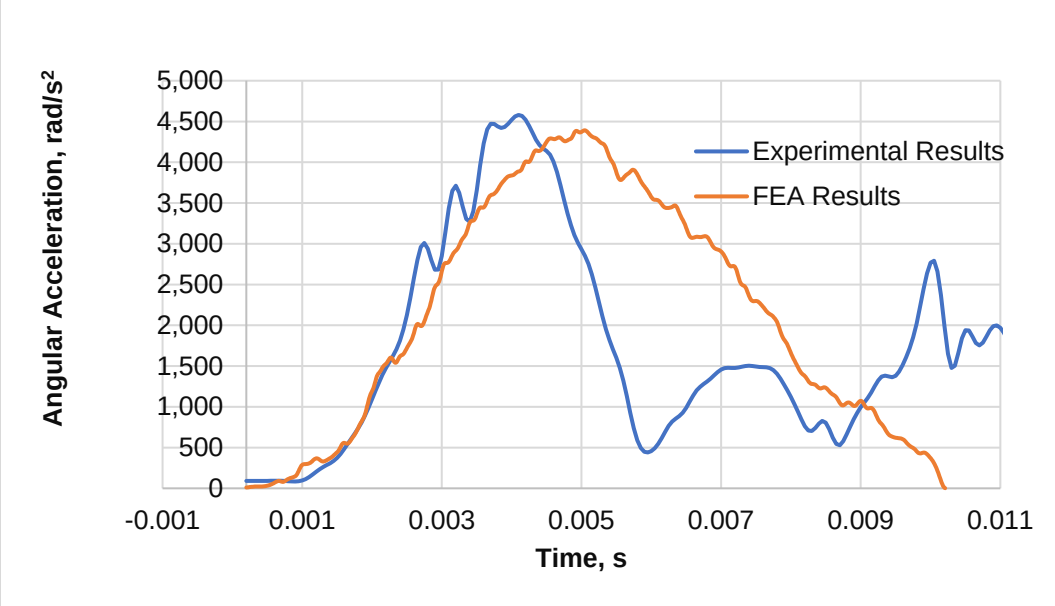

Figure 4.20 Experimental and FEA Angular Accelerations Results Versus Time at Drop Height 0.4m

4.3.2 Comparison Between the Experimental and FEA Model Results for Different Dropped Heights

The results of FEA head-neck assembly based on Abaqus 2017 and the experimental results were performed 10 times for each drop height. Figures 4.21 and 4.22 both show peak translational and angular acceleration versus drop height comparison between the experimental and FEA model results.

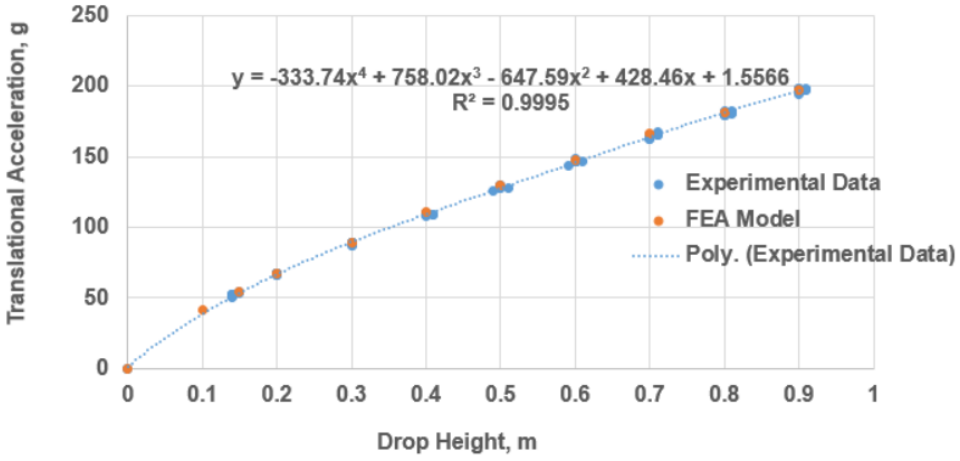

Figure 4.21 Peak Translational Acceleration Comparison Between the Experimental and FEA Model Results Versus Drop Height

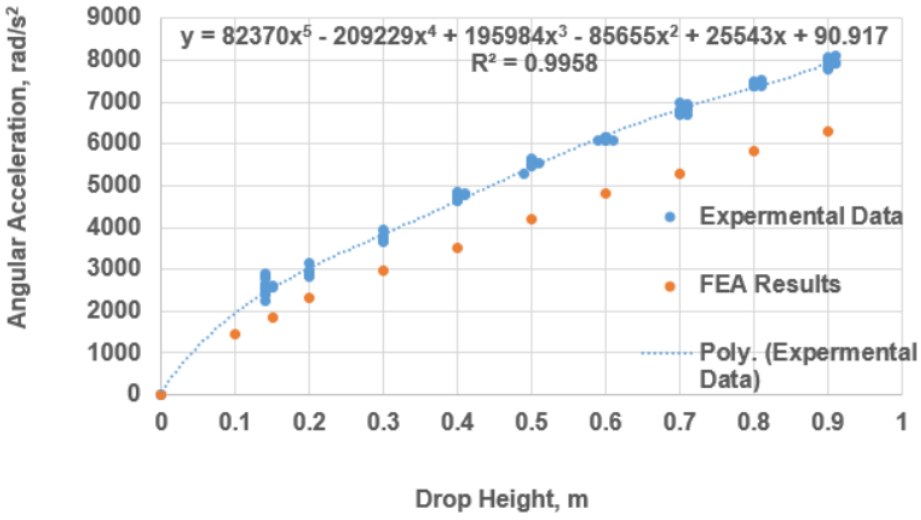

Figure 4.22 Peak Angular Acceleration Comparison Between the Experimental and FEA Model Results Versus Drop Height

In conclusion, the translational acceleration versus time as shown in Figure 4.19 and the peak translational acceleration versus drop height as shown in Figure 4.21 are verified that the FEA head neck assembly model results closely predict the experimental data. In addition, the peak angular acceleration versus drop height results of FEA model with version Abaqus 2016 give a good prediction of the experimental results for the drop height 0.4 m as shown in Figure 4.20. However, the peak angular acceleration versus drop height for FEA model results based on Abaqus 2017 are significantly different than the experimental data as shown in Figure 4.22. In short, the FEA head neck assembly model can be used to obtain the peak translational acceleration in each drop height based on Abaqus 2017 with good reliability. The FEA model based on Abaqus 2016 gives a reliable prediction for both, peak translational and angular accelerations. Reasons for the difference between the two versions need further investigation before the model described can be used to predict the angular acceleration.

REFERENCES

Alquraishi, K. (2017). Impact Resistance of Single-Layer and Multi-Layerd Materials. *University of Maine*.

ASTM. (2015a). Standard Specification for Headgear Used in Soccer 1. *Astm*, *i*(Reapproved), 1–8. https://doi.org/10.1520/F2439-06R11.certification

ASTM. (2015b). Standard Test Methods for Equipment and Procedures Used in Evaluating the Performance Characteristics of Protective Headgear 1. *Astm*, 1–13. https://doi.org/10.1520/F1446-15B.Copyright

Bartsch, A., Benzel, E., Miele, V., Morr, D., & Prakash, V. (2012). Hybrid III anthropomorphic test device (ATD) response to head impacts and potential implications for athletic headgear testing. *Accident Analysis and Prevention*, *48*, 285–291. https://doi.org/10.1016/j.aap.2012.01.032

Brozoski, Frederick ; Logsdon, Katie ; Vasquez, Kimberly ; Lindsey, James ; Phelps, S. (2009). Effects of Magnetic Receiver Unit (MRU) Installation on the Blunt Impact Protection of the HGU-56/P Aircrew Integrated Helmet System (AIHS). *(No. USAARL-2010-10). ARMY AEROMEDICAL RESEARCH LAB FORT RUCKER AL WARFIGHTER PROTECTION DIV.*, *40*.

Bussone, W. R., Bove, R. T., Thomas, R., Richards, D., & Prange, M. T. (2010). Six-Degree-of-Freedom Accelerations : Linear Arrays Compared with Angular Rate Sensors. *Analysis*. https://doi.org/10.4271/2010-01-1017

Caccese, V., Ferguson, J., Lloyd, J., Edgecomb, M., Seidi, M., & Hajiaghamemar, M. (2016). Response of an Impact Test Apparatus for Fall Protective Headgear Testing Using a Hybrid-III Head/Neck Assembly. *Experimental Techniques*, *40*(1), 413–427. https://doi.org/10.1007/s40799-016-0046-4

Darijani, H., & Naghdabadi, R. (2010). Hyperelastic materials behavior modeling using consistent strain energy density functions. *Acta Mechanica*, *213*(3–4), 235–254. https://doi.org/10.1007/s00707-009-0239-3

Edgecomb, M. A. I. (2013). Finite element and experimental analysis of head protective gear to mitigate head injuries due to falls. *Electronic Theses and Dissertations. 1916. http://digitalcommons.library.umaine.edu/etd/1916*.

Faul M, Xu L, Wald MM, C. V. (2010). Traumatic Brain Injury In The United States: Emergency Department Visits, Hospitalizations and Deaths 2002 – 2006. Atlanta, Georgia: Centers for Disease Control and Prevention, National Center for Injury Prevention and Control; 2010.

Feng, W., & Hallquist, J. (2017). On Mooney-Rivlin Constants for Elastomers. *12th International LS-DYNA Users Conference*, *1*(1), 1–10.

Fenner, H., Thomas, D. J., Gennarelli, T., Pintar, F. A., Becker, E. B., Newman, J. A., & Yoganandan, N. (2005). Final Report of Workshop on Criteria for Head Injury and Helmet Standards. *Medical College of Wisconsin and Snell Memorial Foundation Inc.*, (January 2016).

Kimpara, H., & Iwamoto, M. (2012). Mild traumatic brain injury predictors based on angular accelerations during impacts. *Annals of Biomedical Engineering*, *40*(1), 114–126. https://doi.org/10.1007/s10439-011-0414-2

Kimpara, H., Nakahira, Y., Iwamoto, M., Rowson, S., & Duma, S. (2011). Head injury prediction methods based on 6 degree of freedom head acceleration measurements during impact. *International Journal of Automotive Engineering*, *2*(2), 13–19.

King, A. I. (2000). Fundamentals of impact biomechanics: part I-biomechanics of the head, neck, and thorax. *Annual Review of Biomedical Engineering, 2(1), 55-81.*, 1–20. https://doi.org/10.1016/B978-1-4557-5134-1.00001-9

Langlois JA, Rutland-Brown W, T. K. (2004). Traumatic Brain Injury in the United States : Emergency Department Visits, Hospitalizations, and Deaths. *Atlanta (GA): Centers for Disease Control and Prevention, National Center for Injury Prevention and Control; 2004.*, (October).

Marquis, B., Severson, K., & Tyrell, D. (1995). Analysis of Occupant Protection Strategies in Train Collisions. *1995 ASME International Mechanical Engineering Congress and Exposition*, *60*(April 2015), 539–557.

Mueller, B., MacAlister, A., Nolan, J., & D. Zuby. (2015). Comparison of HIC and BrIC Head Injury Risk in IIHS Frontal Crash to Real-World Head Injuries. *Insurance Institute for Highway Safety United States*, *15–0272*(208), 1–18.

National Operating committee on Standards for Athletic Equipment. (2013). Standard Test Method and Equipment Used in Evaluating the Performance Characteristics of Protective Head Gear/Equipment NOCSAE DOC (ND) 001- 11m12, (May 2012), 1–11.

Newman, J. A. (1986). A Generalized Model for Brain Injury Threshold. *In Proceedings of International Conference on the Biomechanics of Impact, 1986 (Pp. 121-131).*, 121–131.

Newman, J. A., Shewchenko, N., & Welbourne, E. (2000). A proposed new biomechanical head injury assessment function - the maximum power index. *Stapp Car Crash Journal*, *44*, 215–247. Retrieved from http://dx.doi.org/

NOCSAE081. (2006). Standard Linear Impact Test Method and Equipment Used in Evaluating the Performance Characteristics of Protective Headgear and face Guard NOCSAE DOC (ND) 081- 04M04. *NATIONAL OPERATING COMMITTEE ON STANDARDS FOR ATHLETIC EQUIPMENT*, (January).

Padgaonkar, A. J., Krieger, K. W., & King, A. I. (1975). Measurement of Angular Acceleration of a Rigid Body Using Linear Accelerometers. *Journal of Applied Mechanics*, *42*(3), 552–556. Retrieved from http://dx.doi.org/10.1115/1.3423640

R. Jakel. (2010). Analysis of Hyperelastic Materials with MECHANICA – Theory and Application Examples –. *PTC Presentation for the 2nd SAXSIM at Technische Universität Chemnitz*. https://doi.org/10.1093/toxsci/kft286

Rowson, S., & Duma, S. M. (2013). Brain injury prediction: Assessing the combined probability of concussion using linear and rotational head acceleration. *Annals of Biomedical Engineering*, *41*(5), 873–882. https://doi.org/10.1007/s10439-012-0731-0

Seidi, M. (2015). Design and Evaluation of Protective Head Gear to Mitigate Head Injuries Due to Falls. *Electronic Theses and Dissertations. 2308. http://digitalcommons.library.umaine.edu/etd/2308 This*, (May), 183. Retrieved from http://myaccess.library.utoronto.ca/login?url=http://search.proquest.com/docview/1688760036?accountid=14771%5Cnhttp://bf4dv7zn3u.search.serialssolutions.com/?ctx_ver=Z39.88-2004&ctx_enc=info:ofi/enc:UTF-8&rfr_id=info:sid/ProQuest+Dissertations+%26+Theses+

Takhounts, E. G., Craig, M. J., Moorhouse, K., McFadden, J., & Hasija, V. (2013). Development of Brain Injury Criteria (BrIC). *Stapp Car Crash Journal, 57, 243.*, *57*(November), 243–266.

Takhounts, E. G., Ridella, S. A., Rowson, S., & Duma, S. M. (2011). Kinematic rotational brain injury criterion (BRIC). *In Proceedings of the 22nd Enhanced Safety of Vehicles Conference. Paper (No. 11-0263)*, 1–10.

Thom, D. R., Hurt Jr, H. H., Smith, T. A., & Ouellet, J. V. (1997). Feasibility Study of Upgrading FMVSS No. 218, Motorcycle Helmets. *Head Protection Research Laboratory, University of Southern California, Final Report.*, (218).

Thompson, H. J., McCormick, W. C., & Kagan, S. H. (2006). Traumatic Brain Injury in Older Adults: Epidemiology, Outcomes, and Future Implications. *Journal of the American Geriatrics Society*, *54*(10), 1590–1595. https://doi.org/10.1111/j.1532-5415.2006.00894.x

U.S. Department of Health and Human Services. (2016). Falls are leading cause of injury and death in older Americans| CDC Online Newsroom | CDC. Retrieved from https://www.cdc.gov/media/releases/2016/p0922-older-adult-falls.html

BIOGRAPHY OF THE AUTHOR

Hussein Sharqi Owaid was born in Nasiriyah city at Thi Qar, Iraq on September 11, 1987. He graduated from Al Marqeziah High School in July of 2005. He graduated from the University of Thi Qar with a Bachelor of Science in Mechanical Engineering in July of 2009. He is a candidate for the Master of Science degree in Mechanical Engineering from the University of Maine in December 2017.